

8-2014

MICROFLUIDIC PARTICLE AND CELL MANIPULATION USING RESERVOIR- BASED DIELECTROPHORESIS

Saurin Patel

Clemson University, saurinp@clemson.edu

Follow this and additional works at: https://tigerprints.clemson.edu/all_dissertations

 Part of the [Mechanical Engineering Commons](#)

Recommended Citation

Patel, Saurin, "MICROFLUIDIC PARTICLE AND CELL MANIPULATION USING RESERVOIR-BASED DIELECTROPHORESIS" (2014). *All Dissertations*. 1323.
https://tigerprints.clemson.edu/all_dissertations/1323

This Dissertation is brought to you for free and open access by the Dissertations at TigerPrints. It has been accepted for inclusion in All Dissertations by an authorized administrator of TigerPrints. For more information, please contact kokeefe@clemson.edu.

MICROFLUIDIC PARTICLE AND CELL MANIPULATION USING
RESERVOIR-BASED DIELECTROPHORESIS

A Dissertation
Presented to
the Graduate School of
Clemson University

In Partial Fulfillment
of the Requirements for the Degree
Doctor of Philosophy
Mechanical Engineering

by
Saurin H. Patel
Aug 2014

Accepted by:
Dr. Xiangchun Xuan, Committee Chair
Dr. John R. Saylor
Dr. Richard S. Miller
Dr. Rui Qiao

ABSTRACT

Controlled manipulation of synthetic particles and biological cells from a complex mixture is important to a wide range of applications in biology, environmental monitoring, and pharmaceutical industry. In the past two decades microfluidics has evolved to be a very useful tool for particle and cell manipulations in miniaturized devices. A variety of force fields have been demonstrated to control particle and cell motions in microfluidic devices, among which electrokinetic techniques are most often used. However, to date, studies of electrokinetic transport phenomena have been primarily confined within the area of microchannels. Very few works have addressed the electrokinetic particle motion at the reservoir-microchannel junction which acts as the interface between the macro (i.e., reservoir) and the micro (i.e., microchannel) worlds in real microfluidic devices. This dissertation is dedicated to the study of electrokinetic transport and manipulation of particles and cells at the reservoir-microchannel junction of a microfluidic device using a combined experimental, theoretical, and numerical analysis.

First, we performed a fundamental study of particles undergoing electrokinetic motion at the reservoir-microchannel junction. The effects of AC electric field, DC electric field, and particle size on the electrokinetic motion of particles passing through the junction were studied. A two-dimensional numerical model using COMSOL 3.5a was developed to investigate and understand the particle motion through the junction. It was found that particles can be continuously focused and even trapped at the reservoir-microchannel junction due to the effect of reservoir-based dielectrophoresis (rDEP). The

electrokinetic particle focusing increases with the increase in AC electric field and particle size but decreases with the increase in DC electric field. It was also found that larger particles can be trapped at lower electric fields compared to smaller counterparts.

Next, we utilized rDEP to continuously separate particles with different sizes at the reservoir-microchannel junction. The separation process utilized the inherent electric field gradients formed at the junction due to the size difference between the reservoir and the microchannel. It was observed, that the separation efficiency was reduced by inter-particle interactions when particles with small size differences were separated. The effect of enhanced electrokinetic flow on the separation efficiency was investigated experimentally and was observed to have a favorable effect. We also utilized rDEP approach to separate particles based on surface charge. Same sized particles with difference in surface charge were separated inside the microfluidic reservoir. The streaming particles interacted with the trapped particles and reduced the separation efficiency. The influences from the undesired particle trapping have been found through experiments to decrease with a reduced AC field frequency.

Then, we demonstrated a continuous microfluidic separation of live yeast cells from dead cells using rDEP. Because the membrane of a cell gets distorted when it loses its viability, a higher exchange of ions results from such viability loss. The increased membrane conductivity of dead cells leads to a different Claussius-Mossotti factor from that of live cells, which enables their selective trapping and continuous separation based on cell viability. A two-shell numerical model was developed to account for the varying

conductivities of different cell layers, the results of which agree reasonably with the experimental observations. We also used rDEP to implement a continuous concentration and separation of particles/cells in a stacked microfluidics device. This device has multiple layers and multiple microchannels on each layer so that the throughput can be significantly increased as compared to a single channel/single layer device.

Finally, we compared the two-dimensional and three-dimensional particle focusing and trapping at the reservoir-microchannel junction using rDEP. We observed that the inherent electric field gradients in both the horizontal and vertical planes of the junction can be utilized if the reservoir is created right at the reservoir-microchannel junction. Three-dimensional rDEP utilizes the additional electric field gradient in the depth wise direction and thus can produce three-dimensional focusing. The electric field required to trap particles is also considerably lower in three-dimensional rDEP as compared to the two-dimensional rDEP, which thus considerably reduces the non-desired effects of Joule heating. A three-dimensional numerical model which accounted for the entire microfluidic device was also developed to predict particle trajectories.

ACKNOWLEDGEMENTS

I would like to express my deepest appreciation and sincere gratitude to my advisor Dr. Xiangchun Xuan, for believing in my abilities. I would like to thank him for his patience, motivation, and several insightful discussions that helped me complete my dissertation. His continued guidelines have greatly helped me in my research and writing of this dissertation.

I would also like to thank my committee members, Dr. John R. Saylor, Dr. Richard S. Miller, and Dr. Rui Qiao for giving up their precious time to be a part of my committee. I am gracious for the constant support and constructive advice I have received on their behalf during my graduate studies.

I would like to thank the National Science Foundation (NSF), for the funding received for my research. I would also like to thank the Department of Mechanical Engineering, Clemson University for providing me with Graduate Laboratory Assistantship which helped me financially support my graduate studies.

I would also like to thank my colleagues Junjie Zhu, Bhaskar Praveen, Litao Liang, Akshay Kale, John DuBose, and Xinyu Lu for being supportive during the past years. I would like to thank my friends Yash Raval and Jasmin Adeshara for creating a cheerful atmosphere which made my years at the graduate school enjoyable.

I would like to thank my father, mother, and brother for their love and support throughout my entire life. I am forever indebted to them and much of this work is a

reflection of the values they installed in me. Finally, I would like to thank my wife, Dhara, for her patience and support while I pursued my education. I am and will always be indebted to her. I dedicate this dissertation to her.

TABLE OF CONTENTS

	Page
ABSTRACT	ii
TABLE OF CONTENTS	vii
LIST OF FIGURES	xii
CHAPTER 1: Introduction and overview	1
1.1 Background and Motivation	1
1.2 Electrokinetic Phenomena	3
1.2.1 The Electric Double Layer.....	4
1.2.2 Electroosmosis	6
1.2.3 Electrophoresis.....	8
1.2.4 Dielectrophoresis	9
1.3 Dissertation Outline	11
CHAPTER 2: Electrokinetic Motion of Particles at the	
Reservoir-Microchannel Junction	13
2.1 Introduction.....	13
2.2 Experiment.....	16
2.2.1 Microfluidic Device Fabrication.....	16
2.2.2 Particle Solution Preparation	18
2.2.3 Particle Manipulation and Visualization.....	18
2.3 Theory	19
2.3.1 Mechanism	19

Table of Contents (Continued)	Page
2.3.2 Trapping and Focusing Number	22
2.4 Numerical Simulation	25
2.5 Results and Discussion	26
2.5.1 AC Electric Field Effects on Particle Focusing.....	26
2.5.2 DC Electric Field Effects on Particle Focusing.....	30
2.5.3 Particle Size Effects on Particle Focusing.....	33
2.5.4 Particle Trapping and Concentration.....	36
2.6 Summary	39
 CHAPTER 3: Particle Separation by Size using Reservoir-based	
Dielectrophoresis	41
3.1 Background on Particle Separation.....	41
3.2 Experiment.....	44
3.3 Theory	45
3.3.1 Separation Mechanism.....	49
3.4 Numerical Simulation	50
3.5 Results and Discussion	52
3.5.1 Size-based Separation of 3 and 10 μm Polystyrene	
Particles Using rDEP	52
3.5.2 Size-based Separation of 3 and 5 μm Polystyrene	
Particles Using rDEP	54
3.5.3 Effects of Electrokinetic Flow on Particle Separation	
Efficiency	58
3.6 Summary	60

Table of Contents (Continued)	Page
CHAPTER 4: Particle Separation by Charge using Reservoir-based	
Dielectrophoresis	62
4.1 Introduction.....	62
4.2 Materials and Methods.....	64
4.2.1 Microfluidic Device Fabrication.....	64
4.2.2 Particle Solution Preparation	65
4.2.3 Particle Manipulation and Visualization.....	66
4.3 Particle Separation Mechanism.....	67
4.4 Numerical Model and Validation.....	71
4.5 Results and Discussion	74
4.5.1 Charge-based Particle Separation using rDEP.....	74
4.5.2 Electrokinetic Flow Effects on Particle Separation	77
4.5.3 AC Field Frequency Effects on Particle Separation	79
4.6 Summary	80
CHAPTER 5: Microfluidic Separation of Live and Dead Yeast Cells using	
Reservoir-based Dielectrophoresis	82
5.1 Introduction.....	82
5.2 Experiment.....	84
5.2.1 Microchannel Fabrication	84
5.2.2 Cell Preparation	86
5.2.3 Experimental Technique	87
5.3 Theory	88
5.3.1 Principle of Reservoir-based Dielectrophoresis (rDEP)	88

Table of Contents (Continued)	Page
5.4 Numerical Modeling	93
5.4.1 Calculation of Complex Permittivities of Live and Dead Yeast Cells	95
5.5 Results and Discussion	96
5.5.1 Focusing and Trapping of Live Yeast Cells with rDEP.....	96
5.5.2 Comparison of rDEP trapping of Live and Dead Yeast Cells	98
5.5.3 Continuous Separation of Live and Dead Yeast Cells with rDEP	101
5.6 Summary	104
CHAPTER 6: Enhanced Throughput for Electrical Manipulation of Particles and Cells in a Stacked Microfluidic Device Using Reservoir-based Dielectrophoresis (rDEP)	
6.1 Introduction.....	106
6.2 Experiment.....	107
6.2.1 Stacked Microfluidic Device	107
6.2.2 Particle and Cell Solution	108
6.2.3 Experimental Technique	109
6.3 Theory	110
6.4 Numerical Simulation	112
6.5 Results and Discussion	113
6.5.1 5 μm Particles Concentration and Separation	

Table of Contents (Continued)	Page
from 3 μm Particles.....	113
6.5.2 Yeast Cells Concentration and Separation from E. coli	116
6.6 Summary	119
CHAPTER 7: Three Dimensional Characterization of Electrokinetic	
Particle Entry Through Reservoir-microchannel Junction	120
7.1 Introduction.....	120
7.2 Experiment.....	121
7.3 Theory	123
7.4 Numerical Simulation	125
7.5 Results and Discussion	126
7.5.1 Comparison Between Two-dimensional and	
Three-dimensional Particle Focusing	126
7.5.2 Comparison Between Two-dimensional and	
Three-dimensional Particle Trapping	130
7.6 Summary	134
CHAPTER 8: Conclusion and Future Work.....	135
8.1 Conclusion	135
8.2 Future work.....	139
REFERENCES.....	140

LIST OF FIGURES

	Page
Figure 1: Schematic of an electric double layer (EDL) formed adjacent to a positively charged surface. Stern layer and zeta potential ζ are also illustrated in the image, reprinted from (129 Masliyah, J. 2005)	5
Figure 2: Schematic of electroosmotic flow in a capillary tube bearing a uniform negative surface charge	7
Figure 3: Dielectrophoresis of a particle in an externally applied electric field is illustrated in the figure 3. Demonstration of translation of particle towards the low electric field region when particle is less polarizable than the medium (a) and the translation of particle towards the high electric field region when particle is more polarizable than the medium (b)	11
Figure 4: Picture of a PDMS-based microfluidic device used in the experiment (green food dye used for clarity). The inset displays a schematic view of the reservoir-microchannel junction with actual dimensions. The block arrow indicates the particle moving direction in the experiments	17
Figure 5: Illustration of rDEP for particles focusing and trapping at the reservoir-microchannel junction. The image also illustrates electric field lines and electric field contour (background color, the darker the higher electric field).....	20
Figure 6: Comparison of experimentally obtained (snapshot and superimposed) and numerically predicted trajectories of 5 μm particles passing through the reservoir-microchannel junction under the influence of rDEP at various DC-biased AC voltages. The DC voltage applied, is fixed at 50 V and the AC (RMS) voltage at 1 kHz frequency is varied from (a) 0 V ($\alpha = 0$) to (b) 200 V ($\alpha = 4$), (c) 400 V ($\alpha = 8$), and (d) 550 V ($\alpha = 11$)	28
Figure 7: Illustration of experimentally measured and numerically	

List of Figures (Continued)**Page**

predicted stream width of 5 μm particles passing through the reservoir-microchannel junction under the influence of rDEP at various DC-biased AC voltages. The DC voltage applied, is fixed at 50 V and the AC (RMS) voltage at 1 kHz frequency is varied	29
Figure 8: Comparison of experimentally obtained (snapshot and superimposed) and numerically predicted trajectories of 5 μm particles passing through the reservoir-microchannel junction under the influence of rDEP at various DC-biased AC voltages. The AC (RMS) voltage applied at 1 kHz frequency, is fixed at 200 V and the DC voltage is varied from (a) 25 V ($\alpha = 8$) to (b) 50 V ($\alpha = 4$), (c) 75 V ($\alpha = 2.67$), and (d) 100 V ($\alpha = 2$)	31
Figure 9: Illustration of experimentally measured and numerically predicted stream width of 5 μm particles passing through the reservoir-microchannel junction under the influence of rDEP at various DC-biased AC voltages. The AC (RMS) voltage applied at 1 kHz frequency is fixed at 200 V and the DC voltage is varied	32
Figure 10: Comparison of experimentally obtained (snapshot and superimposed) and numerically predicted trajectories of 3, 5 and, 10 μm particles passing through the reservoir-microchannel junction under the influence of rDEP at DC-biased AC voltage of 50 V DC and 200 V AC ($\alpha = 4$)	34
Figure 11: Illustration of experimentally measured and numerically predicted stream width of 3, 5 and, 10 μm particles passing through the reservoir-microchannel junction under the influence of rDEP at various DC-biased AC voltages. The DC voltage applied, is fixed at 50 V and the AC (RMS) voltage at 1 kHz frequency is varied	35
Figure 12: Comparison of experimentally obtained (snapshot and superimposed) and numerically predicted trajectories of 3, 5 and 10 μm particles trapped at the reservoir-microchannel junction under the influence of rDEP at various DC-biased AC voltages. The DC voltage applied is fixed at 50 V and the AC (RMS) voltage applied to trap the particles at 1 kHz	

List of Figures (Continued)	Page
frequency, is (a) 975 V ($\alpha = 19.5$) to (b) 550 V ($\alpha = 11$), and (c) 400 V ($\alpha = 8$).....	38
Figure 13: Illustration of rDEP for particles focusing and trapping at the reservoir-microchannel junction. The image also illustrates electric field lines and electric field contour (background color, the darker the higher electric field).....	47
Figure 14: Analysis of electrokinetic and dielectrophoretic velocities of particles undergoing separation at the reservoir microchannel junction. The arrows are proportional to the magnitude of electrokinetic (blue) and dielectrophoretic (red) velocities experienced by particles approaching reservoir-microchannel junction. The electric field lines (black lines) and the contour of electric field (darker the larger) are also illustrated	49
Figure 15: Comparison of experimentally obtained snapshot (a) and superimposed (b) images with numerically predicted trajectories (c) of 3 and 10 μm particle separation at the reservoir-microchannel junction under the influence of rDEP. The DC voltage applied is 50 V and the AC (RMS) voltage applied is 400 V at 1 kHz frequency	52
Figure 16: Comparison of experimentally obtained snapshots and superimposed images with numerically predicted trajectories of 3 and 5 μm particle separation at the reservoir-microchannel junction under the influence of rDEP at various DC-biased AC voltages. The DC voltage applied, is fixed at 25 V and the AC (RMS) voltage at 1 kHz frequency is varied from (a) 0 V ($\alpha = 0$) to (b) 450 V ($\alpha = 4$), and (c) 550 V ($\alpha = 11$)	55
Figure 17: Percentage of 3 and 5 μm particles trapped at the reservoir-microchannel junction during particle separation at various DC-biased AC voltages under rDEP	59
Figure 18: Picture of the microfluidic device (filled with green food dye for clarity) used in the experiment. The inset displays the dimensions of the reservoir-microchannel junction	65
Figure 19: Velocity analysis of a particle at the reservoir-microchannel	

junction due to electrokinetic flow and the induced rDEP. The thin lines represent the electric field lines or equivalently fluid streamlines in the absence of the particle. The background color shows the electric field contour (the darker color, the larger field magnitude)..... 68

Figure 20: Comparison of the experimentally obtained streak images (left column in each panel) and numerically predicted trajectories (right column in each panel) of fluorescent (top row) and non-fluorescent (bottom row) 3 μm particles at the reservoir-microchannel junction under the influence of rDEP. The applied DC voltage was fixed at 25 V and the 1-kHz AC voltage (RMS value) was varied from 0 V (a) to 400 V (b). The block arrow in (a) indicates the particle moving direction..... 74

Figure 21: Demonstration of selective concentration and continuous sorting of 3 μm fluorescent particles from 3 μm non-fluorescent particles at the reservoir-microchannel junction by rDEP. (a) shows a snapshot image of the particle behaviors 45 s after the 50 V DC-biased 800 V AC (RMS value, 1 kHz) voltage was applied. (b) and (c) show the comparison of the experimentally obtained streak images (top row) and the numerically predicted trajectories (bottom row) of the fluorescent and non-fluorescent particles, respectively. The block arrow in (a) indicates the particle moving direction..... 76

Figure 22: Electrokinetic flow effects on charge-based rDEP separation of 3 μm fluorescent and non-fluorescent particles at the reservoir-microchannel junction. Illustrated are the snapshot images taken 2 minutes after the electric voltage at (a) 25 V DC/625 V AC ($\alpha = 25$), (b) 50 V DC/800 V AC ($\alpha = 16$), and (c) 100 V DC/950 V AC ($\alpha = 9.5$) was imposed to the microchannel. The AC voltages are all in RMS value and at 1 kHz frequency. The dashed lines highlight the regions where non-fluorescent particles are trapped due to the influences from the concentrated fluorescent particles. The block arrow in (a) indicates the particle moving direction..... 78

Figure 23: AC field frequency effects on charge-based rDEP

separation of 3 μm fluorescent and non-fluorescent particles at the reservoir-microchannel junction. Illustrated are the snapshot images taken 2 minutes after the application of a 75 V DC-biased 875 V AC voltage (RMS). The AC voltage frequency was varied from 0.5 kHz (a) to 1 kHz (b) and 5 kHz (c). The dashed lines highlight the regions where non-fluorescent particles get trapped due to the influences from the concentrated fluorescent particles. The block arrow in (a) indicates the particle moving direction	80
Figure 24: Picture of the microfluidic device (filled with green food dye for clarity) used in the experiment. The inset displays the dimensions of the reservoir-microchannel junction. The block arrow indicates the cell moving direction in experiments	85
Figure 25: Illustration of cell velocity at the reservoir-microchannel junction due to the combined effects of electrokinetic flow, U_{EK} , and negative rDEP, U_{DEP} . The thin lines represent the electric field lines or equivalently fluid streamlines. The background shows the electric field contour (the darker color, the larger field magnitude)	89
Figure 26: Comparison of the model predicted CM factors of live (solid line) and dead (dashed line) yeast cells suspended in 1 mM phosphate buffer as a function of the electric field frequency. The dash-dot line divides the diagram to positive DEP (top half, $\text{Re}\{f_{CM}\} > 0$) and negative DEP (bottom half, $\text{Re}\{f_{CM}\} < 0$) regions	90
Figure 27: Two-shell model of a yeast cell (not to scale, left panel). The values of the radius, r , electric conductivity, σ , and permittivity, ε , for each layer of the cell are listed in the table (right panel)	96
Figure 28: Comparison between experimentally obtained superimposed images (top row) and numerically predicted trajectories (bottom row) of live yeast cells at the reservoir-microchannel junction under the influence of rDEP. In the experiment the applied DC voltage was fixed at 2 V while the AC voltage (RMS) at 1 kHz frequency was varied from	

List of Figures (Continued)

Page

- (a) 0 V ($\alpha = 0$) to (b) 30 V ($\alpha = 15$) and (c) 50 V ($\alpha = 25$).
The block arrow in (a) indicates the cell moving direction..... 97
- Figure 29: Experimentally recorded (symbols) and numerically predicted (lines) AC to DC electric field ratios, α , for trapping live (a) and dead (b) yeast cells at different AC field frequencies at the reservoir-microchannel junction by rDEP. The DC voltage was maintained at 2 V in both experiments..... 99
- Figure 30: Phase diagram of the experimentally recorded AC to DC field ratios, α , for rDEP trapping of live (triangular symbols) and dead (square symbols) yeast cells at the reservoir-microchannel junction with respect to the AC field frequency. The DC voltage was fixed at 2 V in all measurements. The highlighted area (i.e., Zone 2) indicates the region in which the dead yeast cells can be selectively trapped the continuously separated from live yeast cells by rDEP 100
- Figure 31: Demonstration of selective concentration and continuous separation of live and dead yeast cells at the reservoir-microchannel junction by rDEP. (a) is a snapshot image, and (b) and (c) compare the experimentally obtained superimposed images (top row) of live (b) and dead (c) yeast cells with the numerically predicted cell trajectories (bottom row). The cell separation was driven by a 4 V DC-biased 47.5 V AC (i.e., $\alpha = 11.875$) at 1 kHz frequency. The block arrow in (a) indicates the cell moving direction..... 103
- Figure 32: Illustration of a stacked PDMS-glass microfluidic device with two PDMS layers, each of which is composed of four a 0.5 mm-long straight microchannels with a 5 mm-diameter reservoir at each end. The channel is 500 μm wide and has a constriction section of 50 μm in width and 500 μm in length at the central reservoir microchannel junction (see the inset of figure. 32). The arrow in the inset indicates flow direction..... 108
- Figure 33: Velocity analysis of a particle at the reservoir-microchannel junction due to electrokinetic flow and the induced rDEP. The thin lines represent the electric field lines or equivalently fluid streamlines in the absence of the particle. The background color shows the electric field contour 111

- Figure 34: Comparison of experimentally obtained snapshot and superimposed images and, numerically predicted trajectories for 5 μm particles at the reservoir-microchannel junction. Where, 34(a) and 34(c) are reservoir-microchannel junctions from layer A (see figure 32) representing trapping (50V DC and 500V AC) of particles in the images. Image 34(b) represents the superimposed image of particle trapping from layer B. 34(e), 34(f) and 34(g) are experimentally obtained snapshot images demonstrating the separation of 5 μm and 3 μm particles by the rDEP. 34(d) and 34(h) represents the numerically predicted trajectories for trapping and separation respectively 114
- Figure 35: Experimentally obtained snapshot images of yeast cell trapping and, yeast cell and E. coli separation at the reservoir-microchannel junction. Images 35(a), 35(b) and 35(c) demonstrate the trapping of yeast cells (25V dc and 200V ac) at the reservoir microchannel junction. Image 35(d) represents the numerically predicted cell trajectories. Images 35(e)-35(h) are experimentally obtained snapshot images of yeast and E. coli cell separation at the junction 117
- Figure 36: Schematic view of microfluidic devices used to obtain (a) two-dimensional, and (b) three-dimensional particle focusing and trapping. The inset illustrates the difference in location of the reservoirs in the devices used for two-dimensional and three-dimensional characterization of particles 122
- Figure 37: Illustration of (a) electric field \mathbf{E} and (b) dielectrophoretic force, \mathbf{F}_{DEP} distribution at the reservoir-microchannel junction. The top and bottom image on the left represents the top view and the side view of electric field distribution at the reservoir-microchannel junction. The images on the right represent the dielectrophoretic force (\mathbf{F}_{DEP}) distribution at the junction 124
- Figure 38: Comparison between experimentally obtained (snapshot and superimposed) and numerically predicted trajectories of 5 μm particles subjected to two-dimensional focusing at the reservoir-microchannel junction under the influence of rDEP at various DC-biased AC voltages. The DC voltage

List of Figures (Continued)

Page

applied, is fixed at 25 V and the AC (RMS) voltage at 1 kHz frequency is varied from (a) 0 V ($\alpha=0$) to (b) 150 V ($\alpha=6$), and (c) 300 V ($\alpha=12$)	129
Figure 39: Comparison between experimentally obtained (snapshot and superimposed) and numerically predicted trajectories of 5 μm particles subjected to three-dimensional focusing at the reservoir-microchannel junction under the influence of rDEP at various DC-biased AC voltages. The DC voltage applied, is fixed at 25 V and the AC (RMS) voltage at 1 kHz frequency is varied from (a) 0 V ($\alpha=0$) to (b) 150 V ($\alpha=6$), and (c) 300 V ($\alpha=12$)	130
Figure 40: Comparison of experimentally obtained snapshots and superimposed images with numerically predicted trajectories of 5 μm particles subjected to (a) two-dimensional and (d) three-dimensional trapping at the reservoir-microchannel junction under the influence of rDEP. The DC voltage applied is 25 V and the AC (RMS) voltage at 1 kHz frequency is 375 V ($\alpha=15$) for two-dimensional, and 425 ($\alpha=17$) for three-dimensional trapping.....	131
Figure 41: Comparison between two-dimensional and three-dimensional particle trapping under various DC-biased AC voltages under the influence of rDEP at the reservoir-microchannel junction.....	133

CHAPTER 1: Introduction and overview

1.1 Background and Motivation

Advancement in the field of microfluidics has enabled fluidic components to be miniaturized and integrated together on Lab-on-a-chip (LOC) microfluidic devices. A Lab-on-a-chip microfluidic device is analogous to microelectronic chip and integrates several laboratory operations. The LOC device typically consists of arrays of microchannels, electrodes, micron sized valves and pumps, sensors etc. The microchannels and other miniaturized components tend to consume smaller volumes of fluids reducing reagent consumption. The miniaturization also reduces consumption of experimental materials; reducing waste production and thus decreasing the costs. Microfluidic devices have small length scales making the diffusive mixing fast and often increasing the speed and accuracy of the reactions (DeWitt, S. H. 1999; Watts, P. 2003). A Microfluidic device also reduces measurement times and improves sensitivity, selectivity and repeatability of assays. Microfluidic devices have large surface to volume ratio which facilitates rapid heat transfer, enabling precise temperature control. Integrated microfluidic devices also offers portability feature, permitting mobile applications in forensics, drug delivery for point-of-care medicines, chemical and biological analysis etc. The manufacturing costs of this miniaturized devices being low, they could be disposable, eliminating cross contamination. Occasionally, implementations of microfluidic devices have completely transformed the performances of certain types of

experiments or have enabled large scale parallelization that could not be attained previously.

Typically, particle and cell manipulation includes focusing, trapping, mixing, filtering, separating, sorting, etc. Focusing is termed as concentrating scattered particles at the inlet of the microchannel into a narrow stream at the exit which allows for accurate detection and sorting. Trapping is termed as locally immobilizing particles and increasing the concentration of particles that are otherwise distributed uniformly in the bulk fluid. Separation is isolating of one specific kind of particle from a mixture of different particles. In literature particles have been separated based on properties such as size, charge, shape, density, deformability, magnetic and optical polarizability etc.

Numerous force fields have been utilized for manipulation of particles and cells inside the microfluidic devices. These force fields include but are not limited to magnetic (Pamme, N. 2006; Gijs, M. A. 2010), electric (Gascoyne, P. R. 2002; Hughes, M. P. 2002; Srivastava, S. K. 2011; Regtmeier, J. 2011), acoustic (Laurell, T. 2007; Friend, J.), optical (Wang, M. M. 2005; Kim, S. B. 2008), hydrodynamic (Yamada, M. 2005; Yamada, M. 2006; Davis, J. A. 2006; Choi, S. 2007), inertial (Di Carlo, D. 2009; Kuntaegowdanahalli, S. S. 2009), gravitational (Huh, D. 2007) etc. The studies of particle manipulations have been primarily confined within the microchannels. Very few works have addressed the electrokinetic particle motion at the reservoir-microchannel junction which acts as the interface between the macro (i.e., reservoir) and micro (i.e., microchannels) worlds in the microfluidic devices. Therefore, this proposed work is

dedicated to the study of electrokinetic manipulation of particles and cells at the reservoir-microchannel junction of a microfluidic device. The goal of this work is to obtain fundamental knowledge of electrokinetic particle motion at the reservoir-microchannel junction and to utilize the junction to attain focusing and trapping of particles and cells, having differences in physical properties. The key objective of this thesis work is to apply reservoir-microchannel junction for continuous particle/cell sorting and separation using reservoir-based dielectrophoresis (rDEP).

1.2 Electrokinetic Phenomena

Electrokinetic phenomena can be broadly classified into electroosmosis, streaming potential, electrophoresis, dielectrophoresis, and sedimentation potential. These electrokinetic phenomena arise due to the interaction of the surface charge and ionic aqueous liquids, and are often defined by the presence of an electrical double layer (EDL). The brief descriptions of these electrokinetic phenomena are: 1. Electroosmosis which refers to the flow of liquid along a charged surface when an electric field is applied parallel to the surface. 2. Streaming potential which refers to the inverse of electroosmosis, i.e. an electric potential is created when a liquid is forced to move along a charged surface. 3. Electrophoresis which refers to the movement of suspended, charged particles as a result of an applied electric field. 4. Dielectrophoresis which refers to the movement of neutral particles by the application of an electric field and 5. Sedimentation potential which refers to the inverse of electrophoresis, i.e. an electrical potential is created by the movement of charged particles through a liquid by gravity. The subsequent

sections discuss the source of electrokinetic phenomena, the electrical double layer, and a brief review of electroosmosis, electrophoresis and dielectrophoresis. In this work the focus is on electrokinetic phenomena using an applied electric field to induce motion and hence streaming, and sedimentation potential are beyond the scope of this work.

1.2.1 The Electrical Double Layer

Generally, a solid surface when brought in contact with an ionic aqueous solution tends to attain surface charge. The surface charge attained by the solid surface originates from the adsorption and dissociation of chemical groups within the ionic solution (Hunter, J. 2001; 128 Li, D. 2004). In course of electrokinetic studies, presence of surface charges is accepted and its origin is paid less attention. However, it is important to recognize the origins of these charges. The formation of such electrical surface charge could be explained by variety of mechanisms: 1. Ionization of surface groups. 2. Differential dissolution of ions from surfaces of sparingly soluble crystals. 3. Isomorphic substitution. 4. Charged crystal surfaces. 5. Specific ion adsorption (Masliyah, J. 2005). The charged surface and the surrounding ions undergo an electrostatic interaction wherein counter-ions are attracted and co-ions are repelled from the charged surface. Consequently, a layer consisting of more counter-ions than co-ions is formed close to the charged surface, this layer is known as electrical double layer (EDL). The phenomenon of the electrokinetic transport of particles in microchannels originates from this electric double layer (EDL). The EDL reestablishes ionic electro-neutrality and, consequently, causes an electrokinetic potential which is referred to as the surface or zeta potential ζ .

The magnitude of the zeta potential is a function of the surface charge and the thickness of the electrical double layer. The layer on the ionic aqueous side can be divided into stern layer and diffuse layer. Ions within the stern layer are immobilized due to strong electrostatic forces and the ions within the diffuse layer are free to move. As a result, main focus in electrokinetic studies is on diffuse layer. The zeta potential, ζ , is defined at the interface between the stern layer and diffuse layer. Figure 1 illustrates the formation of an EDL within the presence of a positively charged surface and the corresponding electric potential distribution.

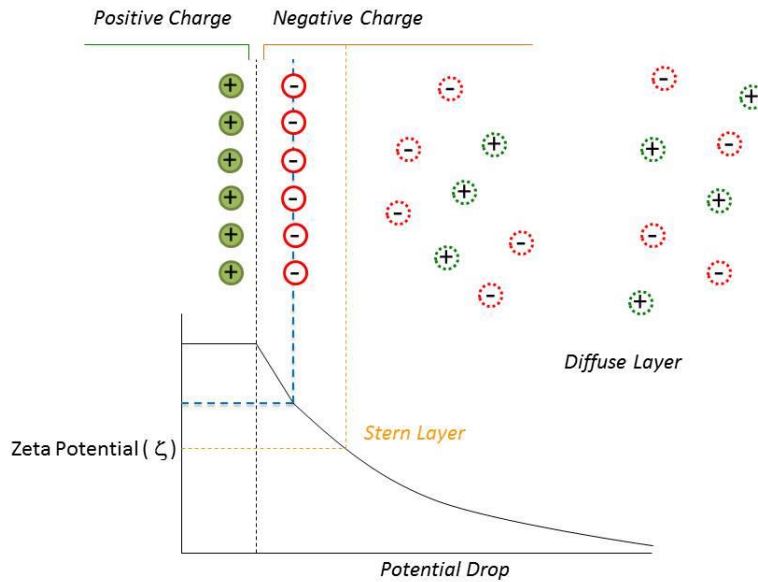


Figure 1: Schematic of an electric double layer (EDL) formed adjacent to a positively charged surface. Stern layer and zeta potential ζ are also illustrated in the image.

The potential distribution, in the direction away from the shear plane, is characterized by the Debye length, κ^{-1} , defined as:

$$\kappa^{-1} = \sqrt{\frac{\epsilon k_B T}{2e^2 z_v^2 n_\infty}} \quad (1-1)$$

Where n_∞ is the bulk ionic concentration, k_B is Boltzmann's constant, T is the fluid temperature, z_v is ionic valence, e is the elementary charge, and ϵ is the dielectric constant in the medium. The Debye length depends on the concentration of the ionic aqueous solution. Typically, the dimension of the EDL is on the order of several nanometers.

1.2.2 Electroosmosis

The introduction of ionic aqueous solution inside a microchannel gives rise to the formation of electrical double layer (EDL) in order to neutralize the charged surfaces. On application of external electric field parallel to the stationary charge surface, the excessive counter-ions within the EDL experience tangential electrical force to the electric field lines and migrate towards the oppositely charged electrodes. The ions drag the viscous fluid along with them and this induced flow motion arising from the electrostatic interaction between the charge within the EDL and the applied electric field is called electroosmotic flow. Assuming the electroosmotic flow is incompressible, steady state, fully developed and there is no external pressure gradient across the charged surface, Navier-Stokes equation, with the addition of an electrical body force term can be written as Eq. (1-2):

$$0 = \mu \left(\frac{\partial^2 u}{\partial y^2} \right) + E_x \rho_e \quad (1-2)$$

where, u and E_x are, respectively, the x component of fluid velocity and electric field imposed, μ is the fluid viscosity, and ρ_e is the net charge density within the channel which can be expressed through the Poisson equation:

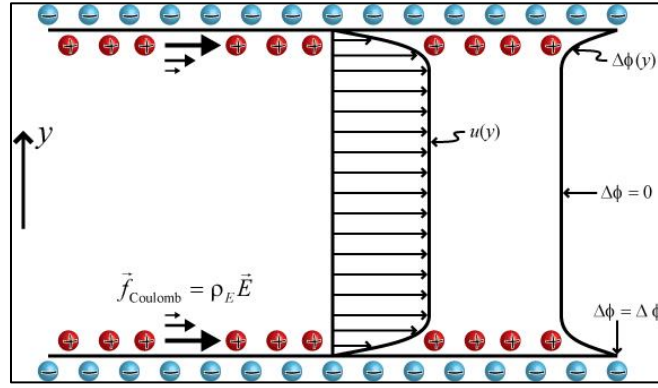


Figure 2: Schematic of electroosmotic flow in a microchannel bearing a uniform negative surface charge, reprinted from (Kirby, J. 2004).

$$\rho_e = -\epsilon \frac{d^2 \phi}{dy^2} \quad (1-3)$$

Substituting Eq. (1-3) into Eq. (1-2) and solving for the electroosmotic flow velocity, u_{eo} , with boundary conditions set such that: $\phi(b) = \phi(-b) = \zeta_w$ and $u(b) = u(-b) = 0$ results in Eq. (1-4);

$$u_{eo} = \frac{\varepsilon E_x}{\mu} (\phi - \zeta_w) \quad (1-4)$$

The electrical double layer thickness being much smaller than the characteristic length of the microfluidic device, the electroosmotic flow profile in a microchannel is almost uniform and referred to as plug-like flow as shown in figure 2. The electroosmotic flow is utilized widely to transport species in microchannel devices (Linan, J. 2002; Hirvonen, J. 1997; Pikal, M. J. 2001; Chen, L. 2007) due to its unique plug-like flow profile that diminishes the dispersion problem, which is a major concern in pressure driven flow (PDF).

1.2.3 Electrophoresis

A charged particle suspended in ionic aqueous solution will migrate when subjected to an external electric field which is referred as electrophoresis. The charged surface in electroosmotic flow being the wall is stationary, while in electrophoresis it is the surface of the particle and is mobile. The particle's steady electrophoretic velocity can be obtained by balancing the hydrodynamic force acting on the particle to the electrostatic force acting on the particle. Under a thin electrical double layer

approximation and application of external electric field, the electrophoretic velocity of the particle can be expressed as shown in Eq. (1-5). The difference between electroosmotic and electrophoretic velocity is that the zeta potential of the wall, ζ_w , is replaced by the zeta potential of the particle, ζ_p .

$$u_{ep} = \frac{\epsilon \zeta_p}{\mu} E_x \quad (1-5)$$

The particles follow the uniform electric field lines of the applied external electric field. The electrophoretic and electroosmotic velocity of the particles and the fluid in microchannels are opposite to each other. Typically, the electroosmotic motion of the fluid dominates the particle electrophoretic motion and the particles are dragged along with the bulk fluid. The electrophoretic and electroosmotic motions in a microchannel are combined together and referred as electrokinetic velocity of the particle. Electrophoresis is widely used in particle separation, concentration, transportation etc. in microfluidic devices (Hunter, J. 2001; Li, D. 2004; Kang, Y. 2008).

1.2.4 Dielectrophoresis

The motion of a polarizable particles immersed in an ionic aqueous solution when subjected to a non-uniform electric field is known as dielectrophoresis (Pohl, H. A. 1978). The direction of the DEP force is determined by the ratio of the polarizability of the particle to that of the electrolyte solution, as shown in figure 3. The motion of the particle towards the region with higher electric field is known as positive DEP (see figure

3(b)) and away from the higher electric field region is known as negative DEP (see figure 3(a)). Dielectrophoresis originates from the electric field gradients resulting in translational particle motion across fluid streamlines. The dielectrophoretic force is proportional to the square of the electric field and third power of the particle size, indicating non-linear electrokinetics. The time averaged DEP force induced on a spherical particle is expressed as;

$$\mathbf{F}_{DEP} = \frac{1}{2} \pi \varepsilon_f d^3 \text{Re}\{f_{CM}\} (\mathbf{E} \cdot \nabla \mathbf{E}) \quad (1-6)$$

where ε_f is the permittivity of the suspending fluid, d the particle diameter, E the electric field and $\text{Re}\{f_{CM}\}$ represents the real part of the Clausius–Mossotti (CM) factor, which is given by;

$$f_{CM} = \frac{\varepsilon_p^* - \varepsilon_m^*}{\varepsilon_p^* + 2\varepsilon_m^*} \quad (1-7)$$

In the above equation, $\varepsilon^* = \varepsilon - i \frac{\sigma}{\omega}$ is the complex permittivity, with σ and ω being the corresponding conductivity and angular frequency of the applied electric field respectively.

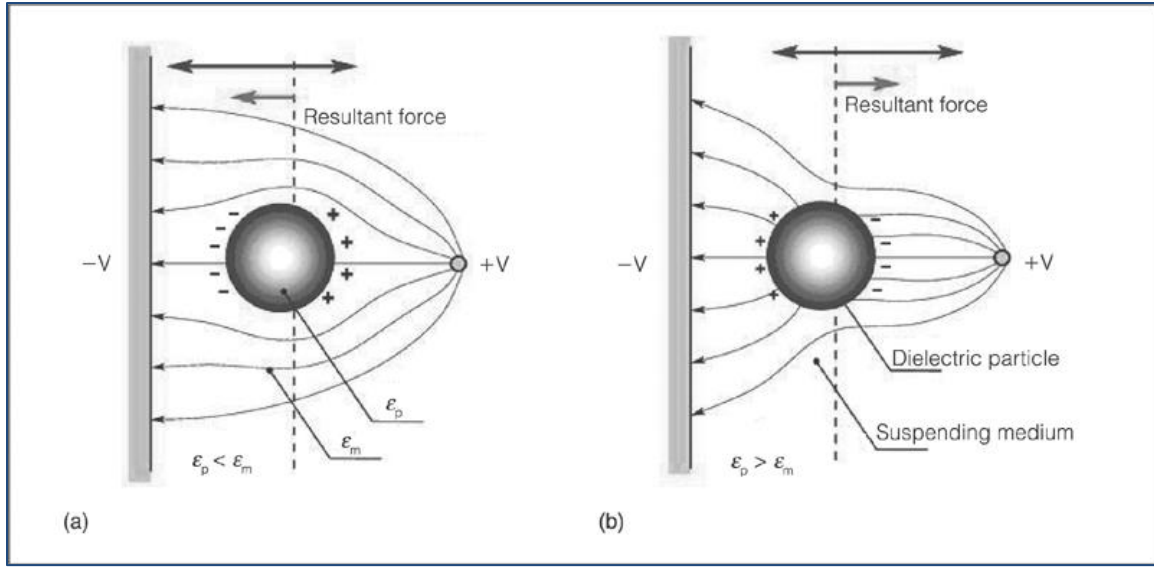


Figure 3: Dielectrophoresis of a particle in an externally applied electric field is illustrated in the figure 3. Demonstration of the translation of particle towards the low electric field region when particle is less polarizable then the medium (a) and the translation of particle towards the high electric field region when particle is more polarizable then the medium (b) (Medora, G.. 2007).

DEP force is widely used in separation, concentration, trapping etc. of particles as it depends to the third power of the particle size. This unique dependence of DEP force on particle size can be utilized to generate dissimilar responses which enable easy particle manipulation within the microfluidic devices.

1.3 Dissertation Outline

This dissertation is organized as follows. Chapter 2 provides the fundamental study of particle motion at a reservoir-microchannel junction under the effects of rDEP. Particle transport, focusing and trapping at the junction and, the parameters affecting them will be demonstrated. The chapter concludes with the discussion of potential applications of the reservoir-microchannel junction for particle separation based on the

differences in their physical properties. In Chapter 3, we utilize the reservoir-microchannel junction to attain size based separation of particles under the application of DC-biased AC voltages. We further investigate the effects of enhanced electroosmotic flow on inter-particle interactions and its effects on the size based separating efficiency of the microfluidic device. Chapter 4 further expands the use of reservoir-microchannel junction to separating particles by charge. We demonstrate separation of same sized particles but having differences of surface charge at the junction. Investigation of effects of enhanced electroosmotic flow and frequency on charge based separation is also studied. The transport, focusing and selective trapping of live and dead yeast cells at the reservoir-microchannel junction under varying DC-biased AC fields and frequency will be demonstrated in chapter 5. In Chapter 6, a stacked microfluidic device to continuously concentrate and separate particles/cells is investigated with the goal to enhance throughput. Chapter 7 presents comparison between two-dimensional and three-dimensional particle focusing and trapping. The electric field gradients in the vertical direction at the reservoir-microchannel junction can be utilized to enhance the dielectrophoretic force which can reduce the external electric field required to trap particles. A three dimensional focusing and trapping of particles to reduce the applied DC-biased AC voltage is proposed. All the experimental results obtained in Chapters 2, 3, 4, 5, 6, and 7 are verified utilizing a numerical model.

The fundamentals of reservoir-based dielectrophoresis are repeated in every chapter to facilitate easier reading of the thesis. Appropriate explanations and modifications are made in accordance to the aim attained in the chapter.

CHAPTER 2: Electrokinetic Motion of Particles at the Reservoir-microchannel Junction

2.1 Introduction

Controlled manipulation of particles and cells is a key requirement for a microfluidic device. With the increased interest in microfluidics several particle manipulation techniques have been proposed. Several microchannel designs and force fields to control the particle manipulations have also been proposed. Particle electrokinetic motion in array of microchannels ranging from straight (Keh, H. J. 1985; Keh, Huan J. 1991; Shugai, A. A. 1999; Yariv, E. 2002; Hsu, J. P. 2004; Xuan, X. 2005; Davison, S. M. 2006; Liu, H. 2007; Unni, H. N. 2007; Hsu, J. P. 2007; Qian, S. 2008; Li, D. 2010; Liang, L. 2010; Liang, L. 2010), curved (Zhu, J. 2009; Church, C. 2009; Ai, Y. 2010; Zhu, J. 2010), constricted (Ai, Y. 2009; Pysher, M. D. 2007; Hawkins, B. G. 2007; Kang, Y. 2008; Jones, P. V. 2011) and methodized (Lapizco-Encinas, B. H. 2004; Xuan, X. 2006; Qian, S. 2006; Zhu, J. 2009) has been extensively studied experimentally and numerically. The studies of particle motion in the above mentioned microchannels have been limited within the microchannel area. Particle motion at the reservoir-microchannel junction has not been paid any particular attention. The applied electric field becomes inherently non-uniform at the reservoir-microchannel junction due to the significant size mismatch between the macro (reservoir) and the micro (microchannel) components of a microfluidic device which can be used to focus, trap and separate particles. Electric field

has been extensively used as an external force field to control and manipulate particles owing to its ease of operation and control. Dielectrophoresis (DEP) is a force generated on application of non-uniform electric field and has become an important tool in microfluidics. Current DEP-based microfluidic separations of particles and cells have been implemented using primarily three approaches. The first approach is electrode-based dielectrophoresis (eDEP), (Gagnon, Z. R. 2011; Cetin, B. 2011; Jesus-Perez, N. M. 2011) where the frequency of AC electric fields imposed upon in-channel microelectrodes is tuned to obtain distinctive dielectrophoretic responses between live and dead cells. The result is a selective retention of one type of particles and cells upon the electrodes while the other type is either washed out by the medium flow (Wang, X. B. 1993; Markx, G. H. 1994; Docoslis, A. 1997; Li, H. 2002; Suehiro, J. 2003; Doh, I. 2005; Urdaneta, M. 2007; Hakoda, M. 2010) or travels itself through a stationary medium in response to a travelling electric field (Talary, M. S. 1996). Such eDEP separation has also been demonstrated in the form a lateral deflection of particles and cells to differential flow paths in the laminar medium stream, which can then be continuously sorted into separate reservoirs (Lewpiriyawong, N. 2011). The second approach to dielectrophoretic separation of particles and cells is insulator-based dielectrophoresis (iDEP), where an array of insulating posts are patterned onto a microchannel wall to periodically vary the externally applied electric field (Srivastava, S. K. 2011; Regtmeier, J. 2011). Due to their dissimilar dielectrophoretic responses, particles or cells can be trapped to different zones (Lapizco-Encinas, B. H. 2004) or only one particle or cell type can be selectively retained by the insulators (Jen, C. P. 2011). The third approach to DEP separation by cell viability

is contactless dielectrophoresis (cDEP), where electrodes are physically isolated from the particle or cell sample and electric field gradients are confined mainly to the smallest gaps between the main and side microchannels (Shafiee, H. 2009). Under the AC electric field of an appropriate frequency, particles and cells can be selectively trapped by positive DEP while other types can pass the trapping zone (Shafiee, H. 2010).

We develop a new dielectrophoretic approach to manipulate particles and cells at the reservoir-microchannel junction which can be utilized to manipulate, selectively concentrate and, separate particles in a lab-on-a-chip device. The approach uses inherent electric field gradients formed at the junction, eliminating the requirement of mechanical or electrical components inside the microchannel. In this chapter, we perform an experimental and numerical study of electrokinetic particle motion at the reservoir-microchannel junction. On application of external electric fields (both AC and DC), the polystyrene micro-particles are deflected away from the corners at the junction towards the centerline of the microchannel under the influence of negative dielectrophoretic force. We perform a fundamental study, to understand the effects of AC electric field, DC electric field and particle size on the electrokinetic motion of particles passing through the reservoir-microchannel junction. We herein also define a trapping number and a focusing number which facilitates in identifying the parameters that affects the trapping and focusing of particles at the junction.

2.2 Experiment

2.2.1 Microfluidic Device Fabrication

The microchannel was fabricated with polydimethylsiloxane (PDMS) using the standard soft lithography technique. Specifically, photoresist (SU 8-25, MicroChem, Newton, MA) was dispensed onto a clean glass slide, which was made to spin at an angular velocity of 2000 RPM (WS-400-NPP-Lite, laurel Technologies, North Wales, PA). The resulting 25 μm thick photoresist film was soft baked on a digital hotplate (HP30A, Torrey Pines Scientific, San Marcos, CA) in two steps at 65°C for 3 min and 95°C for 7 min. It was then exposed to near UV light (ABM, San Jose, CA) through a negative photo mask with the printed microchannel pattern (CAD/Art Services, Bandon, OR). Following a two-step hard bake at 65°C for 1 min and 95°C for 3 min, the cured photoresist was developed in SU-8 developer solution (MicroChem, Newton, MA) for 4 min, the result of which was a positive replica of the microchannel on the glass slide. After a brief rinse with isopropyl alcohol (Fisher Scientific, Pittsburg, PA) and a final hard bake at 150°C for 5 min, the photoresist was ready for use as the mold of the microchannel.

Next, a mixture of 10:1 mass ratio of the pre-polymer and curing agent of PDMS (Sylgard 184 Silicon Elastomer) was mixed thoroughly and poured over the channel mold. After a 30-min degassing in an iso-temp vacuum oven (13-262-280 A, Fisher Scientific, Fair Lawn, NJ), liquid PDMS was cured at 70°C in a gravity convection oven

(13-246-506GA, Fisher Scientific) for 2 hours. The microchannel structure was cut using a scalpel and peeled off from the mold. Two holes were punched through the PDMS slab inside the originally designed circled at the channel ends, which acted as the reservoir in the experiments. The channel side of the PDMS was then plasma treated (PDC-32 G, Harrick Scientific, Ossining, NY) for 1 min along with a clean glass slide. Finally, the two treated surfaces were bonded together to form the microchannel.

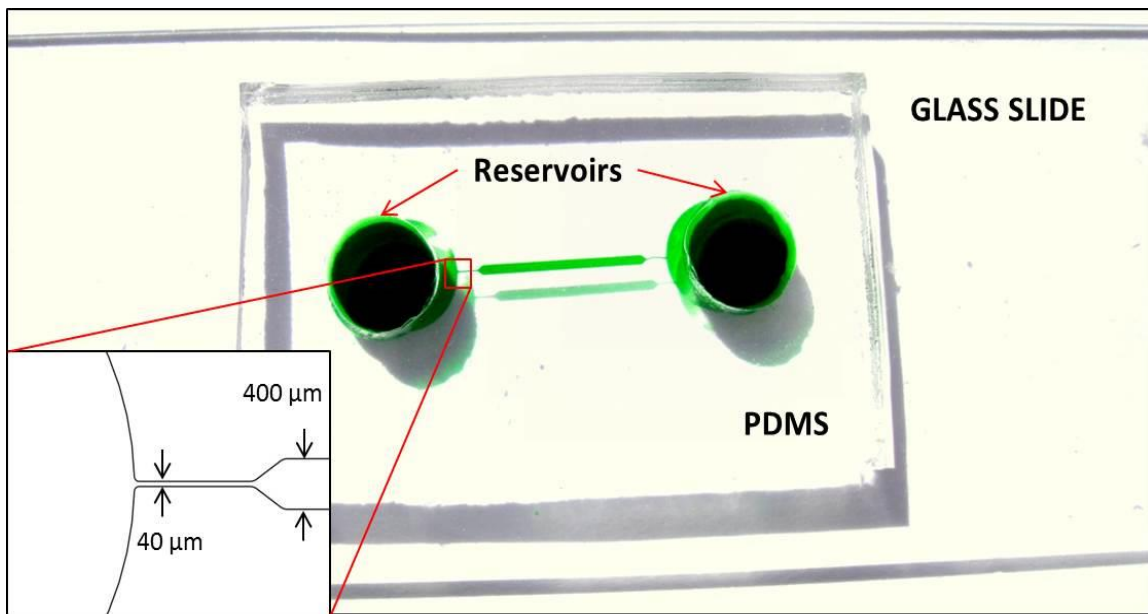


Figure 4: Picture of a PDMS-based microfluidic device used in the experiment (green food dye used for clarity). The inset displays a schematic view of the reservoir-microchannel junction with actual dimensions. The block arrow indicates the particle moving direction in the experiments.

The fabricated PDMS-glass microfluidic device is shown in figure 4. It is composed of a 1.2 cm long straight microchannel with a 5 mm-diameter reservoir at each end. The channel is 400 μm wide and has a constriction section of 40 μm with 1 mm length at the reservoir-microchannel junctions (refer to figure 4). The channel is

uniformly 25 μm in depth. These constrictions are designed for the purpose of reducing the applied electric voltage as the local electric field can be amplified.

2.2.2 Particle Solution Preparation

Polystyrene particles of 3, 5, and, 10 μm in diameter (Sigma-Aldrich, St. Louis, MO, USA) were re-suspended in 1mM phosphate buffer with a concentration of 10^6 - 10^7 particles per milliliter to form three different particle solutions. Tween 20 (0.1% v/v, Fisher Scientific) was added to the particle solution to suppress particle adhesions to channel walls as well as particle aggregations. The particle solutions were mixed in a vortex generator prior to their use in the experiment, to ensure uniform distribution of particles.

2.2.3 Particle Manipulation and Visualization

The microchannel and its reservoirs were primed with the particle-free 1 mM phosphate buffer for 10 min. At the beginning of a separation experiment, the buffer solution in the inlet reservoir was vacated using a pipette and replaced with the respective particle mixture solution. Pressure driven flow was minimized by carefully balancing the liquid heights in the two reservoirs prior to each experiment. The reservoirs were made large with 5 mm in diameter and 3-4 mm in depth in order to minimize the back flow during the course of the experiment. The electrokinetic manipulation of the particles in the microfluidic device was attained by imposing DC-biased AC electric fields across the length of the microchannel. The electric fields were supplied by a function generator

(33220A, Agilent Technologies, Santa Clara, CA, USA) in conjunction with a high voltage amplifier (609E-6, Trek, Medina, NY, USA). The frequency of the AC field was fixed at 1 kHz in all the experiments. Particle motion was monitored using an inverted microscope (Nikon Eclipse TE2000U, Nikon Instruments, Lewisville, TX, USA), through which videos and images at the reservoir-microchannel junction were recorded using a CCD camera (Nikon DS-Qi1Mc).

2.3 Theory

2.3.1 Mechanism

The electric field becomes inherently non-uniform at the reservoir microchannel junction (see figure 5, the darker color, the larger the magnitude) due to the large size mismatch between the reservoir and the microchannel. Particles experience a negative DEP force, F_{DEP} , which induces a dielectrophoretic motion, U_{DEP} , when moving electrokinetically from the reservoir to the microchannel as shown in figure 5. The time averaged U_{DEP} of an isolated spherical particle using the dipole moment approximation under DC and low-frequency (<100 kHz) AC electric field is given by (Morgan, H. 2002; Jones, T. 1995);

$$\mathbf{U}_{DEP} = \frac{\epsilon_f r^2}{3\eta_f} f_{CM} \nabla^2 \mathbf{E} \quad (2-1)$$

$$f_{CM} = \frac{\sigma_p - \sigma_f}{\sigma_p + 2\sigma_f} \quad (2-2)$$

Where r is the particle diameter, ϵ_f is the fluid permittivity; f_{CM} is the Clausius-Mossotti factor, η_f is the fluid dynamic viscosity, E is the local electric field, σ_p and σ_f are the electric conductivities of the particle, and the fluid, respectively. Polystyrene particles (Ermolina, I. 2005) and biological cells (Voldman, J. 2006) often appear poorly conducting in DC and low-frequency AC fields, one can have $\sigma_p < \sigma_f$, and thus f_{CM} is negative, resulting into negative DEP (Jones, T. 1995). Therefore, the F_{DEP} and the resulting U_{DEP} are directed towards the lower electric field region as indicated by the particle velocity in figure 5.

The resulting particle velocity U , is the vector addition of the DC electrokinetic motion (combination of fluid Electroosmosis and particle Electrophoresis), U_{EK} , and the AC/DC dielectrophoretic velocity, U_{DEP} :

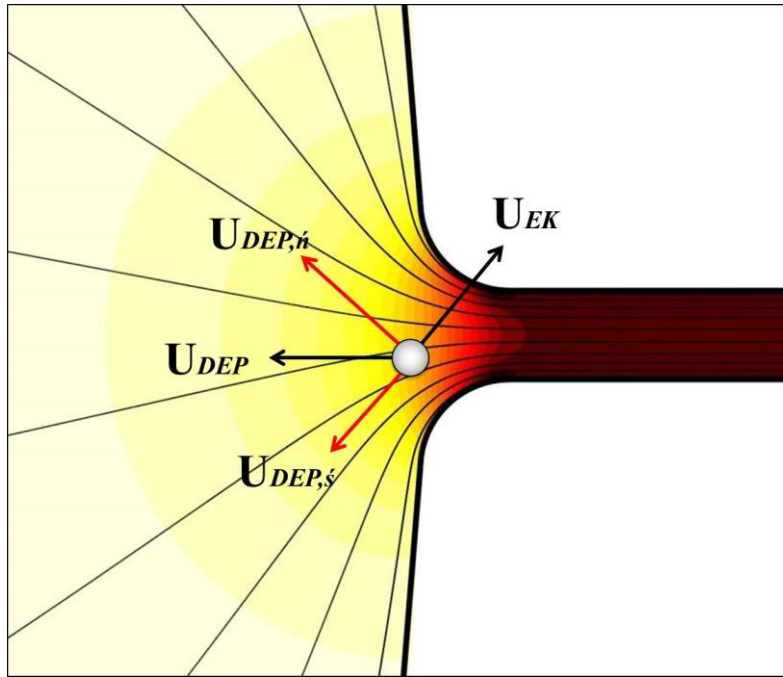


Figure 5: Illustration of rDEP for particles focusing and trapping at the reservoir-microchannel junction. The image also illustrates electric field lines and electric field contour (background color, the darker the higher electric field).

$$\mathbf{U} = \mathbf{U}_{EK} + \mathbf{U}_{DEP} = \mu_{EK} \mathbf{E}_{DC} + \mu_{DEP} \nabla^2 \mathbf{E} \quad (2-3)$$

$$\mu_{EK} = \frac{\varepsilon_f (\zeta_p - \zeta_w)}{\eta_f} \quad (2-4)$$

$$\mu_{DEP} = \frac{\varepsilon_f r^2 f_{CM}}{3\eta_f} \quad (2-5)$$

where μ_{EK} is the particle electrokinetic mobility, \mathbf{E}_{DC} is the DC component of the applied DC-biased AC electric field, μ_{DEP} is the particle dielectrophoretic mobility, ζ_p is the particle zeta potential, and ζ_w is the wall zeta potential. The electrokinetic velocity, \mathbf{U}_{EK} , is parallel to the electric field lines and hence stream-wise as flow field is similar to electric field lines in electrokinetics. However, the \mathbf{U}_{DEP} , exhibits a component along both the stream-wise and cross-stream-wise directions as illustrated in figure 5.

Polystyrene particles experience negative DEP (i.e., $\mu_{DEP} < 0$), $U_{DEP,n}$ is directed towards the centerline of the microchannel as illustrated in figure 5, which produces a focusing effect on the suspended particles at the reservoir-microchannel junction (Zhu, J. 2012). $U_{DEP,s}$, the other component exhibited by rDEP acts against the U_{EK} and slows down the particle motion at the reservoir-microchannel junction. Additionally, since $U_{DEP,s}$ is proportional to square of the total electric field, while U_{EK} is linearly proportional to only the DC field component, \mathbf{E}_{DC} , one can expect $U_{DEP,s}$ to counter-balance U_{EK} at large electric fields, i.e.,

$$\mu_{EK} E_{DC} + \mu_{DEP} \frac{\partial E^2}{\partial s} \leq 0 \text{ or } \frac{\mu_{EK}}{-\mu_{DEP}} \leq 2(1 + \alpha^2) \frac{\partial E_{DC}}{\partial s} \quad (2-1)$$

where α is the AC to DC field ratio, i.e., $E = E_{DC} + E_{AC} = E_{DC} (1 + \alpha)$. When this happens particles can be stagnated and concentrated at the reservoir-microchannel junction (Zhu, J. 2012). Such rDEP trapping is dependent on the electrokinetic to dielectrophoretic particle mobility ratio,

$$\frac{\mu_{EK}}{-\mu_{DEP}} = \frac{3}{2} \frac{(\zeta_p - \zeta_w)}{r^2 f_{CM}} \quad (2-2)$$

which is function of particle size (r) and charge (ζ_p). Particles or cells with distinct extrinsic or intrinsic properties have different mobility ratios, thus we can potentially concentrate one type of particles in the upstream reservoir while the other type can flow through the microchannel and be concentrated in the downstream reservoir.

2.3.2 Trapping and Focusing Number

As shown in figure 5, trapping occurs when the stream-wise dielectrophoretic particle velocity, $U_{DEP,s}$, balances particle motion due to the stream-wise electrokinetic velocity of the particle, U_{EK} ($\eta_T \geq 1$). If particle motion is only considered along the streamline (i.e. analogous to the electric field lines illustrated in figure 5), we can define a trapping number as the ratio of the two velocities. Therefore, the trapping number, η_T , can be expressed as,

$$\eta_T = \frac{\mu_{DEP} \frac{\partial E^2}{\partial S}}{\mu_{EK} E_{DC}} \quad (2-8)$$

In the above equation we know that $E = E_{DC}(1 + \alpha)$, where α is the AC to DC electric field ratio. Also, for a channel having length L , constriction width W and an external applied DC voltage V_{DC} , we can approximate the average DC electric field, E_{DC} , to be V_{DC} / L . Similarly $\partial E^2 / \partial S$ in the trapping number expression can be approximated as E^2 / W , the term increases with the increase in electric field and decrease in the constriction width W . Replacing the expressions in Eq. (2-8) and simplifying, the expression for trapping number reduces to;

$$\eta_T = \frac{d^2 \cdot f_{CM} \cdot V_{DC} \cdot (1 + \alpha^2)}{(\zeta_p - \zeta_w) \cdot L \cdot W} \quad (2-9)$$

The trapping of particles at the reservoir-microchannel junction is governed by particle size, d , the Clausius-Mossotti factor, f_{CM} , which is a function of particle and buffer solution conductivity and, permittivity, the applied average DC electric field, V_{DC} / L , the AC to DC electric field ratio, α , the constriction width, W , and the particle and wall zeta potential difference, $\zeta_p - \zeta_w$, which governs the electrokinetic motion of particles. Based on the trapping number, η_T , define above, particles attributing differences in size, conductivity or zeta potential will generate dissimilar response at the reservoir-microchannel junction and can be potentially separated from each other.

Similarly, we can also define a focusing number, η_F , as the ratio of the cross-stream dielectrophoretic particle velocity, $U_{DEP,n}$, normal to the streamline and the vector addition of the stream-wise dielectrophoretic particle velocity, $U_{DEP,s}$, and electrokinetic particle velocity, U_{EK} . The focusing number can then be defined as,

$$\eta_F = \frac{\mu_{DEP} \frac{E^2}{R}}{\mu_{EK} E_{DC} + \mu_{DEP} \frac{\partial E^2}{\partial S}} \quad (2-10)$$

where, R is the radius of curvature. Using the approximations discussed above and simplifying Eq. (2-10), the focusing number can be reduces to,

$$\eta_F \approx \frac{\left[\frac{1}{R} \right]}{\left[\frac{1}{W} + \frac{(\zeta_p - \zeta_w) \cdot L}{d^2 \cdot f_{CM} \cdot V_{DC} \cdot (1 + \alpha^2)} \right]} \quad (2-11)$$

As seen from Eq. (2-11), the focusing number is a function of radius of curvature, R , the constriction width, W , particle size, d , the Clausius-Mossotti factor, f_{CM} , the applied DC voltage, V_{DC} , the AC to DC electric field ratio, α , and the particle and wall zeta potential difference, $\zeta_p - \zeta_w$.

2.4 Numerical Simulation

We developed a 2D numerical model in COMSOL 3.5a (Burlington, MA) to understand and predict the observed particle electrokinetic motion at the reservoir-microchannel junction in the microchannel. The particle-particle and particle-wall interactions are neglected in the model. The local perturbation of the flow and the electric field due to presence of particles is also neglected, instead a correction factor, λ , is introduced to account for the effects of particle size on the dielectrophoretic velocity. Hence, the particle velocity in Eq. (2-12) is rewritten as

$$\mathbf{U}_p = \mu_{EK} \mathbf{E}_{DC} + \lambda \mu_{DEP} (1 + \alpha^2) \nabla E_{DC}^2 \quad (2-12)$$

Particle trajectory is computed using the particle tracing function (COMSOL 3.5a) which utilizes the modified velocity expression in Eq. (2-12). The microchannel along with the two reservoirs (refer to figure 5) is used as the computational domain. Circle having a 0.5 mm diameter is used to simulate electrodes in each reservoir. The external electric potential is imposed upon these circles. The electrode at the inlet reservoir is imposed with the experimentally applied DC voltage and the outlet reservoir is grounded. The electric conductivity of PDMS and glass being low, the channel walls are assumed electrically non-conducting. The DC electric field, E_{DC} , is obtained by solving the Laplace equation $\nabla^2 \phi = 0$ where ϕ is the DC electric potential.

In numerical simulation, the electrokinetic mobility, μ_{EK} , is determined by experimentally measuring the velocity of individual particles in a straight microchannel

where the DEP effects are negligible. The measured electrokinetic mobility was $3.5 \times 10^{-8} \text{ m}^2 / (\text{V} \cdot \text{s})$ for 3 μm particles and $3.2 \times 10^{-8} \text{ m}^2 / (\text{V} \cdot \text{s})$ for 5 and 10 μm particles. The dielectrophoretic mobility was calculated using Eq. (2-5) with electrical permittivity $\epsilon_f = 6.9 \times 10^{-10} \text{ C} / (\text{v} \cdot \text{m})$ and dynamic viscosity $\eta_f = 1.0 \times 10^{-3} \text{ kg} / (\text{m} \cdot \text{s})$ for pure water at 20°C . The electrical conductivity of polystyrene particles was estimated using $\sigma_p = 4K_s / d$ where $K_s = 1 \text{ nS}$ is the surface conductance. The electrical conductance of the buffer solution (1mM phosphate buffer) was measured to be $200 \mu\text{S} / \text{cm}$. Therefore, the CM factors i.e., f_{CM} for 3, 5 and, 10 μm particles were calculated as -0.45, -0.47 and, -0.49 respectively. The correction factor, λ , used for 3, 5 and, 10 μm particles is 0.8, 0.6 and 0.3 respectively, which is consistent with previous studies (Zhu, J. 2009).

2.5 Results and Discussion

2.5.1 AC Electric Field Effects on Particle Focusing

Experimentally obtained snapshots (top row) and superimposed (middle row) images of 5 μm particles moving through the reservoir-microchannel junction under various DC-biased AC electric fields are shown in figure 6. The applied DC voltage is fixed at 50 V, resulting into an average DC electric field of 50 V/cm and, the AC voltage (RMS) is varied to understand particle electrokinetic motion under various AC to DC voltage ratios, α . Under the application of pure DC voltage (i.e. $\alpha = 0$), 5 μm particles experience pure DC electrokinetic motion and move through the reservoir-microchannel

junction occupying the entire microchannel width as shown in Figure 6(a). The induced negative dielectrophoretic force at the reservoir-microchannel junction is weak resulting into minimal deflection of the particles. However, on application of AC voltage of 200 V (i.e. $\alpha = 4$), 5 μm particles are deflected towards the centerline of the reservoir-microchannel junction which is illustrated in figure 6(b). The electrokinetic velocity, U_{EK} , of the particles is solely a function of applied DC electric field and does not change with the application of AC electric field. On the other hand the dielectrophoretic velocity, U_{DEP} , of the particle is a function of both DC and AC applied electric fields. Increasing the AC voltage induces reservoir-based dielectrophoretic force (rDEP), which deflects the particles towards the center of the microchannel reducing the particle stream width. On further increasing the applied AC voltage, i.e., $\alpha = 8$, the induced rDEP force increases and the particles are further pushed towards the centerline of the channel as seen in figure 6(c). Particles form a single file (pearl chain) and are well focused along the centerline as they move through the reservoir-microchannel junction. When the AC voltage is increased to 550 V (i.e. $\alpha = 11$), particles get trapped inside the reservoir as seen in figure 6(d). The AC voltage of 550 V generates sufficient opposing dielectrophoretic velocity, U_{DEP} , to overcome the electrokinetic velocity, U_{EK} (refer to figure 5) and gets trapped at the reservoir-microchannel junction.

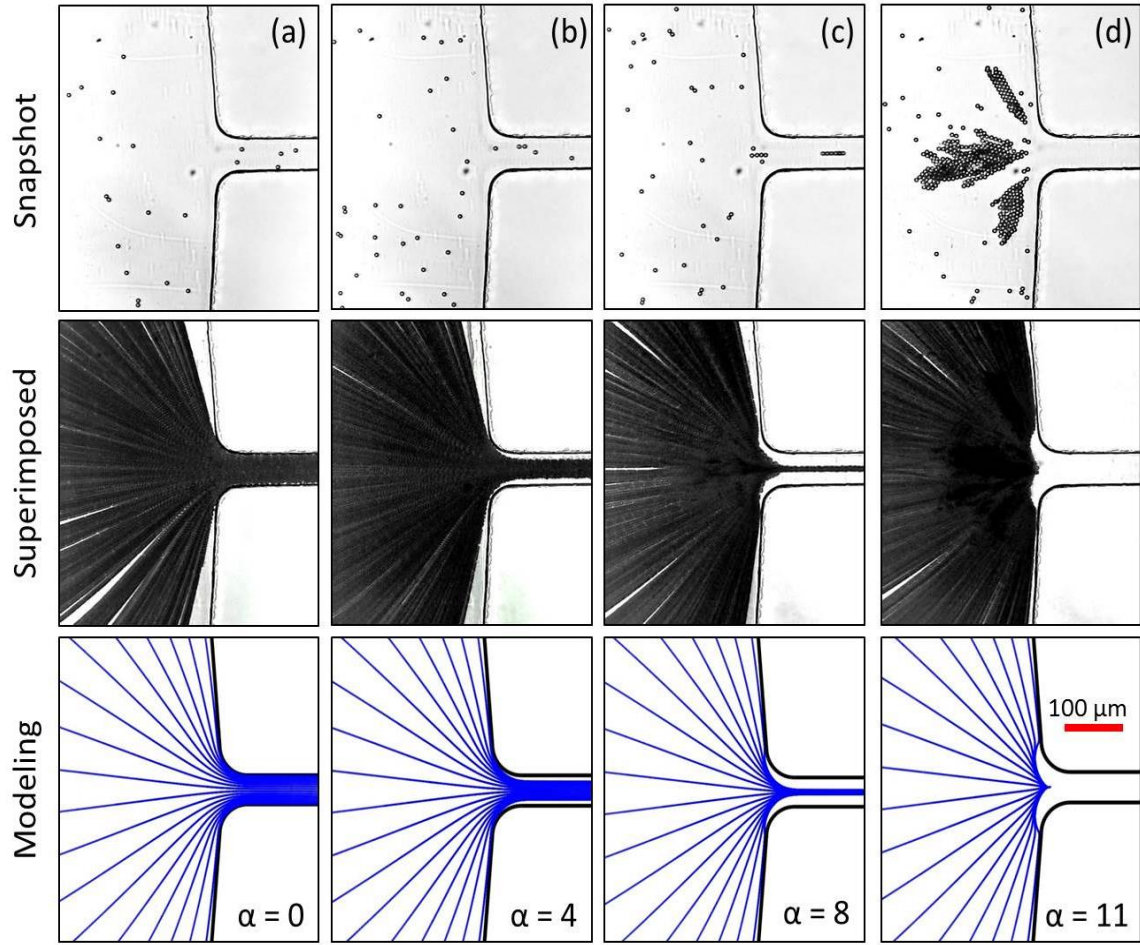


Figure 6: Comparison of experimentally obtained (snapshot and superimposed) and numerically predicted trajectories of 5 μm particles passing through the reservoir-microchannel junction under the influence of rDEP at various DC-biased AC voltages. The DC voltage applied, is fixed at 50 V and the AC (RMS) voltage at 1 kHz frequency is varied from (a) 0 V ($\alpha = 0$) to (b) 200 V ($\alpha = 4$), (c) 400 V ($\alpha = 8$), and (d) 550 V ($\alpha = 11$).

From the results in figure 6, it is apparent that the particle deflection towards the centerline of the microchannel increases with the increase in the applied AC electric field intensity. Figure 6 also shows the comparison between experimentally obtained (top and middle row) and numerically predicted (bottom row) particle trajectories, which agree considerably well in all four cases (6(a) to 6(d)). The agreement between the

experimentally obtained and numerically predicted results validates the numerical model developed. From the focusing number defined in section 2.3.2, we can see that it is a function of AC to DC ratio, α . With the increase in AC voltage the AC to DC ratio, α increases. Application of larger AC fields increases the focusing number corresponding to increased particle focusing which is evident from the experimental and numerical results shown in figure 6 and 7.

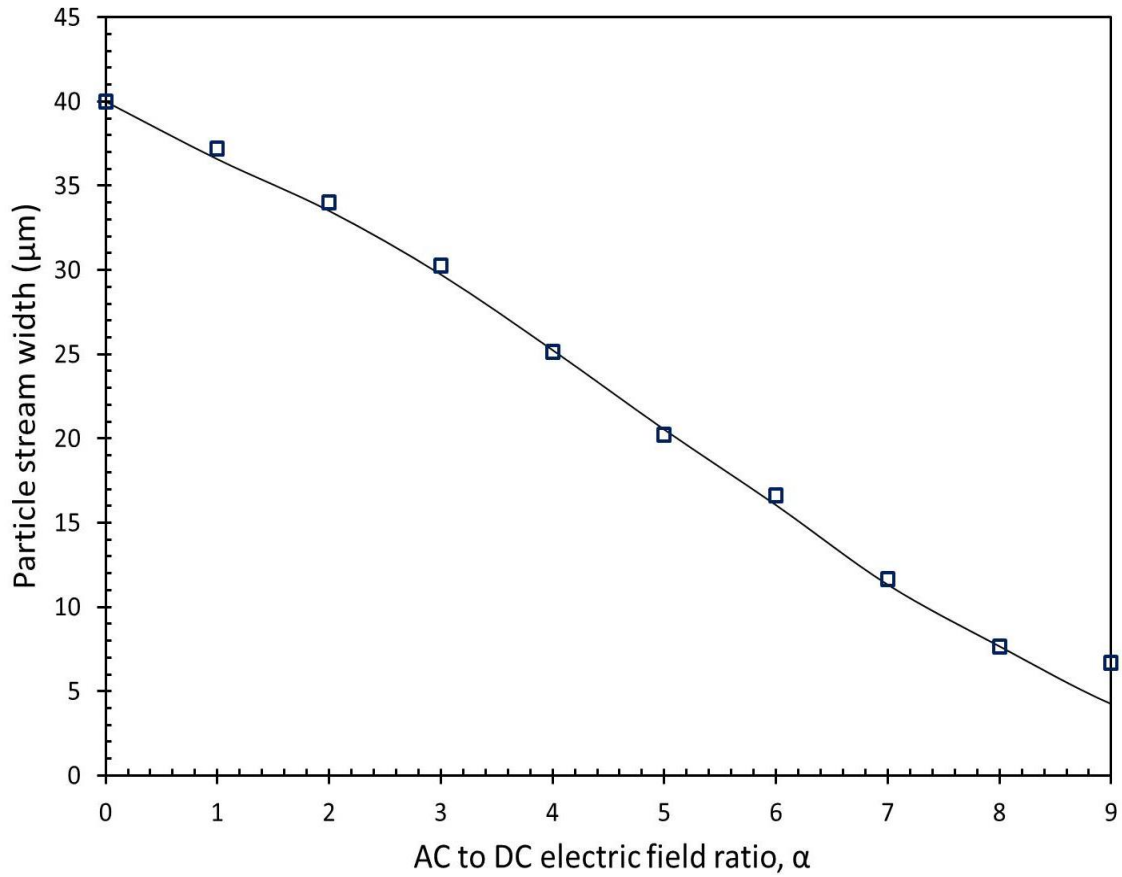


Figure 7: Illustration of experimentally measured and numerically predicted stream width of $5\ \mu\text{m}$ particles passing through the reservoir-microchannel junction under the influence

of rDEP at various DC-biased AC voltages. The DC voltage applied, is fixed at 50 V and the AC (RMS) voltage at 1 kHz frequency is varied.

The 5 μm particle stream width was measured from the experimentally obtained superimposed images at various DC-biased AC electric fields. The measured 5 μm particle stream width was then compared with the numerically predicted particle width, which was extracted from the model. As seen in figure 7, there is a close agreement between the experimentally and numerically obtained widths of the focused particle streams at different DC-biased AC electric fields. Initially the particles are uniformly distributed throughout the microchannel (i.e. Particle stream width is 40 μm at $\alpha = 0$) but gradually get focused under the increasing influence of rDEP force induced with the increase in applied AC voltage.

2.5.2 DC Electric Field Effects on Particle Focusing

Figure 8 shows the experimentally (snapshot and superimposed images) obtained and numerically (modeling images) predicted 5 μm particle trajectories under various DC-biased AC electric fields. In this study the applied AC voltage was fixed at 200 V (RMS) at 1 kHz frequency and the DC voltage was varied from 25 V to 100 V (i.e. $\alpha = 8$ to $\alpha = 2$) to understand particle electrokinetic motion under various DC-biased AC electric fields.

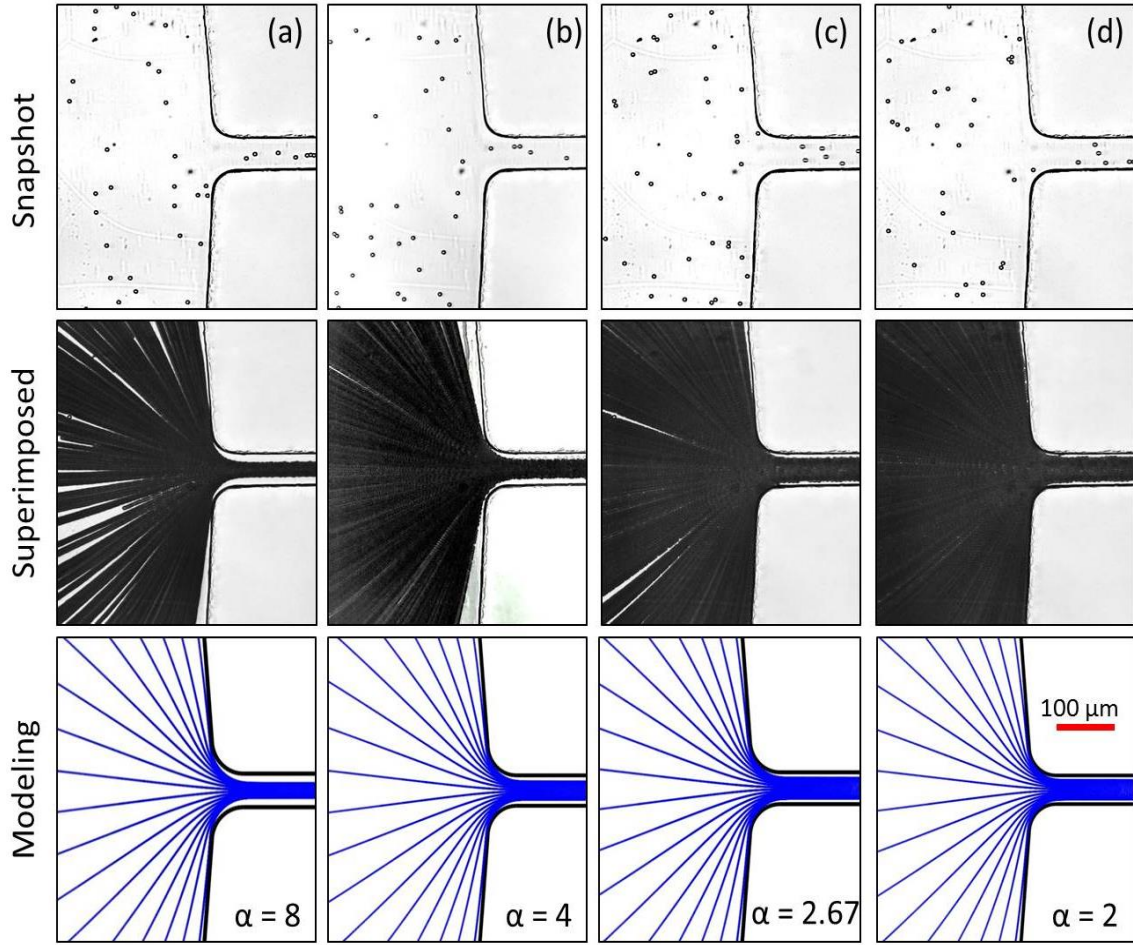


Figure 8: Comparison of experimentally obtained (snapshot and superimposed) and numerically predicted trajectories of 5 μm particles passing through the reservoir-microchannel junction under the influence of rDEP at various DC-biased AC voltages. The AC (RMS) voltage applied at 1 kHz frequency, is fixed at 200 V and the DC voltage is varied from (a) 25 V ($\alpha = 8$) to (b) 50 V ($\alpha = 4$), (c) 75 V ($\alpha = 2.67$), and (d) 100 V ($\alpha = 2$).

At DC voltage of 25 V (i.e. $\alpha = 8$) as seen in figure 8(a) the 5 μm particles move away from the corners of the junctions towards the centerline forming a narrower particle stream compared to the microchannel width. However, when the magnitude of the applied DC voltage is increased the particle stream width also increases as seen in figure 8(b) to 8(d). With the increase in the DC electric field the electrokinetic velocity, U_{EK} , of

the particles also increases and particles move faster through the reservoir-microchannel junction compared to the lower DC electric fields. The duration for which the particles experience rDEP force at the reservoir-microchannel junction under the influence of applied DC-biased AC voltage reduces with the increase in particle electrokinetic velocity. Due to this the focusing width of the particles moving through the reservoir-microchannel junction increases, decreasing the focusing performance.

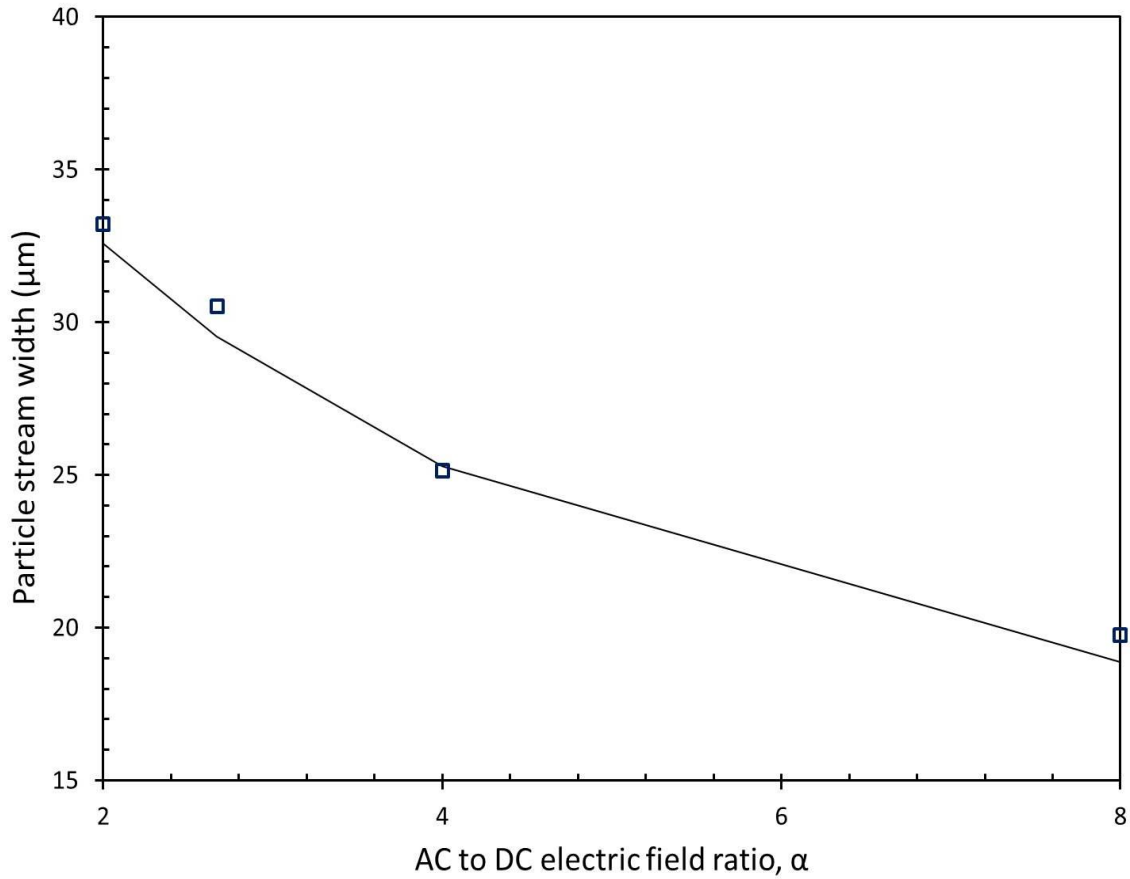


Figure 9: Illustration of experimentally measured and numerically predicted stream width of 5 μm particles passing through the reservoir-microchannel junction under the influence of rDEP at various DC-biased AC voltages. The AC (RMS) voltage applied at 1 kHz frequency is fixed at 200 V and the DC voltage is varied.

Similar to section 2.5.1, the experimentally measured 5 μm particle stream width was compared with the numerically predicted particle width, which was extracted from the model. As seen in figure 9, there is a reasonable agreement between the experimentally and numerically obtained widths of the focused particle streams at different DC-biased AC electric fields. Initially under the application of 25 V DC and 200 V AC, the particles are focused towards the centerline of the microchannel but with the gradual increase in the magnitude of applied DC voltage the particle stream width also increases.

2.5.3 Particle Size Effects on Particle Focusing

As shown in figure 10, particle deflection from the corners of the junction increases with the increase in the particle size under the influence of same applied DC-biased AC electric field. The increase in particle deflection towards the centerline with the increase in particle size can be attributed to the direct dependence of rDEP force on the volume of the particle as illustrated in Eq. (2-1).

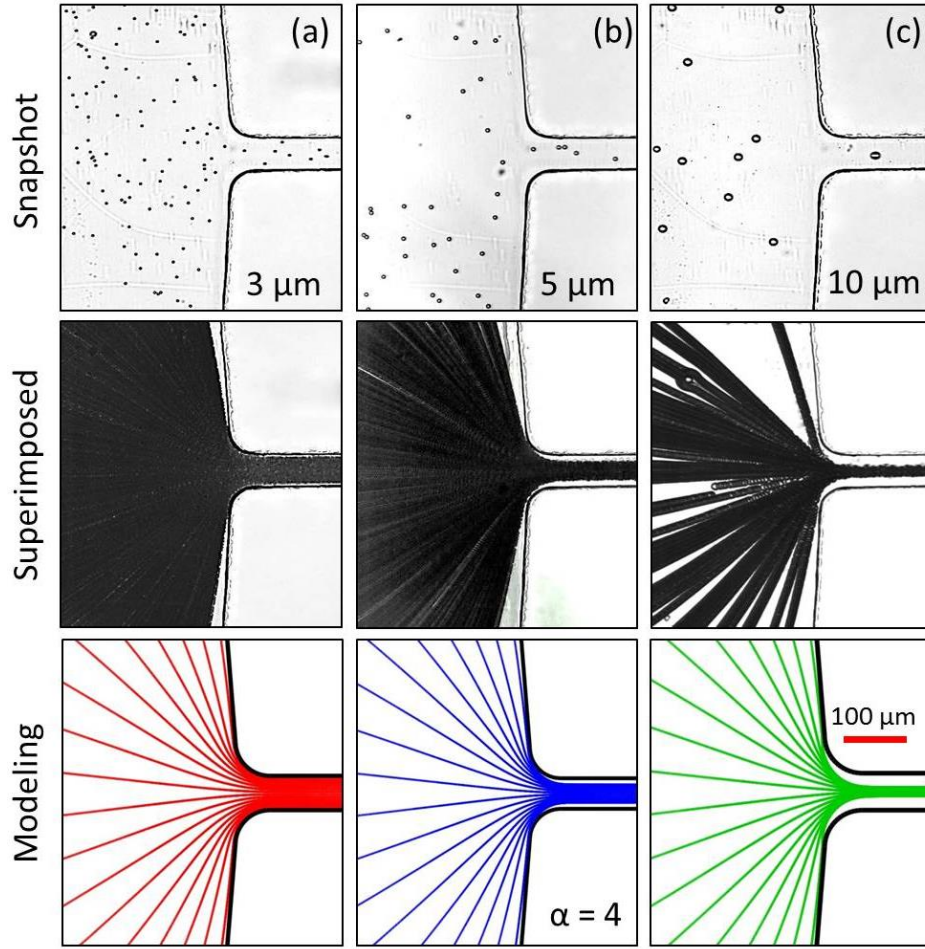


Figure 10: Comparison of experimentally obtained (snapshot and superimposed) and numerically predicted trajectories of 3, 5 and, 10 μm particles passing through the reservoir-microchannel junction under the influence of rDEP at DC-biased AC voltage of 50 V DC and 200 V AC ($\alpha = 4$).

The rDEP force experienced by the 10 μm particles is much larger compared to that of 3 and 5 μm particles due to its large volume, therefore the 10 μm particles observe the largest deflection from the corners of the junction towards the centerline of the microchannel. The observed stream width of 10 μm particles is the smallest compared to the other smaller particle sizes. The deflection of 5 μm particles is also larger compared to the 3 μm particles under the influence of same DC-biased AC electric fields and the

later show the least deflection and thus the maximum stream width. The above demonstrated dissimilar responses of different particle sizes at the reservoir-microchannel junction can be utilized to selectively concentrate and separate particles by size inside the reservoir.

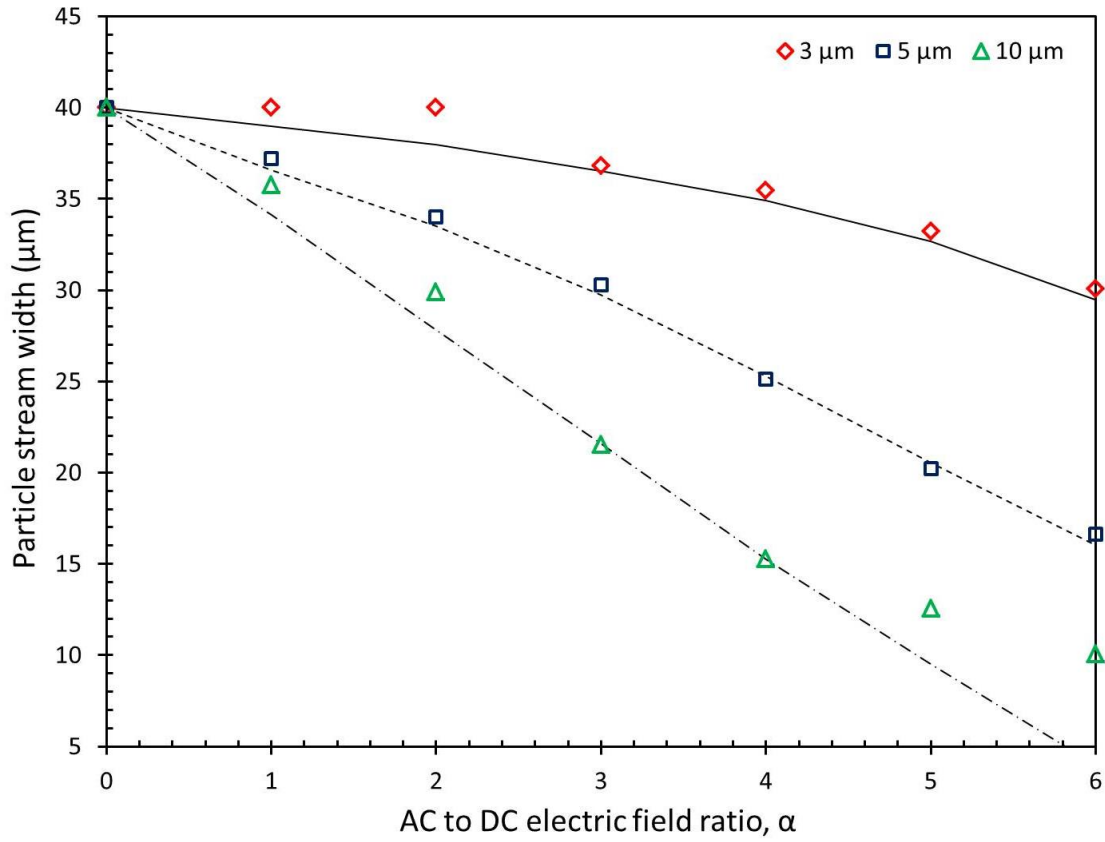


Figure 11: Illustration of experimentally measured and numerically predicted stream width of 3, 5 and, 10 μm particles passing through the reservoir-microchannel junction under the influence of rDEP at various DC-biased AC voltages. The DC voltage applied, is fixed at 50 V and the AC (RMS) voltage at 1 kHz frequency is varied.

Figure 11 shows the comparison of experimentally measured and numerically predicted particle stream width for 3, 5, and, 10 μm particles under the influence of

various DC-biased AC voltages and using the method described in section 2.5.1. It is evident from figure 11 and section 2.5.1, that the particle stream width decreases with the increase in AC to DC ratio, α . However, particles of different sizes experience dissimilar deflection and larger particles are deflected more from the corners of the junction allowing them to focus at lower DC-biased AC voltages compared to their smaller counterparts. 10 μm particles are well focused at a lower AC to DC ratio (i.e. $\alpha = 6$), whereas 5 and 3 μm particles exhibit larger stream width as the magnitude of rDEP force experienced by the smaller particle is lower. From the focusing number defined in section 2.3.2, we can see that it is a function of particle size, d . With the increase in particle size the focusing number also increases corresponding to increased particle focusing which is evident from the experimental and numerical results shown in figure 10 and 11.

2.5.4 Particle Trapping and Concentration

Figure 12 shows the comparison of experimentally obtained (snapshot and superimposed) and numerically predicted trajectories of 3, 5 and 10 μm particles trapped at the reservoir-microchannel junction under the influence of rDEP at various DC-biased AC voltages. The three different sizes of particles are trapped at different DC-biased AC fields. When the stream-wise dielectrophoretic velocity counteracts the electrokinetic velocity particles are trapped at the reservoir microchannel junction. The 3 μm particles as shown in figure 12(a), are trapped at the junction on application of 50 V DC and 975 V AC ($\alpha = 19.5$) whereas the 5 (figure 12(b)) and 10 (Figure 12(c)) μm particles are trapped at 50 V DC and 550 V AC ($\alpha = 11$), and 50 V DC and 400 V AC ($\alpha = 8$) respectively.

The dielectrophoretic force responsible for slowing down of particles and eventually trapping them at the junction is a function of size. Consequently, the 3 μm particles require a relatively larger AC to DC voltage ratio, α , compared to 5 and 10 μm particles. With the increase in size of the particles the DEP force experienced by them at the junction also increases, evident from the lower AC to DC ratio required for trapping of larger particles compared to the smaller counterparts. The numerical modeling results also qualitatively agree with the experimental results in Figure 12. The size dependence of dielectrophoretic force can be utilized to separate particles from a mixture. Potentially, we can apply specific electric field that can trap larger particles in a mixture whereas the smaller ones can pass through the junction into the outlet reservoir resulting into continuous size based separation and concentration of particles.

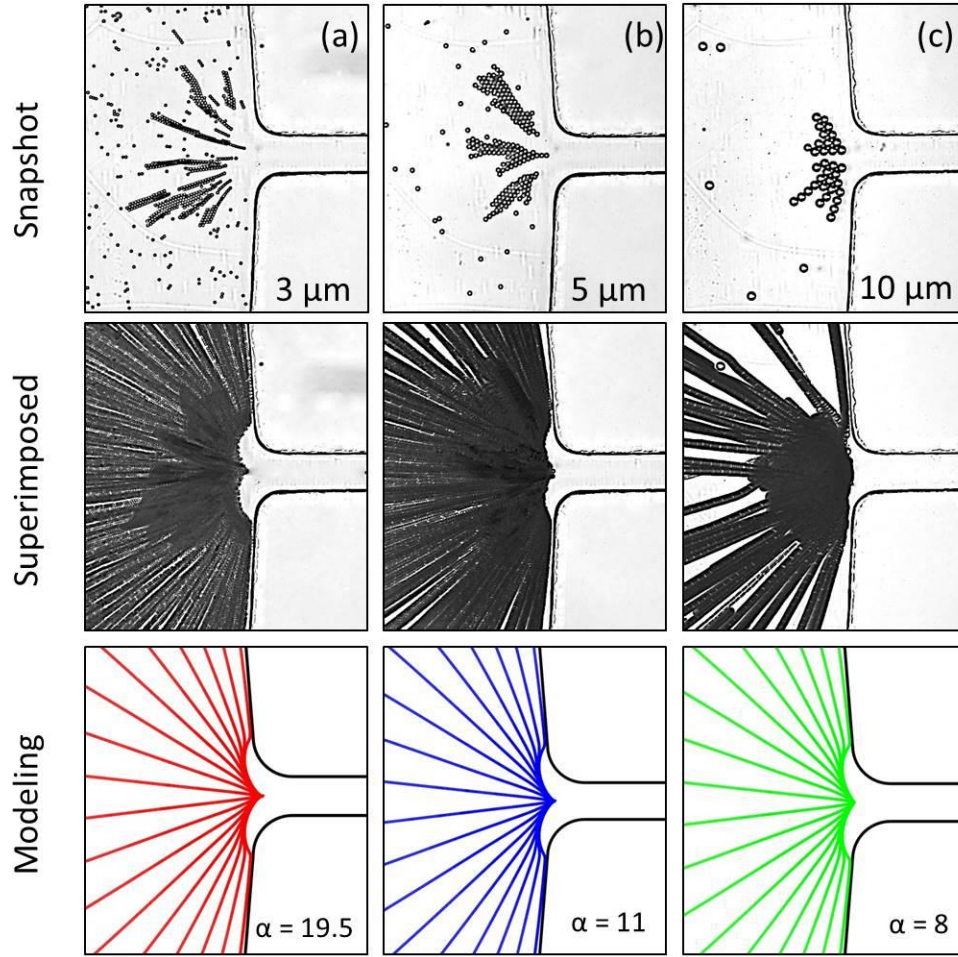


Figure 12: Comparison of experimentally obtained (snapshot and superimposed) and numerically predicted trajectories of 3, 5 and 10 μm particles trapped at the reservoir-microchannel junction under the influence of rDEP at various DC-biased AC voltages. The DC voltage applied is fixed at 50 V and the AC (RMS) voltage applied to trap the particles at 1 kHz frequency, is (a) 975 V ($\alpha = 19.5$) to (b) 550 V ($\alpha = 11$), and (c) 400 V ($\alpha = 8$).

The trapping number is the ratio of stream-wise dielectrophoretic velocity component to electrophoretic velocity and can be used to understand the parameters that affect trapping. The trapping number increases with the increase in particle size. Particles that are larger in size have larger trapping number associated with them and can be trapped easily. From the experimental and numerical results shown in figure 12, larger

particles are trapped at a lower AC to DC voltage ratio, α . The electric field magnitude required to trap larger particles is smaller compared to the smaller particles which is consistent with the trapping number analysis.

2.6 Summary

We have, in this chapter demonstrated the electrokinetic particle motion through the reservoir-microchannel junction under the effects of rDEP force, induced due to the significant size mismatch between the reservoir and the microchannel. A 2D numerical model was also developed using COMSOL 3.5a to simulate the particle motion through the reservoir-microchannel junction, which closely agreed with the experimental results. The experimental and numerical results provides with a potential, to use reservoir-based dielectrophoresis (rDEP) for particle focusing, trapping and sorting in microfluidic devices. The applied electric field becomes inherently non-uniform at the reservoir-microchannel junction due to the significant size mismatch between the macro (reservoir) and the micro (microchannel) components of a microfluidic device. The non-uniform electric field at the reservoir-microchannel junction produces a dielectrophoretic force which induces particle dielectrophoretic motion; we term it as reservoir-based dielectrophoresis (rDEP). Reservoir-based dielectrophoresis differs from traditional methods in that it can be used to manipulate particles completely inside the reservoir, which enables the use of the entire microchannel for other purposes. As miniaturization is an important parameter for lab-on-a-chip devices, integrating such a device can be advantageous. Moreover, the device fabrication and operation is also simple as it does not

require any mechanical or electrical components inside the microchannel. The reservoir-microchannel junction produces inherent non-uniform electric field eliminating the need for fabrication of in-channel microelectrodes. As described in section 2.5.4, the particles can be separated based on the differences they attribute in size, charge, conductivity etc. In the following chapters, we demonstrate the use of reservoir-based dielectrophoresis for continuous particle concentration and separation at the junction.

CHAPTER 3: Particle Separation by Size Using Reservoir-based Dielectrophoresis (rDEP)

3.1 Background on Particle Separation

In the fields of forensics, chemical and biological analysis, biomedical applications etc.; microfluidics has turned out to be a very useful tool and is utilized extensively in separating micron sized species from a mixture. The isolation of different cells from a mixture is one of the fundamental procedures in cell culture, disease diagnostics, and cell therapy or in other clinical areas. In order to reduce power consumption and sample volume utilized for particle separation a number of miniaturized devices have been developed that take advantage of microfluidics. Microfluidic devices generally consume small sample volume and allow for faster operations. For this purpose, electric (Gascoyne, P. R. 2002; Hughes, M. P. 2002; Srivastava, S. K. 2011; Regtmeier, J. 2011), acoustic (Laurell, T. 2007; Friend, J.), optical (Wang, M. M. 2005; Kim, S. B. 2008), magnetic (Pamme, N. 2006; Gijs, M. A. 2010), hydrodynamic (Yamada, M. 2004; Yamada, M. 2005; Yamada, M. 2006; Davis, J. A. 2006; Choi, S. 2007), and inertial (Di Carlo, D. 2009; Kuntaegowdanahalli, S. S. 2009) forces have been widely used to separate particles and these methods can be readily integrated on microfluidic devices (Pamme, N. 2007; Kersaudy-Kerhoas, M. 2008; Tsutsui, H. 2009; Lenshof, A. 2010; Bhagat, A. A. 2010). These separations methods are well developed but require labeling of fluorescent (Fu, A. Y. 1999) or magnetic (Adams, J. D. 2008)

labeling of the targeted or non-targeted particles. Additionally, some of the methods described above also require integration of mechanical moving parts, optical lattice, heaters, micro-pumps etc., which is complex and also difficult to fabricate. Alternate approaches to separate particles in microfluidic devices based on their size is obtained by filtering particles through sieving structures (Yamada, M. 2005) or by differential interaction of particles with local flow profiles (Yamada, M. 2004; Yamada, M. 2004; Yamada, M. 2006). The use of micro-fabricated filters or laminar fluid flow in the above mentioned methods eliminated the use of externally applied force fields, and permitting swift, and efficient particle separation. However, fabrication of micro-filters used in sieving separation is difficult and external pumps for controlling flow rates are required in laminar fluid flow particle separation.

Dielectrophoresis (DEP) is one of the most effective techniques used to separate synthetic as well as biological species. The dependence of DEP force on size and shape of the particles, the magnitude and frequency of the non-uniform electric field, the electrical properties of fluid and particles has been utilized to demonstrate particle manipulation and separation. DEP force in microfluidics has been used to separate micro-particles (Lewpiriyawong, N. 2008; Holmes, D. 2005; Kua, C. H. 2007; Rosenthal, A. 2005; Zhu, J. 2009), yeast cells (Kadaksham, J. 2005), DNA (Parikesit, G. O. 2008), virus (Grom, F. 2006; Docoslis, A. 2007), bacteria (Lapizco-Encinas, B. H. 2004; Yang, L. 2008), red blood cells (Gordon, J. E. 2007; Park, J. 2005) and cancer cells (Kang, Y. 2008). Dielectrophoresis based separation techniques do not require sample modifications, allowing for convenient separation and collection of samples compared to fluorescent or

magnetic marking techniques which requires agent coating to be removed after separation (Wolff, A. 2003; Miltenyi, S. 1990). A number of studies reported in literature utilize electrode-based dielectrophoresis (eDEP). In this type of dielectrophoretic separation high frequency AC electric voltages are imposed on closely spaced microelectrode arrays to produce non-uniform electric fields (Gagnon, Z. R. 2011; Cetin, B. 2011; Jesus-Perez, N. M. 2011). However, microelectrode based DEP systems encounter electrode surface fouling and fabrication of such microfluidic device is complex. An alternate approach to microelectrode based DEP is the Insulator-based dielectrophoresis (iDEP). iDEP eliminates the issues with microelectrode based DEP by using insulating hurdles and posts to locally amplify the electric field and generate non-uniformity (Srivastava, S. K. 2011; Regtmeier, J. 2011). The insulators are made of the microchannel material itself which reduces the fabrication complexity and are less prone to fouling compared to electrodes. Furthermore, external electrical voltage can be applied to the electrodes positioned inside the reservoir at both ends of the channel to create electrokinetic flow rendering the usage of external pumping unnecessary. However, the in-channel micron sized hurdles and posts may cause Joule heating and particle clogging (Kale, A. 2013; Sridharan, S. 2011).

All the methods mentioned above attain non-uniform electric fields with in-channel electrodes or hurdles within the microchannel area. No attention is paid at the reservoir-microchannel junction where the electric field becomes inherently non-uniform due to large size variation between the reservoir and the microchannel. Additionally, separation of particles can be attained inside the reservoir which renders the usage of

microchannel for post analysis. The large volume of fluid inside the reservoir also eliminates the negative effects of Joule heating which is a major concern in iDEP and eDEP devices. We herein propose a new size based particle separation method in microchannels at the reservoir-microchannel junction termed as reservoir-based dielectrophoresis (rDEP). We utilize rDEP to separate 3 μm particles from 10 μm polystyrene particles at the reservoir-microchannel junction. We also utilize rDEP to separate 3 μm particles from 5 μm particles wherein we study the inter-particle interactions affecting the separation efficiency. The effect of enhanced electrokinetic flow on inter-particle interactions during the separation process is studied. The rDEP separation of particles is studied using a combined experimental and numerical analysis.

3.2 Experiment

The microchannel was fabricated with polydimethylsiloxane (PDMS) using the standard soft lithography technique. The detailed procedure is mentioned in chapter 2. The PDMS-glass microfluidic device is composed of a 1 cm-long straight microchannel with a 5 mm-diameter reservoirs at each end. The channel is 400 μm wide and has a constriction section of 40 μm width and 1 mm length at the reservoir microchannel junction. The slab containing the microchannel structure was cut using a scalpel and peeled off. Two holes were punched through the PDMS slab inside the originally designed circles at the channel ends and the center, which served as the reservoirs in experiments. The reservoirs were cut with a diameter of 5 mm and a depth of 3–4 mm, to ensure that their sizes are large enough to minimize the back flow during the course of

experiment. The channel side of the PDMS was then plasma treated (PDC-32 G, Harrick Scientific, Ossining, NY) for 1 min along with a clean glass slide. The two treated surfaces were bonded together to form the glass/PDMS microchannel. Polystyrene particles of 3, 5 and 10 μm in diameter (Sigma-Aldrich, St. Louis, MO) were used to demonstrate the size based separation at the reservoir microchannel junction. The particles were suspended in 1 mM phosphate buffer to a final concentration of 10^6 – 10^7 particles per milliliter. Tween 20 (Fisher Scientific, Waltham, MA, USA) was added to the particle solution at 0.1% v/v to suppress the aggregation of particles and their adhesion to channel walls.

3.3 Theory

Electric field gradients are formed at the reservoir-microchannel junction as the electric field becomes inherently non-uniform due to the size difference between the reservoir and the microchannel. The electric field gradients induce dielectrophoretic force, \mathbf{F}_{DEP} at the reservoir-microchannel junction. The \mathbf{F}_{DEP} force is encountered by the particles when moving electrokinetically from the reservoir to the microchannel as shown in figure 13. The time averaged \mathbf{F}_{DEP} on an isolated spherical particle at low AC field frequency is given by (Morgan, H. 2002)

$$\mathbf{F}_{\text{DEP}} = \frac{1}{2} \pi \epsilon_f d^3 f_{\text{CM}} (\mathbf{E} \cdot \nabla \mathbf{E}) \quad (3-1)$$

$$f_{\text{CM}} = \frac{\sigma_p - \sigma_m}{\sigma_p + 2\sigma_m} \quad (3-2)$$

where d is the particle diameter, ω is the medium permittivity and f_{CM} is the Clausius-Mossotti (CM) factor. The Clausius-Mossotti (CM) factor for DC biased low frequency AC electric field is given by Eq. (3-2) with σ_p and σ_m being the particle and medium conductivities respectively. Particles experience poor conductivity in DC and low-frequency AC fields, consequently $\sigma_p < \sigma_m$, and thus f_{CM} (Clausius-Mossotti factor) is negative, resulting into negative DEP (Jones, T. 1995). Particles experiencing negative DEP force, \mathbf{F}_{DEP} , induce a dielectrophoretic motion, \mathbf{U}_{DEP} , as shown in figure 13.

The resulting particle and cell velocity \mathbf{U} , is the vector addition of the DC electrokinetic motion (combination of fluid electroosmosis and particle electrophoresis), \mathbf{U}_{EK} , and the AC/DC dielectrophoretic velocity, \mathbf{U}_{DEP} :

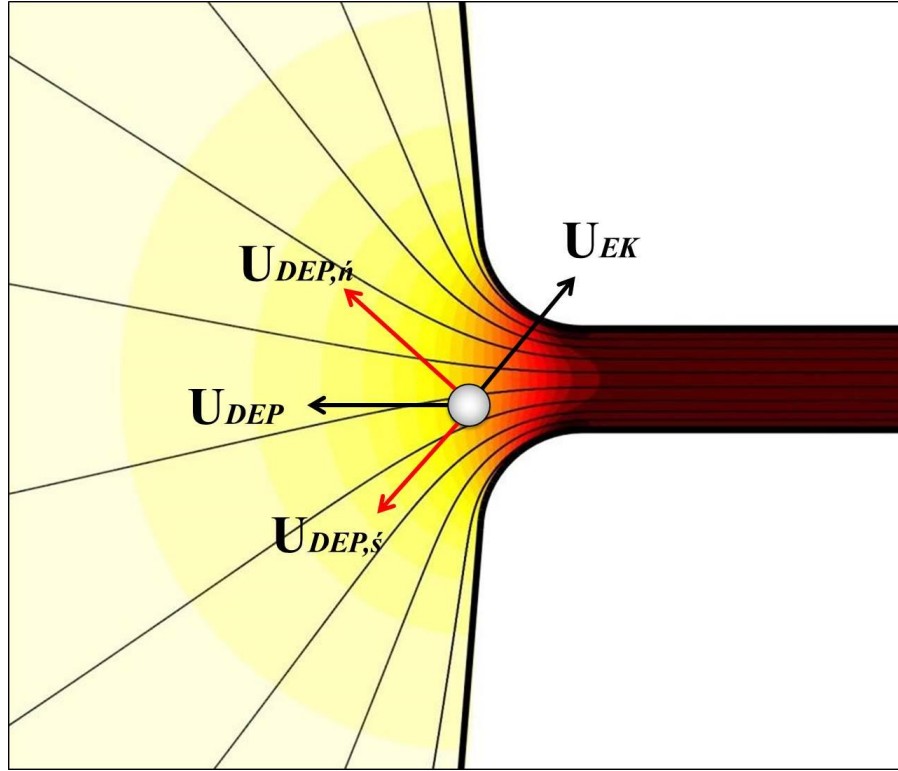


Figure 13: Illustration of rDEP for particles focusing and trapping at the reservoir-microchannel junction. The image also illustrates electric field lines and electric field contour (background color, the darker the higher electric field).

$$\mathbf{U} = \mathbf{U}_{EK} + \mathbf{U}_{DEP} = \mu_{EK} \mathbf{E}_{DC} + \mu_{DEP} \nabla \mathbf{E}^2 \quad (3-3)$$

$$\mu_{EK} = \frac{\varepsilon_f (\zeta_p - \zeta_w)}{\eta_f} \quad (3-4)$$

$$\mu_{DEP} = \frac{\varepsilon_f d^2 f_{CM}}{12\eta_f} \quad (3-5)$$

where μ_{EK} is the electrokinetic particle mobility, \mathbf{E}_{DC} is the DC component of the applied DC-biased AC electric field, μ_{DEP} is the dielectrophoretic particle mobility, ζ_p is the particle zeta potential, and ζ_w is the wall zeta potential.

$U_{DEP,n}$ for particles and cells experiencing negative DEP is directed towards the centerline of the microchannel as shown in figure 13, producing a focusing effect on the particles or cells moving electrokinetically at the reservoir-microchannel junction (Zhu, J. 2012). $U_{DEP,s}$, the stream wise component exhibited by rDEP acts against the U_{EK} and slows down the particle motion at the reservoir-microchannel junction. $U_{DEP,s}$ is proportional to square of the total electric field, whereas U_{EK} is linearly proportional to only the DC field component, E_{DC} . At large electric fields this proportionality difference on the electric field can be utilized to counter-balance U_{EK} with $U_{DEP,s}$, i.e.,

$$\mu_{EK} E_{DC} + \mu_{DEP} \frac{\partial E^2}{\partial s} \leq 0 \text{ or } \frac{\mu_{EK}}{\mu_{DEP}} \leq -2(1 + \alpha^2) \frac{\partial E_{DC}}{\partial s} \quad (3-6)$$

where α is the AC to DC field ratio, i.e., $E = E_{DC} + E_{AC} = E_{DC} (1 + \alpha)$. When the condition in Eq. (3-6) is satisfied particles and cells can be selectively trapped and concentrated at the reservoir-microchannel junction (Zhu, J. 2012). Particle trapping at the reservoir-microchannel junction is governed by the electrokinetic to dielectrophoretic mobility ratio shown in Eq. (3-7)

$$\frac{\mu_{EK}}{\mu_{DEP}} = -\frac{12f_g(\zeta_p - \zeta_w)}{d^2} \frac{\sigma_p + 2\sigma_m}{\sigma_p - \sigma_m} \quad (3-7)$$

Essentially, the particles with lower electrokinetic mobility and higher dielectrophoretic mobility can be trapped at lower AC to DC field ratio, α . The dielectrophoretic mobility

is a function of particle size, d , which indicates that particles with larger size can be trapped at the junction and the smaller sized particles can be swept downstream towards the other reservoir.

3.3.1 Separation Mechanism

As seen from figure 14(a), two particles different in size are moving from the reservoir towards the reservoir-microchannel junction. Both the particles possess almost identical electrokinetic mobility and move at uniformly velocity. The particles encounter small electric field gradients at the corresponding location away from the reservoir-microchannel junction and consequently the stream-wise dielectrophoretic velocity component acting against the electrokinetic velocity is also weak.

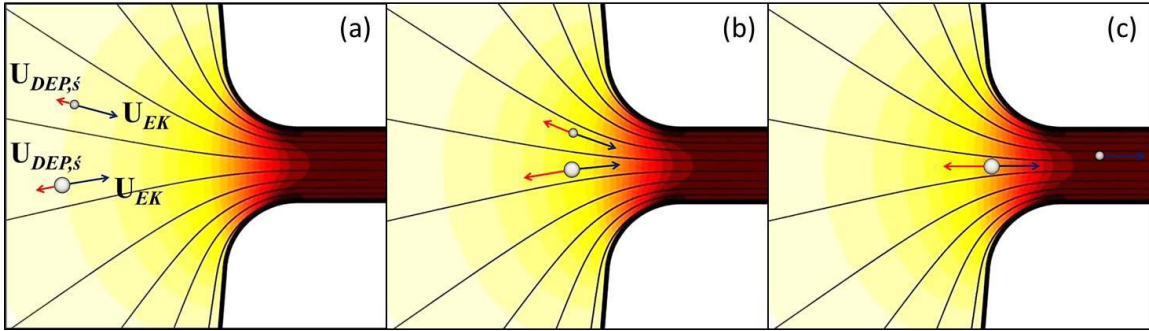


Figure 14: Analysis of electrokinetic and dielectrophoretic velocities of particles undergoing separation at the reservoir microchannel junction. The arrows are proportional to the magnitude of electrokinetic (blue) and dielectrophoretic (red) velocities experienced by particles approaching reservoir-microchannel junction. The electric field lines (black lines) and the contour of electric field (darker the larger) are also illustrated.

As the particles approach the reservoir-microchannel junction seen in figure 14(b), the electrokinetic velocity, which is a linear function of electric field increases.

The electrokinetic velocity increases because of the local amplification of electric field caused by the sudden variation in cross sectional area from the reservoir to the microchannel. Alternately, the stream-wise dielectrophoretic velocity component which is a second-order function of electric field increases sharply. The increased stream-wise dielectrophoretic velocity component counteracts the electrokinetic velocity, slowing down the particles. The dielectrophoretic force inducing the dielectrophoretic velocity is a function of size as well. Therefore, larger particle will experience a larger opposing dielectrophoretic velocity to counter the electrokinetic velocity. Consequently, larger particles at sufficient DC-biased AC voltages will get trapped at the reservoir-microchannel junction and comparatively smaller particles will pass through the junction towards the outlet reservoir. The schematic of particle separation at the reservoir microchannel junction can be seen in figure 14(c). Theoretically, any two particle that attribute differences in the stream-wise dielectrophoretic velocity to electrokinetic velocity ratio can be selectively trapped and separated at the reservoir-microchannel junction.

3.4 Numerical Simulation

The experimental observations are validated by a model numerically solved using commercial finite element package, COMSOL Multiphysics 4.3a (Burlington, MA). Neglecting the effects of the particle on the electric field distribution, the DC electric field distribution $E_{DC} = -\nabla\phi_{DC}$, on the plane of channel length and width is obtained by solving 2D Laplace equation $\nabla^2\phi_{DC} = 0$, for the electric potential with electric insulation

boundary condition on the channel wall, and imposed voltages on the surfaces of the electrodes. With the known electric field the particle velocity is calculated by:

$$\mathbf{U} = \mu_{EK} \mathbf{E}_{DC} + \lambda \mu_{DEP} (1 + \alpha^2) (\mathbf{E}_{DC} \cdot \nabla \mathbf{E}_{DC}) \quad (3-8)$$

The value of λ varies from 0 to 1 and decreases with the increase in particle size. To compute the particle velocity using Eq. (3-8), the electrokinetic mobility, μ_{EK} , was determined by tracking the motion of individual particles in the main body of the microchannel where DEP force is negligible under a small DC field. The measured electrokinetic mobility was $3.5 \times 10^{-8} m^2 / (V \cdot s)$ for 3 μm particles and $3.2 \times 10^{-8} m^2 / (V \cdot s)$ for 5 and 10 μm particles respectively. The dielectrophoretic particle mobility, μ_{DEP} , in Eq. (3-3) was calculated from Eq. (3-4) with the typical dynamic viscosity, $\eta_f = 1.0 \times 10^{-3} kg / (m \cdot s)$ and permittivity $\epsilon_f = 6.9 \times 10^{-10} C / (v \cdot m)$ for pure water at 20 °C. The correction factors for the 3, 5 and 10 μm particles are, respectively, 0.8, 0.6 and 0.4. Particle tracing function within COMSOL 4.3a was utilized to numerically predict the particle separation process. Velocity expression shown in Eq. (3-8) was calculated for the two particles undergoing the separation. Simultaneously plotting the particle trajectories of both the particles at voltage applied during the separation process produced the results which were utilized to demonstrate the numerically predicted separation.

3.5 Results and Discussion

3.5.1 Size-based separation of 3 and 10 μm polystyrene particles using rDEP

Experimentally obtained snapshots (figure 15(a)) and superimposed (figure 15(b)) images of 3 and 10 μm particle separation at the reservoir-microchannel junction under a DC-biased AC electric field of 50 V DC and 400 V AC is shown in figure 15.

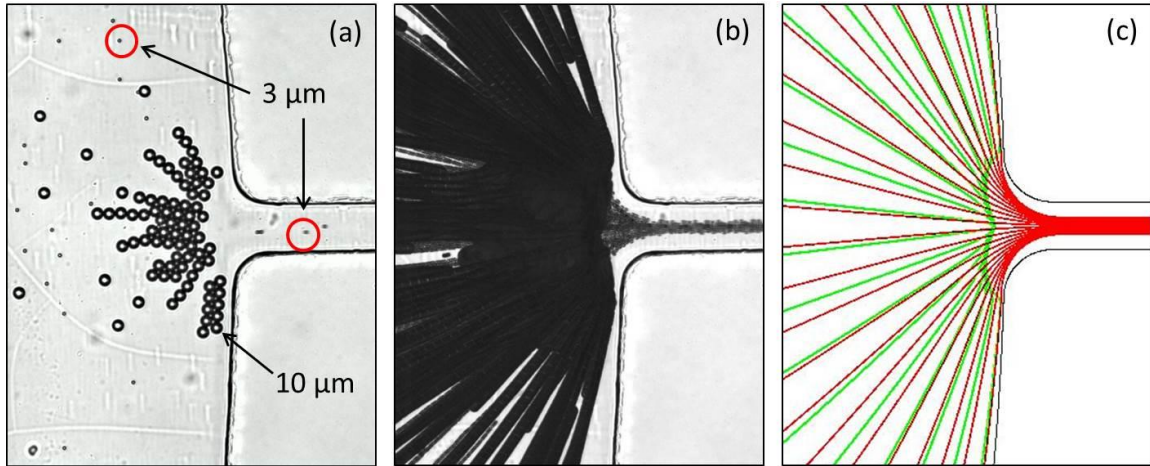


Figure 15: Comparison of experimentally obtained snapshot (a) and superimposed (b) images with numerically predicted trajectories (c) of 3 and 10 μm particle separation at the reservoir-microchannel junction under the influence of rDEP. The DC voltage applied is 50 V and the AC (RMS) voltage applied is 400 V at 1 kHz frequency.

The 3 μm particles are driven through the microchannel by electroosmotic flow, while the 10 μm particles are trapped and form pearl chains within the reservoir near the entrance of the microchannel on application of 50 V DC biased 400 V AC voltages. The two particles have approximately the same electrokinetic mobility, however, 10 μm particles possess a smaller mobility ratio, $\mu_{EK}/(-\mu_{DEP})$, than 3 μm particles indicated by

Eq. (3-7). Therefore, we are able to selectively concentrate 10 μm particles at the reservoir-microchannel junction under the applied DC-biased AC electric field, at which 3 μm particles are too small to be trapped by rDEP and thus swept to the exit reservoir. Since the DEP force is proportional to particle volume, DEP force acting on the 3 μm particles is lower than that on the 10 μm particles, and is not enough to overcome the hydrodynamic force. Therefore, 3 μm particles cannot be trapped by the DEP force at the reservoir-microchannel junction at the applied voltage, and flows through the microchannel towards the downstream reservoirs. In contrast, 10 μm particles are trapped inside the reservoir near the entrance due to sufficiently generated DEP at the applied voltage. Figure 15 clearly shows that we can continuously separate 10 μm particles and 3 μm particles using rDEP. The theoretical predictions of trajectories of 3 and 10 μm particles shown in figure 15(c) shows that the 3 μm particles passes along the centerline of the microchannel towards the downstream, while the large 10 μm particles are trapped inside the reservoir. The theoretical predictions qualitatively agree very closely with the experimental observations. The trapping number associated with 10 μm particles is much larger than 3 μm particles owing to its large size difference, which suggests they can be easily separated. We can see from the experimental analysis the separation efficiency of 3 and 10 μm particles is much higher compared to 3 and 5 μm particles. The inter-particle interaction between the 3 μm particles being swept from the inlet to outlet reservoirs, and 10 μm particles trapped at the reservoir-microchannel junction is low which results into very high separation purity. The low inter-particle interaction can be attributed to a very

large size difference between the 3 and 10 μm particles and, the AC field applied to separate the particles being small.

3.5.2 Size-based separation of 3 and 5 μm polystyrene particles using rDEP

In order to study the separation of polystyrene particles having size differences we studied the separation of 3 and 5 μm size particles at the reservoir-microchannel junction. Experimentally obtained snapshots (top row) and superimposed (middle row) images of 3 and 5 μm particles moving through the reservoir-microchannel junction under various DC-biased AC electric fields is shown in figure 16. The applied DC voltage is fixed at 25 V, resulting into an average DC electric field of 25 V/cm and, the AC voltage (RMS) is varied to understand particle electrokinetic motion under various AC to DC voltage ratios, α . Under the application of pure DC voltage (i.e. $\alpha = 0$), 3 and 5 μm particles experience pure DC electrokinetic motion and move through the reservoir-microchannel junction occupying the entire microchannel width as shown in figure 16(a). The induced negative dielectrophoretic force under pure DC field at the reservoir-microchannel junction is weak resulting into minimal deflection of the particles. However, on application of AC voltage of 450 V (i.e. $\alpha = 18$), 3 and 5 μm particles are deflected towards the centerline of the reservoir-microchannel junction under the effect of negative dielectrophoresis which is illustrated in figure 16(b). The electrokinetic velocity, U_{EK} , of the particles is solely a function of applied DC electric field and does not change with the application of AC electric field.

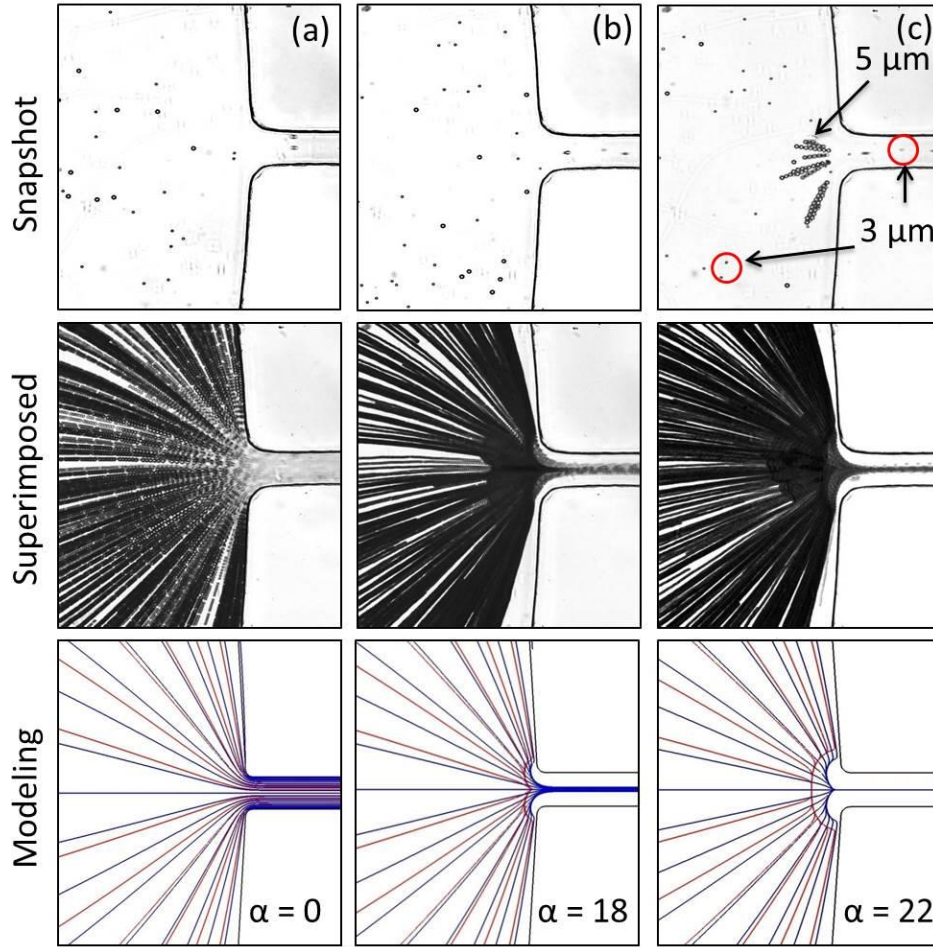


Figure 16: Comparison of experimentally obtained snapshots and superimposed images with numerically predicted trajectories of 3 and 5 μm particle separation at the reservoir-microchannel junction under the influence of rDEP at various DC-biased AC voltages. The DC voltage applied, is fixed at 25 V and the AC (RMS) voltage at 1 kHz frequency is varied from (a) 0 V ($\alpha = 0$) to (b) 450 V ($\alpha = 18$), and (c) 550 V ($\alpha = 22$).

On the other hand the dielectrophoretic velocity, U_{DEP} , of the particle is a function of both DC and AC applied electric fields. Increasing the AC voltage induces stronger dielectrophoretic velocity compared to pure DC voltage without changing the electrokinetic velocity. The normal dielectrophoretic velocity component, $U_{DEP,n}$, gives rise to particle motion normal to the electric field lines, which deflects the particles

towards the center of the microchannel reducing the particle stream width. The DEP force acting on the particles at the reservoir-microchannel junction is a strong function of particle size. A larger particle, which is 5 μm in this particular case, experiences a larger magnitude of DEP force acting on it compared to smaller 3 μm particles. Therefore, the 5 μm particles are deflected more towards the centerline of the microchannel forming a narrower stream compared to the 3 μm particles. When the AC voltage is increased to 550 V (i.e. $\alpha = 22$), 5 μm particles get trapped inside the reservoir as seen in figure 16(c) as the stream-wise component of the dielectrophoretic velocity counteracts to the electrokinetic velocity. The two particles have approximately the same electrokinetic mobility, however, 5 μm particles possess a smaller mobility ratio, $\mu_{EK}/(-\mu_{DEP})$, than 3 μm particles indicated by Eq. (3-7). The AC voltage of 550 V generates sufficient opposing dielectrophoretic velocity, U_{DEP} , to overcome the electrokinetic velocity, U_{EK} of the larger 5 μm particles and they get trapped at the reservoir-microchannel junction. However, for the smaller 3 μm particles dielectrophoretic velocity, U_{DEP} , is not sufficient to overcome the electrokinetic velocity, U_{EK} , and they are swept from the inlet reservoir into the outlet reservoir resulting into continuous particle separation at the reservoir-microchannel junction.

Based on the trapping number, η_T , analysis introduced in Chapter 2 section 2.3.2, particles that are inherently different by size, charge or conductivity possess a different trapping number at the same applied DC-biased AC voltages. Trapping number is essentially the ratio of particle dielectrophoretic velocity in the stream-wise direction to

that of the electrokinetic velocity. The trapping number can be used to better understand the parameters that affect trapping of particles at the reservoir-microchannel junction. The trapping number increases with the increase in particle size, Clausius-Mossotti factor, DC voltage and AC to DC voltage ratio. Trapping number can also be increased by decreasing the particle's electrokinetic mobility, length of the channel and constriction width. Particles in a mixture those are different in size, charge or conductivity properties will possess a different trapping number and can be potentially separated. For size based separation we can see that trapping number is a function of particle diameter. The particle that has a larger diameter tends to attribute a larger trapping number compared to the smaller counterpart. As trapping number corresponding to 5 μm particles is larger than the 3 μm particles, we can trap the 5 μm particles at the reservoir-microchannel junction. Therefore, we are able to selectively concentrate 5 μm particles at the reservoir-microchannel junction under the applied DC-biased AC electric field, at which 3 μm particles are too small to be trapped by rDEP and thus swept to the exit reservoir. The numerical predictions of trajectories of 3 and 5 μm particles shown in figure 16(c) shows that the 3 μm particles passes along the centerline of the microchannel towards the downstream, while the large 5 μm particles are trapped inside the reservoir. The numerical predictions qualitatively agree closely with the experimental observations. However, our numerical model does not account for the inter-particle interactions and its effects on the separation. The model can predict the particle trapping at the reservoir-microchannel junction but does not simulate the behavior of particles after it gets trapped.

The inter-particle interaction between the 3 μm particles being swept from the inlet to outlet reservoirs, and 5 μm particles trapped at the reservoir-microchannel junction is considerably high. We observe that when sufficient numbers of 5 μm particles are trapped, the 3 μm particles under the effect of inter-particle force start getting trapped along with the 5 μm particles. We attribute these interactions to the disturbance in the local electric field due to the trapped particles which considerably enhances the rDEP force. These interactions greatly influence the separation process efficiency and the time for which the separation experiment can function. When the size difference between the particles within a mixture that needs to be separated is small, the inter-particle interactions can significantly affect the separation process. In order to better understand the interactions and improve the size based particle separation efficiency we experimentally investigate the effects of enhanced electrokinetic flow on the separation process at the junction. The electrokinetic flow is enhanced with the application of larger DC voltage in the DC-biased AC voltage. The experimentally obtained results for the separation process and particle interactions at larger DC voltages are discussed in section 3.5.3.

3.5.3 Effects of electrokinetic flow on particle separation efficiency

We conducted the size based separation of 3 and 5 μm particles using rDEP at three other DC voltages, which are 50, 75 and 100 V respectively. As seen in Eq. (3-6), the increase of DC field should cause a drop in the required AC to DC ratio, α , for the particle trapping. This theoretical prediction is verified by our experimental predictions,

which were implemented at 50 V DC/ 725 V AC ($\alpha = 14.5$), 75 V DC/ 750 V AC ($\alpha = 10$), and 100 V DC/ 900 V AC ($\alpha = 9$), respectively.

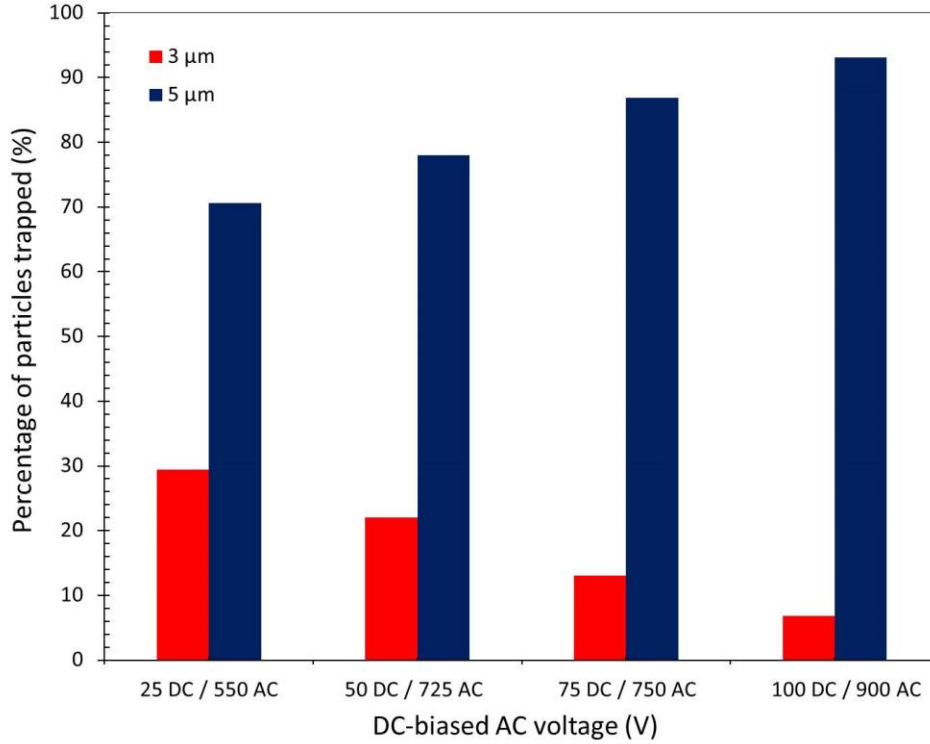


Figure 17: Percentage of 3 and 5 μm particles trapped at the reservoir-microchannel junction during particle separation at various DC-biased AC voltages under rDEP.

The videos of the separation experiment at various DC-biased AC fields were utilized to quantify the separation purity. The videos were analyzed frame by frame counting the number of 3 μm particles entering the reservoir-microchannel junction and the number of 3 μm particles passing through the microchannel into the outlet reservoir until one minute after the electric field is applied. The difference in the number of particles entering the reservoir-microchannel junction and exiting it was undergoing inter-particle interactions. Particles experiencing inter-particle interactions were captured

and pulled into the 5 μm particle pearl chain due to the increased rDEP force caused by the disturbances of the local electric field from the trapped 5 μm particles. The number of 5 μm particles entering the reservoir-microchannel junction and getting trapped was also counted. The plot in figure 17 shows the percentage of 3 μm particles getting trapped along with the 5 μm particles at the reservoir-microchannel junction under the influence of inter-particle interactions. It can be seen from the plot that a significant number of 3 μm particles are trapped along with the 5 μm particles at the 25 V DC case. This phenomenon, however, diminishes with the increase of the DC voltage as seen in figure. 17, and becomes almost negligible at the 100 V DC case. The increase in purity of the separation process is attributed to the enhanced electrokinetic flow at a higher DC field, which acts to move around the 5 μm particle cluster and drag the 3 μm particles into the microchannel quickly. With the increase in the DC field the electrokinetic velocity of the particles is enhanced which also enables the particles to move faster towards the reservoir-microchannel junction and thus more particles can be trapped in small time duration.

3.6 Summary

We applied the rDEP approach to separate particles based upon size inside a microfluidic reservoir. This separation has been demonstrated through continuous separation of 3 and 5 μm and, 3 and 10 μm particles under various DC-biased AC fields at the reservoir-microchannel junction. The experimentally obtained particle images agree closely with the numerically predicted particle trajectories. However, the separation

efficiency is greatly affected by the inter-particle interactions between the streaming 3 μm particles and the accumulated 5 and 10 μm particles trapped inside the reservoir at the junction. The 3 μm particles also start getting trapped due to the interactions which hinders the continuous separation of particles and requires it to be operated in a semi-continuous manner. The interactions can be attributed to the disturbance in local electric caused by the trapped particles and the increased AC voltage in the DC-biased voltages. The effect of enhanced electrokinetic flow with increased DC voltage in the DC-biased AC voltage on the inter-particle interactions is also studies. The interaction decreases with the enhanced electrokinetic flow and improves the separation efficiency considerably. Additionally, it can be speculated that particles that attribute differences in surface charge and conductivity can also be separated based upon the trapping number analysis which will be studied in the coming chapters.

CHAPTER 4: Particle Separation by Charge Using Reservoir-based Dielectrophoresis (rDEP)

4.1 Introduction

Separating particles (either synthetic or biological) from a complex mixture is important to a wide range of applications in industry, biology and medicine etc. In the past two decades microfluidics has evolved to be a very useful tool for particle separation and manipulation in miniaturized devices (Pamme, N. 2007; Kersaudy-Kerhoas, M. 2008; Tsutsui, H. 2009; Lenshof, A. 2010; Bhagat, A. A. 2010). A variety of microfluidic approaches have so far been developed to separate particles through the use of the force- or flow-field induced electric (Srivastava, S. K. 2011; Regtmeier, J. 2011; Cetin, B. 2011), acoustic (Laurell, T. 2007), optical (Kim, S. B. 2008; 75 Wang, M. M. 2005), magnetic (Pamme, N. 2006; Gijs, M. A. 2010), hydrodynamic (Yamada, M. 2004; Davis, J. A. 2006; Choi, S. 2007), and inertial (Di Carlo, D. 2009; Kuntaegowdanahalli, S. S. 2009) particle motions etc. Some of these separations need an extrinsic fluorescent (Fu, A. Y. 1999) or magnetic labeling (Adams, J. D. 2008) of the targeted or non-targeted particles to establish the specificity, which is usually complex and expensive. The rest of the separations, which cover the majority of the demonstrated microfluidic approaches, are label free and based upon the intrinsic particle properties such as size, shape, density, charge, deformability, polarizability (including electric, magnetic and optical), and compressibility etc. (Gossett, D. R. 2010).

Surface charge is an important particle property. It determines the particle's electrophoretic mobility and plays an important role in keeping particle suspension dispersed. Charge-based particle separation has been achieved in microfluidic devices using several approaches, which can be classified as batch-wise or continuous-flow based on the separation process. The former includes capillary-based electrophoresis (Rodriguez, M. A. 2004) and electrical field-flow fractionation (EFFF) (Giddings, J. C. 1993), where particles of dissimilar charges migrate through a separation column at different times due to their unequal electrophoretic velocities (Subirats, X. 2011) and their residences in stream laminae of unequal velocities (Gale, B. K. 1998), respectively. Free-flow electrophoresis (FFE) is a continuous-flow approach (Krivankova, L. 1998), where particles of dissimilar charges are split up into different lanes by their transverse electrophoretic migrations relative to a pressure-driven carrier electrolyte flow (Kohlheyer, D. 2008). Another continuous-flow microfluidic approach for charge-based particle separation is curvature-induced dielectrophoresis (C-iDEP) (Zhu, J. 2011), which exploits the inherent electric field gradients within turns (Zhu, J. 2009; Zhu, J. 2010), to focus and deflect particles to mobility-dependent flow paths in a double-spiral microchannel (Zhu, J. 2011). Additionally charge-based particle separation has been demonstrated using a bi-directional flow in a converging-diverging microchannel to trap particles carrying a specific charge (Jellema, L. C. 2009). As a net flow was observed experimentally when the particle trapping occurred (Lettieri, G. L. 2003), this separation can be viewed as a continuous-flow approach.

We developed a new microfluidic approach for manipulating particles inside a reservoir. It exploits the particle dielectrophoresis that is induced by the inherent electric field gradient at the reservoir-microchannel junction to focus, trap and concentrate particles (Zhu, J. 2012), which we termed as reservoir-based dielectrophoresis (rDEP). In this work we apply such an rDEP approach to continuous-flow particle separation based upon surface charge. The factors that may affect the separation are studied. A theoretical model is also developed to understand and predict the electrokinetic particle transport behaviors at the reservoir-microchannel junction during separation.

4.2 Materials and Methods

4.2.1 Microfluidic Device Fabrication

The microfluidic device in our experiment was fabricated with polydimethylsiloxane (PDMS) using the standard soft lithography technique. The detailed procedure is given in chapter 2. As shown in Fig. 18, the device is composed of a 1.2 cm-long straight microchannel with a 5 mm-diameter reservoir at each end. The channel is 500 μm wide in the main body and has a constriction section of 50 μm in width and 1 mm in length at the reservoir-microchannel junction in both ends (see the inset in figure 18). These constrictions are designed for the purpose of reducing the applied electric voltage as the electric field can be locally amplified. The channel is uniformly 25 μm deep with a constant radius of 20 μm for all corners.

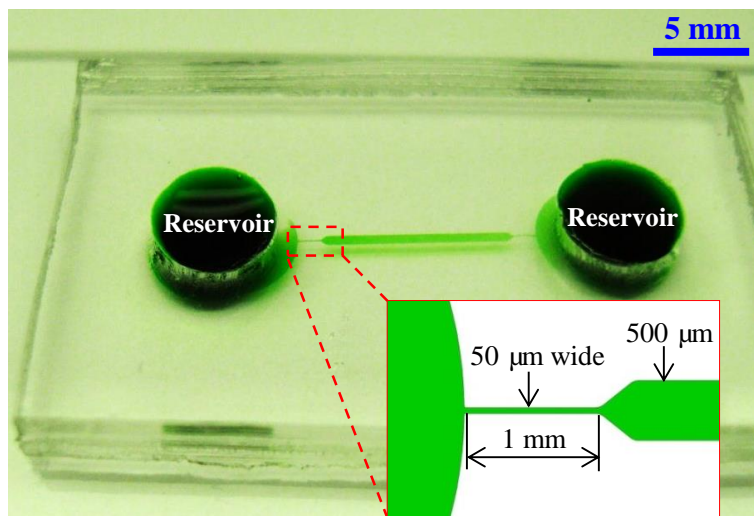


Figure 18: Picture of the microfluidic device (filled with green food dye for clarity) used in the experiment. The inset displays the dimensions of the reservoir-microchannel junction.

4.2.2 Particulate Solution Preparation

To demonstrate the surface charge-based particle separation, we mixed green fluorescent (Bangs Laboratories, Fisher, IN) and non-fluorescent (Sigma Aldrich, St Louis, MO) polystyrene particles at 1:2 number ratio and re-suspended them in 0.1 mM phosphate buffer to a final concentration of 10^7 – 10^8 particles per ml. Both types of particles have a diameter of 3 μm while bearing dissimilar surface charges. The latter is evidenced by the discrepancy in their electrokinetic mobility values, which can be experimentally measured and will be presented in the Theory section below (see section 3.2). Tween 20 (Fisher Scientific, Waltham, MA) was added to the particle solution at 0.1% v/v to suppress the aggregation of particles and their adhesion to channel walls. Prior to use the particle solution was stirred in a vortex generator to ensure a uniform distribution of each type of particles.

4.2.3 Particle Manipulation and Visualization

The electrokinetic manipulation of the particle mixture in the microfluidic device was attained by imposing DC-biased AC electric fields across the length of the microchannel. The electric fields were supplied by a function generator (33220A, Agilent Technologies, Santa Clara, CA) in conjunction with a high-voltage amplifier (609E-6, Trek, Medina, NY). The frequency of AC field was fixed at 1 kHz in most experiments and was varied from 0.5 kHz to 5 kHz in examining its influence on particle separation. Pressure-driven flow was eliminated by carefully balancing the liquid heights in the two reservoirs prior to each experiment. The particle mixture solution was introduced only to the inlet reservoir and the outlet reservoir was devoid of particles at the beginning of a separation experiment. Visual inspection of the outlet reservoir at the end of the experiment could therefore be used to determine the separation purity. Particle motion was monitored using an inverted microscope (Nikon Eclipse TE2000U, Nikon Instruments, Lewisville, TX), through which videos (at around 12 frames/s) and images at the reservoir-microchannel junction were recorded using a CCD camera (Nikon DS-Qi1Mc). To visualize the fluorescent and non-fluorescent particles simultaneously, we used a green fluorescent light along with a relatively weak white light to illuminate the reservoir-microchannel junction.

4.3 Particle Separation Mechanism

As illustrated by its contour (the darker color, the larger magnitude) in figure 19, electric field, \mathbf{E} , becomes inherently non-uniform at the junction of the reservoir and microchannel due to their size mismatch. Therefore, particles experience a dielectrophoretic motion, \mathbf{U}_{DEP} , when moving electrokinetically through the junction. Using the dipole moment approximation, the time averaged \mathbf{U}_{DEP} of an isolated spherical particle under DC and low frequency (< 100 kHz) AC electric fields is given by (Morgan, H. 2002)

$$\mathbf{U}_{DEP} = \frac{\varepsilon_f d^2}{12\eta_f} f_{CM} \nabla \mathbf{E}^2 \quad (4-1)$$

$$f_{CM} = \frac{\sigma_p - \sigma_f}{\sigma_p + 2\sigma_f} \quad (4-2)$$

where d is the particle diameter, ε_f is the fluid permittivity, f_{CM} is the so-called Clausius-Mossotti (CM) factor and has been assumed approximately identical for DC and low frequency (< 100 kHz) AC electric fields, η_f is the fluid dynamic viscosity, \mathbf{E} is the local electric field in root-mean-square (RMS) value, σ_p and σ_f are the electric conductivities of the particle and the suspending fluid, respectively. As polymer particles (Ermolina, I. 2005) and biological cells (Voldman, J. 2006) often appear poorly conducting in DC and low-frequency AC electric fields, one can have $\sigma_p < \sigma_f$ and thus $f_{CM} < 0$ leading to negative DEP (Jones, T. 1995). Therefore, \mathbf{U}_{DEP} points towards the lower electric field region as indicated by the particle velocity analysis in figure 19.

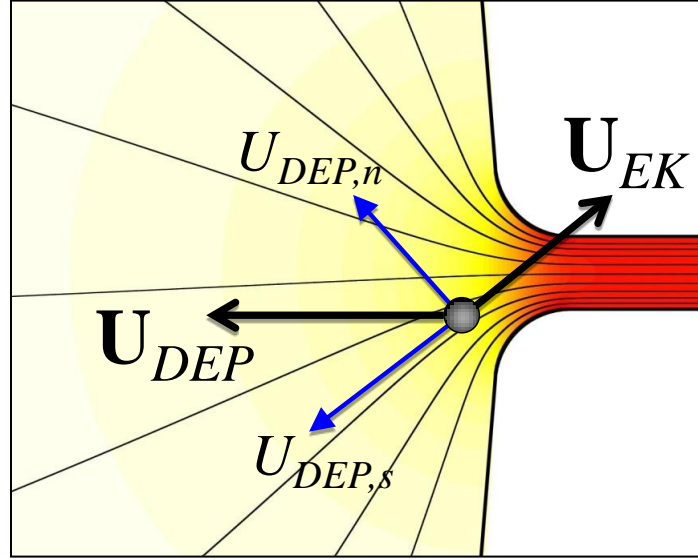


Figure 19: Velocity analysis of a particle at the reservoir-microchannel junction due to electrokinetic flow and the induced rDEP. The thin lines represent the electric field lines or equivalently fluid streamlines in the absence of the particle. The background color shows the electric field contour (the darker color, the larger field magnitude).

The observed particle velocity, \mathbf{U}_p , is the vector addition of the DC electrokinetic motion (a combination of fluid electroosmosis and particle electrophoresis), \mathbf{U}_{EK} , and the AC/DC dielectrophoretic velocity, \mathbf{U}_{DEP} ,

$$\mathbf{U}_p = \mathbf{U}_{EK} + \mathbf{U}_{DEP} = \mu_{EK} \mathbf{E}_{DC} + \mu_{DEP} \nabla \mathbf{E}^2 \quad (4-3)$$

$$\mu_{EK} = f_g \frac{\varepsilon_f (\zeta_p - \zeta_w)}{\eta_f} \quad (4-4)$$

$$\mu_{DEP} = \frac{\varepsilon_f d^2 f_{CM}}{12 \eta_f} \quad (4-5)$$

where μ_{EK} is the electrokinetic particle mobility, \mathbf{E}_{DC} is the DC component of the applied DC-biased AC electric field, μ_{DEP} is the dielectrophoretic particle mobility, f_g is the factor

that accounts for the wall effects on particle motion and is close to 1 for the particles used in our experiments (Anderson, J. 1989), ζ_p is the particle zeta potential that is controlled by the surface charge, and ζ_w is the wall zeta potential. Note that the Brownian, inertial, and gravitational motions of particles have been neglected in Eq. (4-3), which is reasonable for micron-sized particles in electrokinetic microfluidics (Li, D. 2004). The electrokinetic velocity, \mathbf{U}_{EK} , is parallel to the electric field lines and hence stream-wise due to the similarity of electric field and flow field in pure electrokinetics (Cummings, E. B. 2000). In contrast, the rDEP velocity, \mathbf{U}_{DEP} , can have a component in both the stream-wise and the cross-stream directions. Therefore, we rewrite Eq. (4-3) in streamline coordinates as follows,

$$\mathbf{U}_p = (U_{EK} + U_{DEP,s})\hat{\mathbf{s}} + U_{DEP,n}\hat{\mathbf{n}} = \left(\mu_{EK}E_{DC} + \mu_{DEP}\frac{\partial E^2}{\partial s} \right)\hat{\mathbf{s}} + \left(2\mu_{DEP}\frac{E^2}{\mathfrak{R}} \right)\hat{\mathbf{n}} \quad (4-6)$$

where U_{EK} is the magnitude of the electrokinetic velocity, $U_{DEP,s}$ is the magnitude of the stream-wise dielectrophoretic particle velocity, $\hat{\mathbf{s}}$ is the unit vector of the coordinate s along the streamlines, $U_{DEP,n}$ is the magnitude of the cross-stream dielectrophoretic particle velocity, $\hat{\mathbf{n}}$ is the unit vector of the coordinate n normal to the streamlines, and \mathfrak{R} is the local radius of curvature of the streamline.

For particles experiencing negative DEP (i.e., $\mu_{DEP} < 0$), $U_{DEP,n}$ is directed towards the centerline of the microchannel (see the velocity analysis in figure 19), which produces a focusing effect on the suspended particles at the reservoir-microchannel junction (Patel, S. 2012; Zhu, J. 2012). Meanwhile, $U_{DEP,s}$ is against U_{EK} and hence slows

down the particle motion at the reservoir-microchannel junction. Moreover, since $U_{DEP,s}$ is a second-order function of the total electric field, E , while U_{EK} is linearly proportional to only the DC field component, E_{DC} , one can expect $U_{DEP,s}$ to counter-balance U_{EK} at large electric fields, i.e.,

$$\mu_{EK}E_{DC} + \mu_{DEP} \frac{\partial E^2}{\partial s} \leq 0 \text{ or } \frac{\mu_{EK}}{-\mu_{DEP}} \leq 2(1 + \alpha^2) \frac{\partial E_{DC}}{\partial s} \quad (4-7)$$

where α is the AC to DC field ratio, i.e., $E = E_{DC} + E_{AC} = E_{DC} (1 + \alpha)$. When this happens particles can be stagnated and concentrated at the reservoir-microchannel junction (Patel, S. 2012; Zhu, J. 2012). Such rDEP trapping is dependent on the electrokinetic to dielectrophoretic particle mobility ratio,

$$\frac{\mu_{EK}}{-\mu_{DEP}} = \frac{6f_g(\zeta_p - \zeta_w)}{d^2 f_{CM}} \quad (4-8)$$

which is an explicit function of particle size (d) and charge (ζ_p). The larger the mobility ratio is, the more difficult (e.g., a higher AC to DC field ratio, α , is required if the DC field is fixed) it is to trap the particle. This indicates that we can potentially trap and concentrate one type of particles in the upstream reservoir while sweeping the other type to the downstream reservoir based upon one of these properties. We have recently reported the microfluidic separation of particles by size using rDEP (Zhu, J. 2012). In this work we aim to demonstrate the application of rDEP to continuous-flow charge-based separation of particles with a similar size.

4.4 Numerical Model and Validation

The simulation of electrokinetic particle motion from reservoir to microchannel was conducted in COMSOL 3.5a (Burlington, MA) using a 2D model we developed earlier (Zhu, J. 2009; Church, C. 2009). This model neglects the perturbations of finite-sized particles to the flow and electric fields, which in turn causes errors in the computation of particle velocity. To account for such particle size effects (and other effects as well if any), a correction factor, λ_c , was introduced to Eq. (4-3) to correct the dielectrophoretic particle velocity, i.e.,

$$\mathbf{U}_p = \mu_{EK} \mathbf{E}_{DC} + \lambda_c \mu_{DEP} (1 + \alpha^2) \nabla \mathbf{E}_{DC}^2 \quad (4-9)$$

This corrected particle velocity was used as an input to the particle tracing function in COMSOL, where the involving parameters were obtained as follows. The DC electric field, $\mathbf{E}_{DC} = -\nabla \phi_{DC}$, was calculated by solving for the DC electric potential, ϕ_{DC} , from Laplace equation $\nabla^2 \phi_{DC} = 0$. To do so, the electrode in each reservoir was simulated as a 0.5 mm-diameter concentric circle, upon which an electric potential was imposed. Specifically the experimentally applied DC voltage was imposed to the electrode in the entry reservoir. The electrode in the exit reservoir was grounded. All microchannel walls were assumed to be electrically insulated.

The dielectrophoretic particle mobility, μ_{DEP} , in Eq. (4-9) was calculated from Eq. (4-5) with the typical dynamic viscosity, $\eta_f = 1.0 \times 10^{-3}$ kg/(m·s) and permittivity $\epsilon_f = 6.9 \times 10^{-10}$ C/(v·m) for pure water at 20 °C. To obtain the CM factor, f_{CM} , the electric

conductivity of polystyrene particles was computed from $\sigma_p = 4K_s/d$ with $K_s = 1$ nS being the recommended value for surface conductance (Ermolina, I. 2005), which gave $\sigma_p = 13.3$ $\mu\text{S}/\text{cm}$ for $d = 3$ μm particles. Considering the measured electric conductivity of 0.1 mM phosphate buffer, $\sigma_f = 25$ $\mu\text{S}/\text{cm}$, we obtained $f_{CM} = -0.19$ for both the fluorescent and non-fluorescent particles used in our experiment. The electrokinetic particle mobility, μ_{EK} , was determined by tracking the motion of individual particles in the main body of microchannel (where DEP is negligible) under a small pure DC electric field. Specifically we imposed a 25 V DC voltage across the 1.2 cm long microchannel, which produced an average electric field of about 20 V/cm. At this electric field, Joule heating effects were estimated to be negligible (Xuan,X. 2008; Sridharan,Sriram 2011). The resultant electrokinetic velocity of particles in the working buffer was measured in the middle of the channel length, which was then divided by the numerically computed local electric field to give the electrokinetic mobility. Using this method we obtained $\mu_{EK} = 5.9 \times 10^{-8}$ ($\text{m}^2/\text{V}\cdot\text{s}$) and 2.8×10^{-8} ($\text{m}^2/\text{V}\cdot\text{s}$) for the non-fluorescent and fluorescent particles, respectively. In other words, these two types of particles indeed carry different amounts of surface charges, which may be due to the incorporation of dyes into the polymer of the fluorescent particles.

To select the correction factor, λ_c , in Eq. (4-9), we compared the simulated trajectories of the two types of particles at the reservoir-microchannel junction with the experimentally obtained particle streak images. Figure 20 shows this comparison for the motion of the particle mixture in two circumstances: one is under 25 V DC and the other

is under 25 V DC plus 400 V AC (RMS value, 1 kHz frequency). Note that the streak images of the fluorescent and non-fluorescent particles were each obtained by superimposing the same sequence of over 600 images with respect to the bright and dark bases, respectively. The correction factor was set to 0.8 for both particles, which is consistent with the values for particles and cells of comparable sizes used in our previous studies (Zhu, J. 2009; Zhu, Junjie 2011; Zhu, J. 2012; Patel, S. 2012; Zhu, J. 2009; Church, C. 2009; Xuan, X. 2006). On the application of a small pure DC field, fluorescent (top row) and non-fluorescent (bottom row) particles both enter into the microchannel in a uniformly distributed manner because the influence from rDEP is very weak [see figure 20(a)]. However, when the AC electric field is added, fluorescent particles (top row, the right image) are focused to a tight stream along the centerline of the microchannel. In contrast, non-fluorescent particles (bottom row, the right image) still cover more than one half of the channel as seen in figure 20(b). This discrepancy is attributed to the larger electrokinetic mobility of non-fluorescent particles as presented above. Therefore, fluorescent particles are exposed to rDEP focusing (which is identical for the two types of similar-sized particles) for a longer time. The simulated trajectories [right columns in figure 20(a) and figure 20(b)] agree closely with the experimental images (left columns) for both particles in both circumstances, which validates the numerical model and verifies the correction factor value as well.

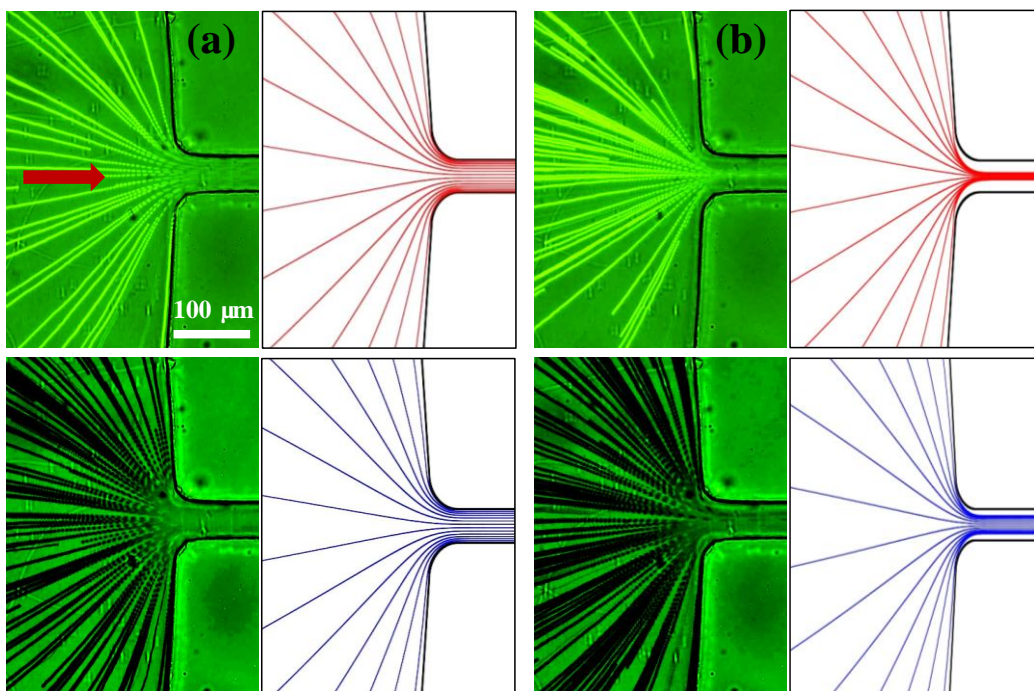


Figure 20: Comparison of the experimentally obtained streak images (left column in each panel) and numerically predicted trajectories (right column in each panel) of fluorescent (top row) and non-fluorescent (bottom row) $3\text{ }\mu\text{m}$ particles at the reservoir-microchannel junction under the influence of rDEP. The applied DC voltage was fixed at 25 V and the 1-kHz AC voltage (RMS value) was varied from 0 V (a) to 400 V (b). The block arrow in (a) indicates the particle moving direction.

4.5 Results and Discussion

4.5.1 Charge-based Particle Separation using rDEP

Figure 21 demonstrates the continuous-flow separation of $3\text{ }\mu\text{m}$ fluorescent and non-fluorescent particles by charge at the reservoir-microchannel junction using rDEP. It was implemented by applying a 50 V DC-biased 800 V AC voltage across the microchannel. The frequency of the AC voltage was maintained at 1 kHz. Figure 21(a) shows a snapshot image of the particle behaviors at the junction 45 s after the electric

field was turned on. One can see that the fluorescent particles are concentrated inside the reservoir while the non-fluorescent particles can migrate through the junction in a focused stream along the centerline of the microchannel. This continuous separation happens because the fluorescent particles possess a smaller electrokinetic to dielectrophoretic mobility ratio [see the definition in Eq. (4-8)] than the non-fluorescent ones and hence can be trapped more easily [see Eq. (4-7)]. It is simply a result of the fluorescent particles' lower electrokinetic mobility as measured experimentally (see section 4.4 and also figure 20) considering that the two types of particles possess a similar value for dielectrophoretic mobility. The streak images of the fluorescent and non-fluorescent particles are illustrated in the top row of figure 21(b) and figure 21(c), respectively. Numerically predicted trajectories of these two particles are displayed in the bottom row, and agree with the experimental results.

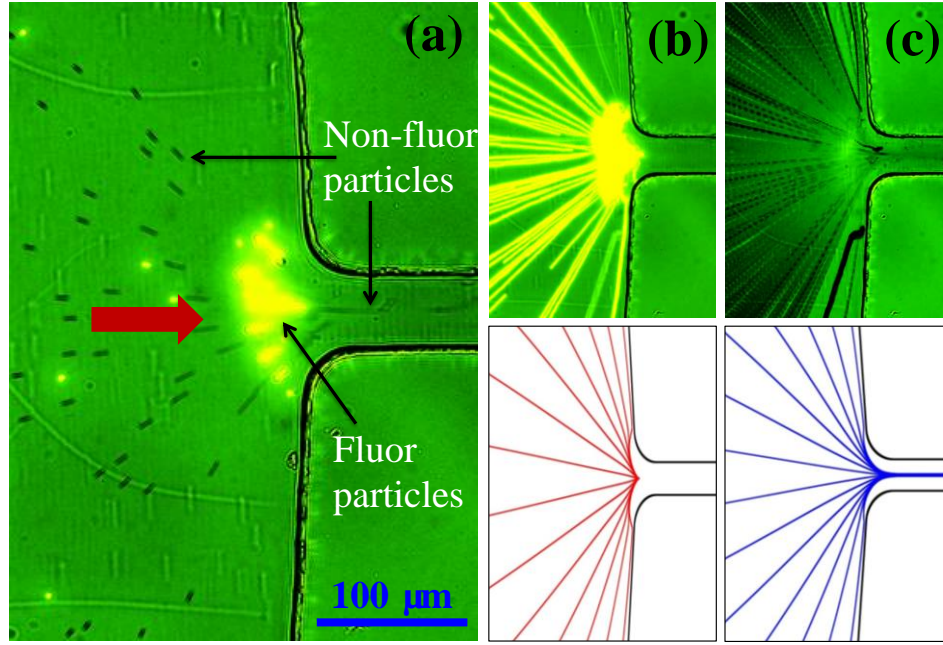


Figure 21: Demonstration of selective concentration and continuous sorting of 3 μm fluorescent particles from 3 μm non-fluorescent particles at the reservoir-microchannel junction by rDEP. (a) shows a snapshot image of the particle behaviors 45 s after the 50 V DC-biased 800 V AC (RMS value, 1 kHz) voltage was applied. (b) and (c) show the comparison of the experimentally obtained streak images (top row) and the numerically predicted trajectories (bottom row) of the fluorescent and non-fluorescent particles, respectively. The block arrow in (a) indicates the particle moving direction.

The estimated flow rate of this continuous charge-based particle separation is 0.25 $\mu\text{l}/\text{min}$, which is more than 5 times larger than the approach we reported in an earlier work through the use of curvature-induced dielectrophoresis (C-iDEP). It can be easily enhanced by increasing the DC voltage (see section 4.5.2 below) and/or employing a parallel operation (e.g., design multiple microchannels in the radial direction to form a circle about the inlet reservoir). The purity of this separation was examined by visually inspecting both the reservoir-microchannel junction during the experiment and the outlet reservoir after the experiment. We found that fluorescent particles first formed chains and then clusters inside the inlet reservoir and none of them could escape from the trapping

zone. This is also confirmed by the nearly absence of fluorescent particles in the outlet reservoir except for the few that were already in the microchannel before the electric field was applied. However, once many fluorescent particles were concentrated some of the non-fluorescent particles could also get captured and pulled into the chains of fluorescent particles. This is mainly caused by the increase of rDEP force due to the disturbances of the local electric field from the trapped non-conducting fluorescent particles. It is speculated that the dipole interactions between the two types of particles and those among the non-fluorescent particles themselves (Morgan, H. 2002; Jones, T. 1995) may also play a role in this process. Unfortunately, neither of these factors was taken into consideration in our numerical model. To better understand this phenomenon, we experimentally investigated the effects of electrokinetic flow and AC field frequency on the separation, which are presented in the sections below.

4.5.2 Electrokinetic Flow Effects on Particle Separation

We conducted the charge-based separation of 3 μm fluorescent and non-fluorescent particles using rDEP at three other DC voltages, which are 25 V, 75 V and 100 V, respectively. As seen from Eq. (4-7), the increase of DC field should cause a drop in the required AC to DC field ratio, α , for particle trapping. This theoretical prediction is verified by our experiments, which were implemented at 25 V DC/625 V AC ($\alpha = 25$), 50 V DC/800 V AC ($\alpha = 16$), 75 V DC/875 V AC ($\alpha = 11.7$), and 100 V DC/950 V AC ($\alpha = 9.5$), respectively. The AC voltages are all in RMS value and at 1 kHz frequency. Figure 22 compare the snapshot particle images at the reservoir-microchannel junction in these

circumstances (except for the 75 V DC case, which will be presented in figure 21), which were all taken at least 2 minutes after the electric field was applied. As highlighted by the dashed lines in the images, there are a significant number of non-fluorescent particles trapped along with fluorescent ones at the 25 V DC case in figure 22(a). This phenomenon, however, diminishes with the increase of the DC voltage as seen in figure 22(b), and becomes almost invisible at the 100 V DC case in figure 22(c). It is attributed to the enhanced electrokinetic flow at a higher DC field, which acts to move around the fluorescent particle cluster and drag the non-fluorescent particles into the microchannel in a quicker matter.

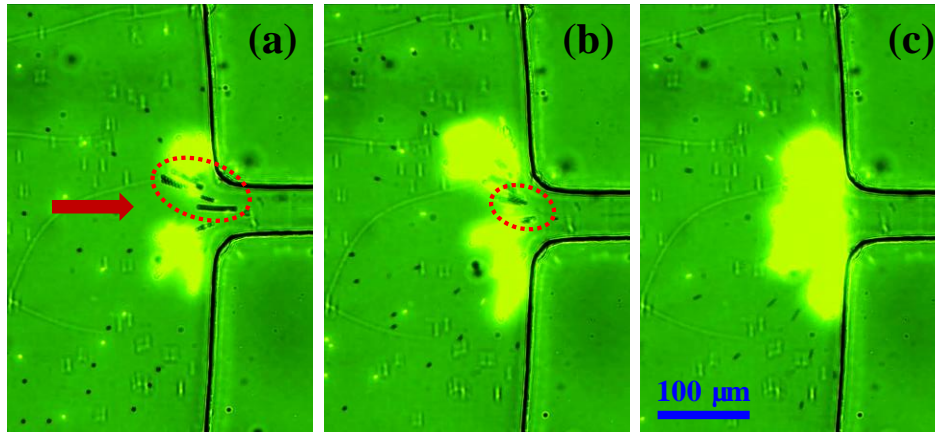


Figure 22: Electrokinetic flow effects on charge-based rDEP separation of 3 μm fluorescent and non-fluorescent particles at the reservoir-microchannel junction. Illustrated are the snapshot images taken 2 minutes after the electric voltage at (a) 25 V DC/625 V AC ($\alpha = 25$), (b) 50 V DC/800 V AC ($\alpha = 16$), and (c) 100 V DC/950 V AC ($\alpha = 9.5$) was imposed to the microchannel. The AC voltages are all in RMS value and at 1 kHz frequency. The dashed lines highlight the regions where non-fluorescent particles are trapped due to the influences from the concentrated fluorescent particles. The block arrow in (a) indicates the particle moving direction.

4.5.3 AC Field Frequency Effects on Particle Separation

We also performed the charge-based separation of 3 μm fluorescent and non-fluorescent particles using rDEP under a fixed 75 V DC/875 V AC voltage while at various AC voltage frequencies. Figure 23 compares the snapshot particle images at the reservoir-microchannel junction when the frequency is varied from 0.5 kHz (a) to 1 kHz (b) and 5 kHz (c). All three images were once again taken at least 2 minutes after the application of the electric field. It is evident that the non-selective trapping of non-fluorescent particles becomes more significant with the increase of the AC voltage frequency. Moreover, the particle trapping zone is greatly expanded at larger frequencies. We don't expect that the variation of AC voltage frequency can affect the rDEP motion of particles to such a considerable extent because the frequency we used in experiments is well below the 100 kHz low-frequency limit (Ermolina, I. 2005; Voldman, J. 2006). It is speculated that the increasing AC voltage frequency greatly enhances the particle-particle interactions (Morgan, H. 2002; Jones, T. 1995) and hence strengthens the trapping of non-fluorescent particles. Additionally as the particles are concentrated near the bottom wall of the microchannel, we speculate that the particle-wall interactions may also contribute to the observed phenomenon in figure 23.

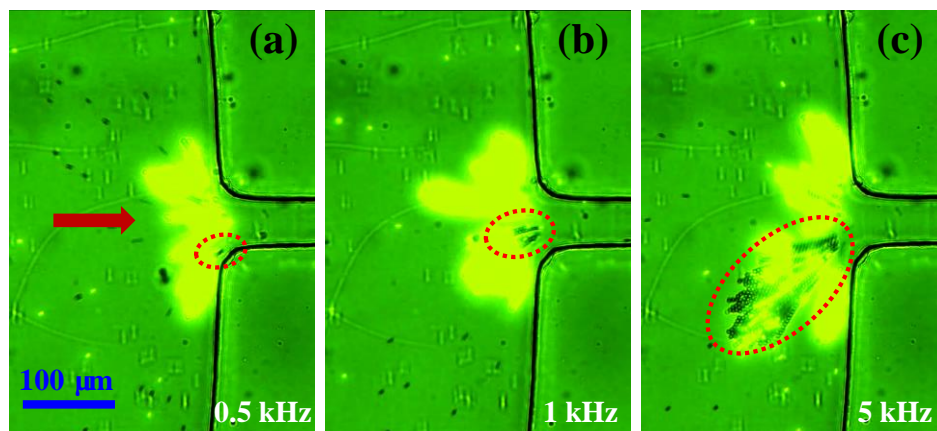


Figure 23: AC field frequency effects on charge-based rDEP separation of 3 μm fluorescent and non-fluorescent particles at the reservoir-microchannel junction. Illustrated are the snapshot images taken 2 minutes after the application of a 75 V DC-biased 875 V AC voltage (RMS). The AC voltage frequency was varied from 0.5 kHz (a) to 1 kHz (b) and 5 kHz (c). The dashed lines highlight the regions where non-fluorescent particles get trapped due to the influences from the concentrated fluorescent particles. The block arrow in (a) indicates the particle moving direction.

4.6 Summary

We have applied a recently developed rDEP approach to continuously separate particles based upon surface charge inside a microfluidic reservoir. This separation has been demonstrated through a selective concentration and continuous sorting of 3 μm fluorescent particles from 3 μm non-fluorescent particles under DC-biased AC electric fields. The obtained particle images agree closely with the predicted particle trajectories from a 2D numerical model. It is, however, found that the streaming non-fluorescent particles may also get trapped in the reservoir due to the influences from the accumulated fluorescent particles, which can significantly lower the separation purity. These influences have been found through experiments to decrease with the enhanced electrokinetic flow (by increasing the applied DC electric field) and the lowered AC field

frequency. We speculate that besides the tested electric field effects (i.e., DC and AC field magnitudes and AC field frequency) the channel and solution properties (e.g., channel width and depth, corner radius, and solution ionic concentration etc.) can also impact the charge-based particle separation. These factors will be studied in future works. Since it takes place inside the reservoir and no in-channel mechanical or electrical parts are needed, the demonstrated rDEP particle sorter can be conveniently integrated with other functional components (e.g., pretreatment and post-analysis of particles) into lab-on-a-chip devices for numerous applications.

CHAPTER 5 - Microfluidic Separation of Live and Dead Yeast Cells Using Reservoir-based Dielectrophoresis (rDEP)

5.1 Introduction

Cell separation is an essential step in biological research, and has important applications in many areas such as environmental monitoring, food production, and pharmaceutical industry. Microfluidic devices have been increasingly used to separate cells due to their advantages in cost, accuracy, and efficiency etc. as compared to their macroscopic counterparts (Pamme, N. 2007; Kersaudy-Kerhoas, M. 2008; Tsutsui, H. 2009; Lenshof, A. 2010; Bhagat, A. A. 2010). A variety of force fields have been demonstrated to implement microfluidic cell separations, ranging from the ubiquitous gravity(Huh, D. 2007) to hydrodynamic (Yamada, M. 2004; 89 Yamada, M. 2004), electric (Gascoyne, P. R. 2002; Hughes, M. P. 2002; Srivastava, S. K. 2011; Regtmeier, J. 2011), acoustic (Laurell, T. 2007; Friend, J. 2008), optical (Wang, M. M. 2005; Kim, S. B. 2008), magnetic (Pamme, N. 2006; Gijs, M. A. 2010), and inertial (Di Carlo, D. 2009; Kuntaegowdanahalli, S. S. 2009) forces etc. These separations can take place either with or without the use of biochemical labels to identify cells. Fluorescence (Fu, A. Y. 1999) and magnetic-activated (Adams, J. D. 2008) cell sorters are the two examples that use external labeling (through fluorescent or magnetic bonding) of the targeted or non-

targeted cells to establish the specificity. For label-free cell separations, numerous intrinsic biomarkers have been exploited to sort cells including size, shape, density, charge, and deformability etc (Gossett, D. R. 2010).

Cell viability is another intrinsic property that has been explored for label-free cell separations. The sorting of live and dead cells is critical to the diagnosis of early-stage diseases and to the efficacy test of drug screening etc (Del Bene, F. 2009; Tatosian, D. A. 2009). Previous studies on this separation are primarily based on dielectrophoresis (DEP), which is the translation of cells either towards (called positive dielectrophoresis) or away from (called negative dielectrophoresis) the high electric field region if the cell is more or less polarizable than the suspending medium (Cheng, I. F. 2007; Pethig, Ronald 2010). The polarizability of a cell is dependent on its electrical (i.e., conductivity and permittivity) and mechanical (i.e., size and shape) properties as well as the electric field frequency (Gagnon, Z. R. 2011; Lei, U. 2011). This enables the label-free separation of cells by one or more of their intrinsic properties via DEP (Cetin, B. 2011; Zhu, J. 2011). It has been reported that cells have a decreased conductivity in the nucleus and an increased conductivity in the membrane when losing viability (Huang, Y. 1992; Pethig, R. 1997; Suehiro, J. 2003). Therefore, the dielectrophoretic responses of live and dead cells to electric fields can become different, especially significant under high-frequency (larger than 100 kHz) AC electric fields.

We develop herein a new microfluidic approach to dielectrophoretic separation of cells by viability. We make use of the reservoir-based dielectrophoresis (rDEP), which is

induced by the inherent electric field gradient at the reservoir-microchannel junction, to selectively trap dead yeast cells and continuously separate them from live ones inside the reservoir. As compared to the existing dielectrophoretic approaches, our approach does not rely on any mechanical or electrical parts inside a microchannel. This not only simplifies the device fabrication and control, but also eliminates the negative issues caused by electrochemical reactions on the in-channel microelectrode surfaces and Joule heating effects around the in-channel micro-insulators. We demonstrate and examine the rDEP trapping and separation of live and dead yeast cells using a combined experimental and numerical method.

5.2 Experiment

5.2.1 Microchannel Fabrication

The microchannel was fabricated with PDMS using the soft lithography technique. Briefly, photoresist (SU 8-25, MicroChem, Newton, MA) was dispensed onto a clean glass slide, which was made to spin at an angular velocity of 2000 RPM (WS-400E-NPP-Lite, Laurell Technologies, North Wales, PA). The resulting 25 μm thick photoresist film was soft baked on a digital hotplate (HP30A, Torrey Pines Scientific, San Marcos, CA) in two steps at 65 $^{\circ}\text{C}$ for 3 minutes and 95 $^{\circ}\text{C}$ for 7 minutes. It was then exposed to near UV light (ABM, San Jose, CA) through a negative photo mask with the printed microchannel pattern (CAD/Art Services, Bandon, OR). Following a two-step hard-bake at 65 $^{\circ}\text{C}$ for 1 minute and 95 $^{\circ}\text{C}$ for 3 minutes, the cured photoresist was

developed in SU-8 developer solution (MicroChem, Newton, MA) for 4 minutes, the result of which was a positive replica of the microchannel on the glass slide. After a brief rinse with isopropyl alcohol (Fisher Scientific, Pittsburg, PA) and a final hard bake at 150 °C for 5 minutes, the photoresist was ready for use as the mold of the microchannel.

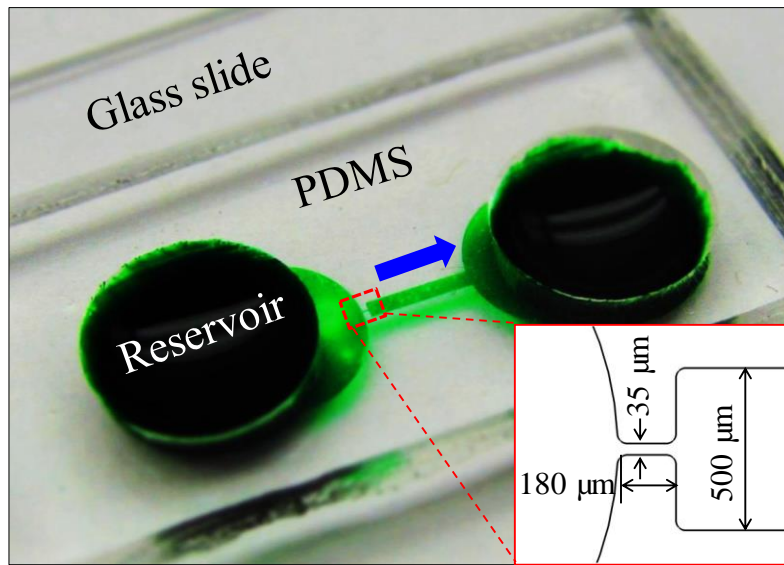


Figure 24: Picture of the microfluidic device (filled with green food dye for clarity) used in the experiment. The inset displays the dimensions of the reservoir-microchannel junction. The block arrow indicates the cell moving direction in experiments.

Next, a mixture of 10:1 mass ratio of the pre-polymer and curing agent of PDMS (Sylgrad 184 Silicon Elastomer) was mixed thoroughly and poured over the channel mold. After a 30-minute degassing in an iso-temp vacuum oven (13-262-280A, Fisher Scientific, Fair Lawn, NJ), liquid PDMS was cured at 70 °C in a gravity convection oven (13-246-506GA, Fisher Scientific) for 2 hours. The microchannel structure was cut using a scalpel and peeled off from the mold. Two holes were punched through the PDMS slab

inside the originally designed circles at the channel ends, which acted as the reservoirs in experiments. The channel side of the PDMS was then plasma treated (PDC-32G, Harrick Scientific, Ossining, NY) for 1 minute along with a clean glass slide. Finally, the two treated surfaces were bonded together to form the microchannel.

Figure 24 shows a picture of the fabricated PDMS-glass microfluidic device. It is composed of a 3.3 mm-long straight microchannel with a 5 mm-diameter reservoir at each end. The channel is 500 μm wide and has a constriction section of 35 μm width and 180 μm length at the entrance, i.e., the reservoir-microchannel junction (see the inset in figure 24). The constriction is designed for the purpose of reducing the applied electric voltage as the local electric field can be amplified. The channel is uniformly 25 μm deep with a constant radius of 20 μm for all corners.

5.2.2 Cell Preparation

Yeast cells (*Saccharomyces Cerevisiae*) were cultured in Sabouraud Dextrose Broth in a shake incubator at 30 °C. After about 24 hours, 25 ml of the culture was concentrated by centrifugation at 10,000 \times g for 10 minutes. The supernatant was removed and the cells were re-suspended in 2 ml 0.85% NaCl. Then, one ml each of this suspension was added to two 30–40 ml centrifuge tubes that originally contained 20 ml 0.85% NaCl (for live yeast) and 20 ml 70% isopropyl alcohol (for dead yeast), respectively. Both cell samples were incubated at room temperature for 1 hour, which were stirred every 15 minutes. After that, they were each pelleted by centrifugation at 10,000 \times g for 10 minutes, which were subsequently re-suspended in separate tubes

containing 10 ml 0.85% NaCl. Prior to experiment, the live and dead yeasts were each rinsed at least three times with DI water using a mini centrifuge (Fisher Scientific, Pittsburg, PA). Both cells were then re-suspended in 1 mM phosphate buffer solution (electric conductivity was measured as 210 $\mu\text{S}/\text{cm}$) to a final concentration of 10^6 cells per ml. In the separation experiment live yeast cells were stained with SYTO 9 green fluorescent before being mixed with dead ones. The average diameter was measured as 6 μm for both types of cells.

5.2.3 Experimental Technique

The dielectrophoretic separation of cells at the reservoir-microchannel junction was attained by imposing DC-biased AC electric fields across the channel. The electric field was supplied by a function generator (33220A, Agilent Technologies, Santa Clara, CA) in conjunction with a high frequency power amplifier (2100HF, Trek Inc., Medina, NY). The AC field frequency was varied from 1 kHz to a few hundred kHz that is dictated by the function generator when the output voltage is over 100 V in root-mean-square (RMS). Pressure-driven flow was eliminated by carefully balancing the liquid heights in the two reservoirs prior to experiment. The reservoirs were made large with more than 5 mm in diameter and 3-4 mm in depth in order to minimize the back flow during the course of measurement. Cell motion was monitored using an inverted microscope (Nikon Eclipse TE2000U, Nikon Instruments, Lewisville, TX), through which videos and images at the reservoir-microchannel junction were recorded using a CCD camera (Nikon DS-Qi1Mc).

5.3. Theory

5.3.1 Principle of Reservoir-based Dielectrophoresis (rDEP)

Due to the significant size-mismatch between the reservoir (5 mm in diameter) and the microchannel (35 μm wide in the constriction region, see the inset in figure 24), electric field becomes inherently non-uniform at the reservoir-microchannel junction. This is illustrated by the electric field contour (the darker color, the larger field magnitude) in figure 25. The consequence is an induced dielectrophoretic motion, \mathbf{U}_{DEP} , when cells move electrokinetically through the macro-micro interface as seen from the cell velocity analysis in figure 25. This motion is thus named reservoir-based dielectrophoresis (rDEP). Under the point-dipole moment approximation, the time averaged \mathbf{U}_{DEP} of a spherical rigid cell is given by (Jones, T. 1995; Church, C. 2009)

$$\mathbf{U}_{DEP} = \mu_{DEP} \nabla \mathbf{E}_{RMS}^2 \quad (5-1)$$

$$\mu_{DEP} = \frac{\pi r^2 \epsilon_f}{3\eta_f} \text{Re}\{f_{CM}\} \quad (5-2)$$

$$f_{CM} = \frac{\epsilon_c^* - \epsilon_f^*}{\epsilon_c^* + 2\epsilon_f^*} . \quad (5-3)$$

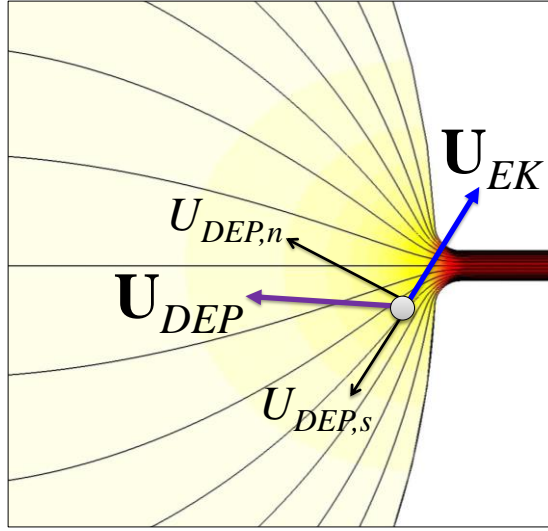


Figure 25: Illustration of cell velocity at the reservoir-microchannel junction due to the combined effects of electrokinetic flow, \mathbf{U}_{EK} , and negative rDEP, \mathbf{U}_{DEP} . The thin lines represent the electric field lines or equivalently fluid streamlines. The background shows the electric field contour (the darker color, the larger field magnitude).

In the above, μ_{DEP} is the dielectrophoretic mobility of cells, \mathbf{E}_{RMS} is the local electric field in RMS value, r is the cell radius, ϵ_f is the permittivity of the suspending fluid, η_f is the fluid dynamic viscosity, $\text{Re}\{f_{CM}\}$ represents the real part of the complex Clausius-Mossotti (CM) factor, f_{CM} , and $\epsilon^* = \epsilon - i\sigma/\omega$ is the complex permittivity with i being the imaginary number, σ the electric conductivity, and ω the field frequency. The subscripts c and f in Eq. (5-3) denote the cell and suspending fluid, respectively.

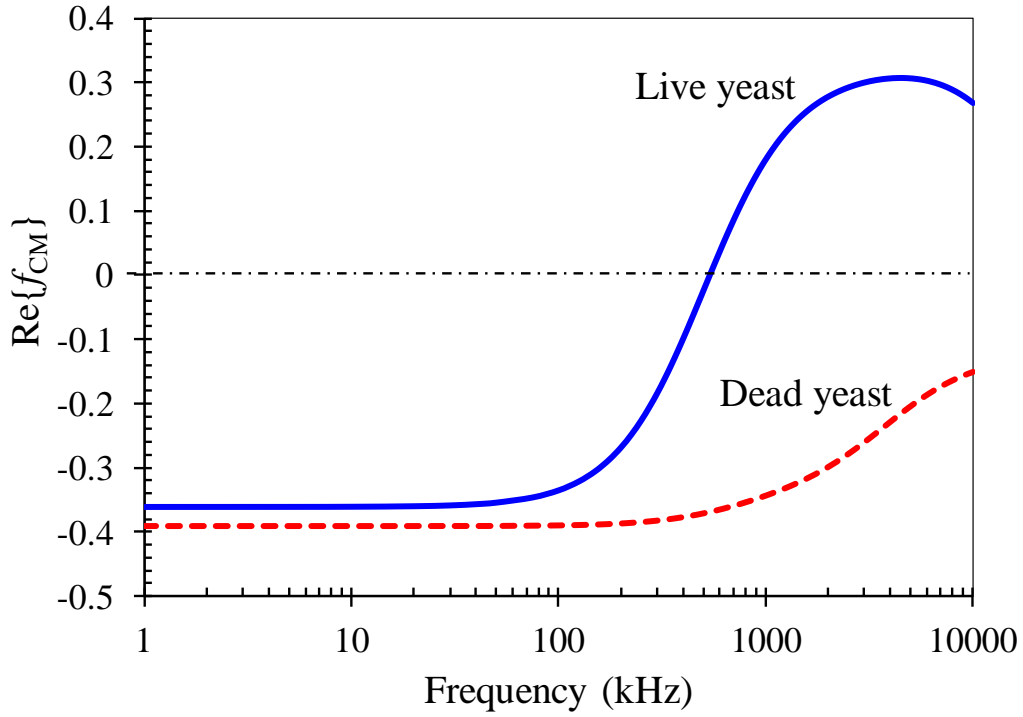


Figure 26: Comparison of the model predicted CM factors of live (solid line) and dead (dashed line) yeast cells suspended in 1 mM phosphate buffer as a function of the electric field frequency. The dash-dot line divides the diagram to positive DEP (top half, $\text{Re}\{f_{CM}\} > 0$) and negative DEP (bottom half, $\text{Re}\{f_{CM}\} < 0$) regions.

The complex permittivities of live and dead yeast cells can be calculated using the so-called multi-shell model (Huang, Y. 1992), where cells are assumed to possess three concentric layers of different electric and dielectric properties in this work. The details of this model and the involving parameters are presented in the section 5.4.1. Figure 26 compares the model predicted CM factors of the two types of cells suspended in 1 mM phosphate buffer as a function of the AC field frequency. Due mainly to their discrepancies in the electric conductivities of cell membrane and cytoplasm (see the 5.4.1), live and dead yeast cells respond dissimilarly to AC electric fields, especially significant when the frequency is over 100 kHz. In the range from DC field (i.e.,

frequency is zero) to 500 kHz AC field, both types of cells possess a negative CM factor while that of dead yeast have a larger magnitude. Therefore, live yeast cells experience a weaker negative rDEP than the dead ones as long as the AC field frequency is less than 500 kHz.

The observed cell velocity, \mathbf{U}_c , at the reservoir-microchannel junction is the vector addition of the DC electrokinetic cell velocity (a combination of fluid electroosmosis and cell electrophoresis), \mathbf{U}_{EK} , and the AC/DC dielectrophoretic velocity, \mathbf{U}_{DEP}

$$\mathbf{U}_c = \mathbf{U}_{EK} + \mathbf{U}_{DEP} = \mu_{EK} \mathbf{E}_{DC} + \mu_{DEP_DC} \nabla E_{DC}^2 + \mu_{DEP_AC} \nabla E_{AC}^2 \quad (5-4)$$

where μ_{EK} is the electrokinetic cell mobility that can be measured experimentally by tracking individual cells at pure DC electric fields, and the dielectrophoretic cell velocity has been split into the DC (zero frequency, i.e., $\omega = 0$) and AC field (RMS value) components. Note that cell inertial, Brownian, and gravity motions are all neglected in Eq. (5-4), which is reasonable for micron-sized cells in microfluidics. Similar to what we have done previously (Zhu, J. 2012; Cummings, E. B. 2000), the cell velocity, \mathbf{U}_c , can be rewritten as follows with respect to the streamline coordinates (see the velocity analysis in figure 24),

$$\begin{aligned} \mathbf{U}_c &= (U_{EK} + U_{DEP,s}) \mathbf{s} + U_{DEP,n} \mathbf{n} \\ &= \left(\mu_{EK} E_{DC} + \mu_{DEP_DC} \frac{\partial E_{DC}^2}{\partial s} + \mu_{DEP_AC} \frac{\partial E_{AC}^2}{\partial s} \right) \mathbf{s} + 2 \left(\mu_{DEP_DC} \frac{E_{DC}^2}{\mathfrak{R}} + \mu_{DEP_AC} \frac{E_{AC}^2}{\mathfrak{R}} \right) \mathbf{n} \end{aligned} \quad (5-5)$$

where U_{EK} is the magnitude of the stream-wise electrokinetic velocity, $U_{DEP,s}$ is the magnitude of the stream-wise dielectrophoretic cell velocity, \hat{s} is the unit vector of the coordinate s along the streamline (equivalent to the electric field lines illustrated in figure 24) (Cummings, E. B. 2000), $U_{DEP,n}$ is the magnitude of the cross-stream dielectrophoretic cell velocity, \hat{n} is the unit vector of the coordinate normal to the streamline, and \mathfrak{R} is the local radius of curvature of the streamline.

In our experiments the frequency of AC electric fields was kept smaller than 500 kHz to ensure negative rDEP for both live and dead yeast cells at the reservoir-microchannel junction (refer to figure 26). Therefore, $U_{DEP,n}$ is directed towards the centerline of the microchannel (see the velocity analysis in figure 24), which produces a focusing effect on the suspended cells at the reservoir-microchannel junction. Meanwhile, $U_{DEP,s}$ is against U_{EK} and thus slows down the entering cells at the junction (figure 24). Moreover, since $U_{DEP,s}$ is a second-order function of both the AC and DC electric fields while U_{EK} is only linearly proportional to the DC field [see, for example, Eq. (5-5), it is certain that $U_{DEP,s}$ can counter-balance U_{EK} when either E_{DC} or E_{AC} increases. At that point and beyond, the stream-wise cell velocity vanishes and cells can be stagnated in front of the reservoir-microchannel junction by rDEP, i.e.,

$$\mu_{EK}E_{DC} + \mu_{DEP_DC}\frac{\partial E_{DC}^2}{\partial s} + \mu_{DEP_AC}\frac{\partial E_{AC}^2}{\partial s} \leq 0 \quad \text{or} \quad \frac{\mu_{EK}}{-\mu_{DEP_DC}} \leq 2 \left(1 + \frac{\mu_{DEP_AC}}{\mu_{DEP_DC}} \alpha^2 \right) \frac{\partial E_{DC}}{\partial s} \quad (5-6)$$

where $\alpha = E_{AC}/E_{DC}$ is the RMS AC to DC field ratio. Note that $\mu_{DEP_DC} < 0$ for negative cell DEP and so $\mu_{EK}/(-\mu_{DEP_DC}) > 0$. The required value of α for trapping cells is a function of two cell mobility ratios: one is the DC electrokinetic to DC dielectrophoretic cell mobility ratio, $\mu_{EK}/(-\mu_{DEP_DC})$, which is dimensional, and the other is the AC to DC dielectrophoretic cell mobility ratio, i.e., $\mu_{DEP_AC}/\mu_{DEP_DC}$, which is non-dimensional. Therefore, we can potentially trap and concentrate one type of cells (e.g., with a smaller $\mu_{EK}/(-\mu_{DEP_DC})$ or larger $\mu_{DEP_AC}/\mu_{DEP_DC}$) in the upstream reservoir while sweeping the other type (e.g., with a larger $\mu_{EK}/(-\mu_{DEP_DC})$ or smaller $\mu_{DEP_AC}/\mu_{DEP_DC}$) to the downstream reservoir. This is likely to happen for the separation of live and dead yeast cells because their CM factors or equivalently the dielectrophoretic mobilities, μ_{DEP} , are different as demonstrated in figure 26.

5.4 Numerical Modeling

The simulation of electrokinetic cell motion from reservoir to microchannel was performed in COMSOL 3.5a (Burlington, MA) using a 2D model developed in our group (Zhu, J. 2009; Church, C. 2009). This model neglects the perturbations on the fluid flow and the electric field caused by the presence of cells. Instead a correction factor, λ_c , is used to account for the effects of cell size (and others if any) on the dielectrophoretic cell velocity. As such, the cell velocity in Eq. (5-4) is rewritten as

$$\mathbf{U}_c = \mu_{EK} \mathbf{E}_{DC} + \lambda_c \mu_{DEP_DC} \left(1 + \frac{\mu_{DEP_AC}}{\mu_{DEP_DC}} \alpha^2 \right) \nabla \mathbf{E}_{DC}^2 \quad (5-7)$$

The DC electric field distribution, $\mathbf{E}_{DC} = -\nabla\phi_{DC}$, was obtained by solving the Laplace equation $\nabla^2\phi_{DC} = 0$ where the DC electric potential, ϕ_{DC} , was experimentally applied. The electrode in each reservoir was simulated by a 0.5 mm-diameter concentric circle, upon which an electric potential is imposed. Specifically the experimentally applied DC voltage was imposed to the electrode in the entry reservoir. The electrode in the exit reservoir was grounded. All microchannel walls are assumed to be electrically insulated.

The cell velocity in Eq. (5-7) was used as an input for the particle tracing function in COMSOL 3.5a. The electrokinetic mobility, μ_{EK} , was determined by tracking the motion of individual cells in the main body of microchannel (where DEP is negligible) under a small DC electric field. They were measured at 2.0×10^{-8} ($\text{m}^2/\text{V}\cdot\text{s}$) and 1.0×10^{-8} ($\text{m}^2/\text{V}\cdot\text{s}$) for the live and dead yeast cells, respectively. The dielectrophoretic mobility was determined using Eq. (5-2) with the typical dynamic viscosity, $\mu = 1.0 \times 10^{-3}$ $\text{kg}/(\text{m}\cdot\text{s})$ and permittivity $\varepsilon_f = 6.9 \times 10^{-10}$ $\text{C}/(\text{V}\cdot\text{m})$ for pure water at 20 °C. A MATLAB code was developed to calculate the CM factors at different electric field frequencies for the live and dead yeast cells using multi-shell model (see the Appendix). The correction factor, λ_c , for both types of yeast (with a diameter of 6 μm) was set to 0.5, which is consistent with our previous studies (Zhu, J. 2011).

5.4.1 Calculation of Complex Permittivities of Live and Dead Yeast Cells

The dielectrophoretic responses of live and dead yeast cells to electric field, i.e., the CM factor f_{CM} in Eq. (5-2), were both calculated using a two-shell model (Huang, Y. 1992; Suehiro, J. 2003). As shown schematically in figure 27, a cell in this model is treated as a dielectric sphere (layer 3, nucleus) covered by two concentric layers (layer 2 for cytoplasmic membrane and layer 1 for cell wall). The complex permittivity of such a cell, i.e., ε_c^* in Eq. (5-8), is computed from (Lewpiriyawong, N. 2011)

$$\varepsilon_c^* = \varepsilon_1^* \frac{\left(\frac{r_1}{r_2}\right)^3 + 2\left(\frac{\varepsilon_{23}^* - \varepsilon_1^*}{\varepsilon_{23}^* + 2\varepsilon_1^*}\right)}{\left(\frac{r_1}{r_2}\right)^3 - \left(\frac{\varepsilon_{23}^* - \varepsilon_1^*}{\varepsilon_{23}^* + 2\varepsilon_1^*}\right)} \quad (5-8)$$

$$\varepsilon_{23}^* = \varepsilon_2^* \frac{\left(\frac{r_2}{r_3}\right)^3 + 2\left(\frac{\varepsilon_3^* - \varepsilon_2^*}{\varepsilon_3^* + 2\varepsilon_2^*}\right)}{\left(\frac{r_2}{r_3}\right)^3 - \left(\frac{\varepsilon_3^* - \varepsilon_2^*}{\varepsilon_3^* + 2\varepsilon_2^*}\right)} \quad (5-9)$$

In the above ε_1^* , ε_2^* , and ε_3^* are, respectively, the complex permittivities of the cell wall, membrane, and nucleus, and are all defined as $\varepsilon^* = \varepsilon - i\sigma/\omega$. The values of the radius r , electric conductivity σ , and permittivity ε for each of the three layers are listed in the table in figure 27.

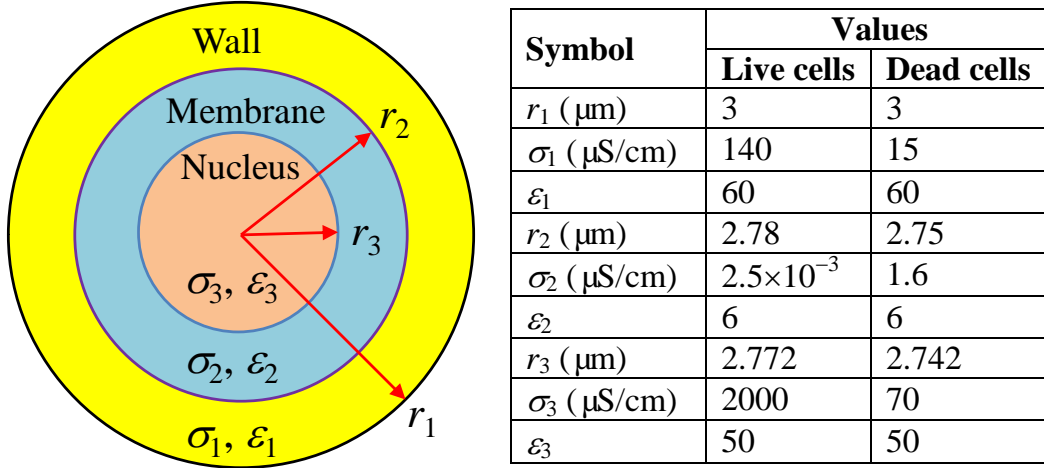


Figure 27: Two-shell model of a yeast cell (not to scale, left panel). The values of the radius, r , electric conductivity, σ , and permittivity, ε , for each layer of the cell are listed in the table (right panel).

5.5 Results and Discussion

5.5.1 Focusing and Trapping of Live Yeast Cells with rDEP

The streak images (top row, obtained by superimposing a sequence of snapshot images) in figure 28 illustrate the typical behaviors of electrokinetic cell motion through the reservoir-microchannel junction under DC-biased AC electric fields. Live yeast cells are used for this demonstration. The applied DC voltage was maintained at 2 V, producing an average DC electric field of 6 V/cm across the microchannel length. The applied AC voltage (RMS value) was fixed at 1 kHz frequency while its magnitude was varied from (a) 0 V (i.e., the AC to DC field ration is $\alpha = 0$) to (b) 30 V (i.e., $\alpha = 15$) and (c) 50 V (i.e., $\alpha = 25$). Under a pure DC electric field, cells migrate through the reservoir-microchannel junction in a nearly uniform distribution over the entire channel width as

seen in figure 28(a). This is attributed to the negligible rDEP induced at the junction under a small DC field.

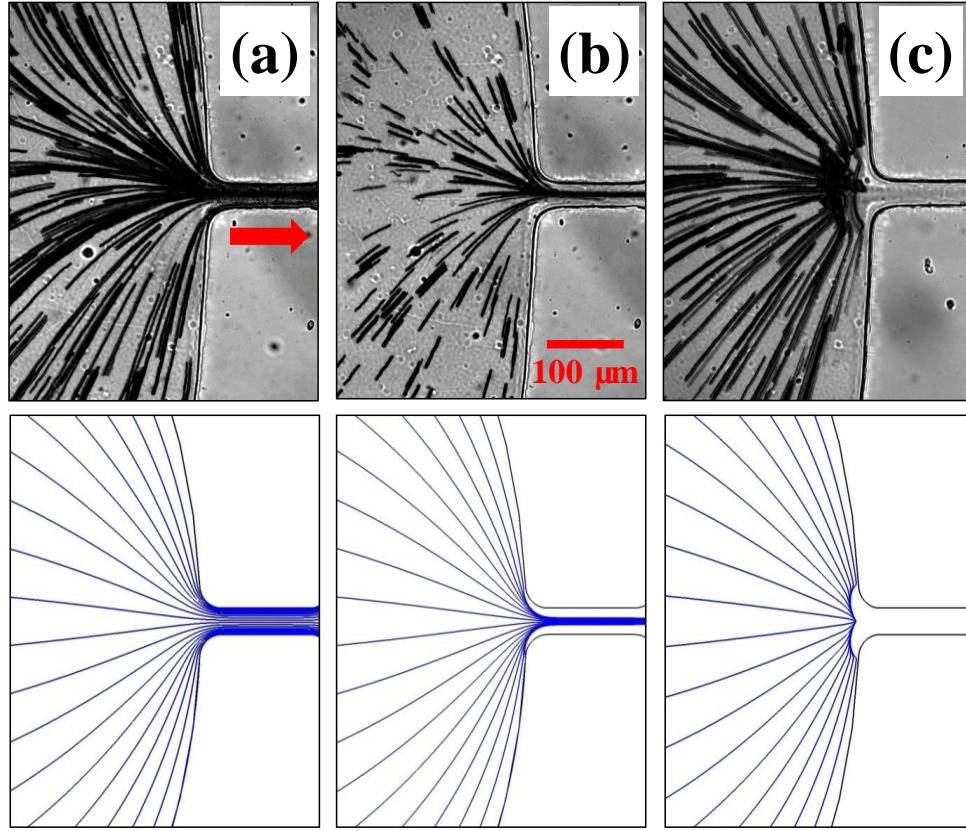


Figure 28: Comparison between experimentally obtained superimposed images (top row) and numerically predicted trajectories (bottom row) of live yeast cells at the reservoir-microchannel junction under the influence of rDEP. In the experiment the applied DC voltage was fixed at 2 V while the AC voltage (RMS) at 1 kHz frequency was varied from (a) 0 V ($\alpha = 0$) to (b) 30 V ($\alpha = 15$) and (c) 50 V ($\alpha = 25$). The block arrow in (a) indicates the cell moving direction.

However, with the inclusion of a 30 V AC voltage, cells get focused due to rDEP and move exclusively along the centerline of the microchannel. This observation in figure 28(b) is consistent with our previous study of polymer bead motions at the reservoir-microchannel junction (Cummings, E. B. 2000). When the AC voltage is further

increased to 50 V, cells, as analyzed in the Theory section, become trapped and concentrated in the reservoir before entering the microchannel [see figure 28(c)]. The numerically predicted cell trajectories at the corresponding experimental conditions are shown in figure 28 (bottom row). A close agreement is obtained for all the three cases discussed above. During the experiment Joule heating effects were found insignificant even at the largest applied electric field [i.e., 156 V/cm on average in case (c)]. This was verified by monitoring the electric current in each test.

5.5.2. Comparison of rDEP Trapping of Live and Dead Yeast Cells

We tested the rDEP trapping of live yeast cells under DC-biased AC electric fields with frequency in the range of 1 kHz to 500 kHz. The DC voltage was fixed at 2 V throughout the measurement. The minimum AC to DC field ratio, α , for a stable cell trapping to occur at the reservoir-microchannel junction is presented in figure 29(a) as a function of the AC field frequency. Due to the decrease in magnitude of the CM factor with increasing frequency (Figure 26), cells should experience a weakened rDEP as the frequency increases, especially significant when the frequency is over 100 kHz. This explains why the experimentally measured (symbols) AC to DC field ratio rises along with frequency figure 29(a). Such a trend is consistent with the numerical prediction (solid line) in figure 29(a). We also tested the rDEP trapping of dead yeast cells using exactly the same approach as for the live ones. The experimental data (symbols) and the corresponding numerical predictions (solid line) are shown in figure 29(b). A similar trend is obtained in between the live and dead yeast cells.

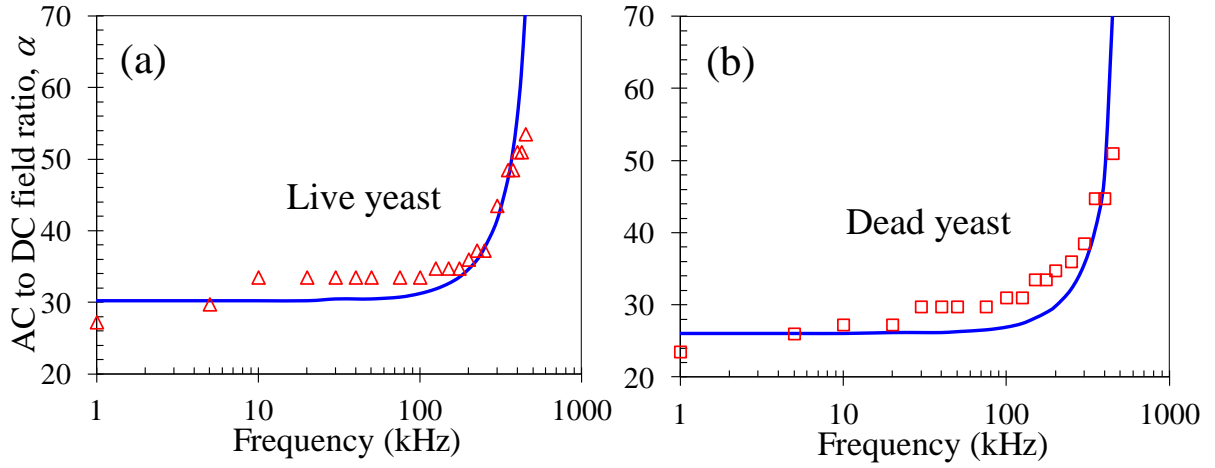


Figure 29: Experimentally recorded (symbols) and numerically predicted (lines) AC to DC electric field ratios, α , for trapping live (a) and dead (b) yeast cells at different AC field frequencies at the reservoir-microchannel junction by rDEP. The DC voltage was maintained at 2 V in both experiments.

However, the AC to DC field ratio for trapping live yeast is larger than that for trapping dead cells in the entire range of the tested AC field frequency. This can be better viewed in figure 30, where the experimentally measured ratios for both types of cells are combined into one plot. As illustrated in figure 26, live yeast cells experience a smaller magnitude of rDEP than do dead cells and so the former possess a smaller AC to DC dielectrophoretic cell mobility ratio, $\mu_{DEP_AC}/\mu_{DEP_DC}$ between the two. Moreover, as they undergo a faster electrokinetic motion, live yeast cells should have a larger DC electrokinetic to DC dielectrophoretic cell mobility ratio, $\mu_{EK}/(-\mu_{DEP_DC})$, than dead yeast cells. The discrepancies in these two ratios mutually explain why the dead yeast cells can be more easily trapped, i.e., at a smaller AC to DC field ratio [refer to Eq. (5-6)].

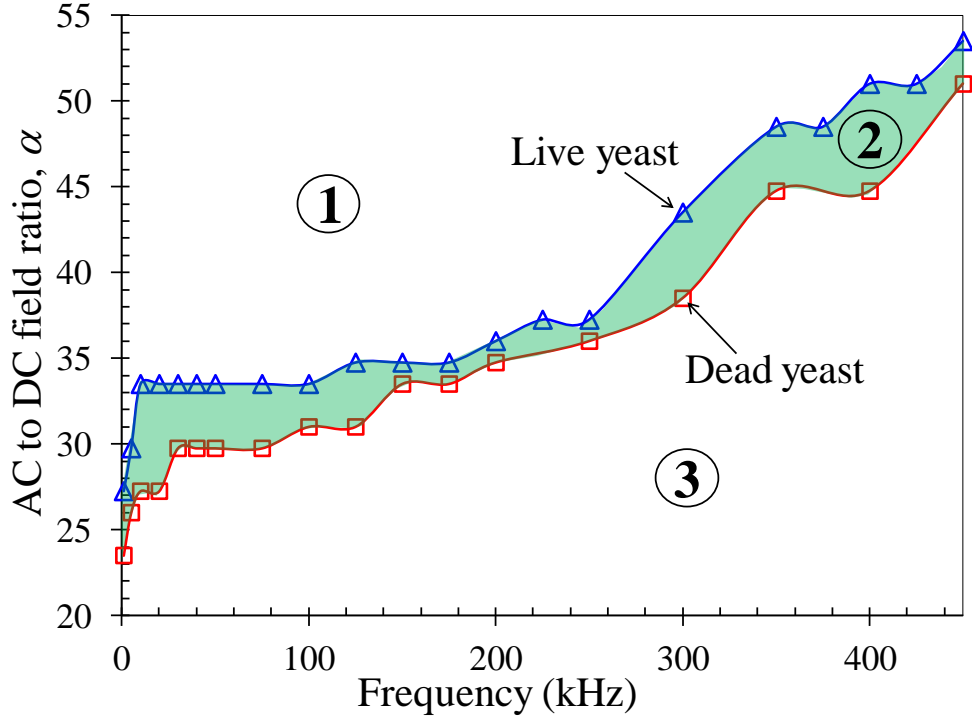


Figure 30: Phase diagram of the experimentally recorded AC to DC field ratios, α , for rDEP trapping of live (triangular symbols) and dead (square symbols) yeast cells at the reservoir-microchannel junction with respect to the AC field frequency. The DC voltage was fixed at 2 V in all measurements. The highlighted area (i.e., Zone 2) indicates the region in which the dead yeast cells can be selectively trapped the continuously separated from live yeast cells by rDEP.

Figure 30 can be used as a phase diagram to guide the electrical manipulation of live and dead yeast cells at the reservoir-microchannel junction using rDEP. The experimentally obtained AC to DC field ratio curves for the two types of cells divide the map into three regions, i.e., Zones 1 to 3 as labeled in figure 30. In Zone 1, the AC to DC field ratio is larger than that for trapping live yeast cells and hence both live and dead cells can get trapped [see figure 28(c)]. In contrast, Zone 3 is the region where the AC to DC field ratio is smaller than that for trapping dead yeast cells. Hence, the induced rDEP is only able to focus both types of cells to the center plane of the microchannel [see figure

28(b)]. In Zone 2, i.e., the highlighted region in figure 30, the AC to DC field ratio is in between the two values required for trapping live and dead yeast cells, respectively. Therefore, dead yeast cells are trapped and concentrated inside the reservoir while live yeast can still travel through the microchannel and be separated from the dead ones. The transition from Zone 1 to Zone 2 and Zone 3, or vice versa, can be easily implemented in two ways. One is to vary the AC to DC field ratio at a fixed AC field frequency, and the other is to adjust the AC field frequency while keeping the AC to DC field ratio constant.

5.5.3 Continuous Separation of Live and Dead Yeast Cells with rDEP

Technically the rDEP separation of live and dead yeast cells at the reservoir-microchannel junction can be realized using a DC-biased AC electric field at any frequency as long as the AC to DC field ratio is within Zone 2 of figure 30. Practically, however, we need to consider a couple of factors in experiments. One factor is that the gap between the AC to DC field ratios for trapping live and dead cells should be the larger the better, which will make the device design and control relatively easy. Figure 30 indicates that we can use the frequency in the range of either 1-100 kHz or 300-400 kHz. The second factor is that the AC field frequency should be the lower the better. It is because a larger AC field needs to be used at a higher frequency (suppose the DC field is fixed), which has two consequences: (1) Joule heating and electrothermal effects may become significant causing adverse influences on the sample and device (Xuan, X. 2008; Sridharan, S. 2011), and (2) the choices of commercially available voltage amplifiers are

significantly limited as the voltage amplification is compromised by the AC field frequency.

Taking these factors into consideration, we conducted the rDEP separation experiment with DC-biased AC electric fields at 1 kHz frequency. It was observed that the application of a 4 V DC-biased 47.5 V AC voltage (i.e., $\alpha = 11.875$) could achieve a selective concentration and continuous separation of live and dead yeast cells at the reservoir-microchannel junction. The experimental and numerical results are displayed in figure 31. Figure 31(a) shows a snapshot image of the cell behaviors at the junction, where the non-fluorescent dead yeast (appearing as dark hollow circles due to optical reflections) are trapped inside the reservoir while the fluorescent live yeast (appearing bright green) enter into the microchannel. The streak images of the live and dead cells are shown in the top row of figure 31(b) and figure 31(c), respectively. Also shown are the numerically predicted cell trajectories in the bottom row, which both agree reasonably well with the experimental results.

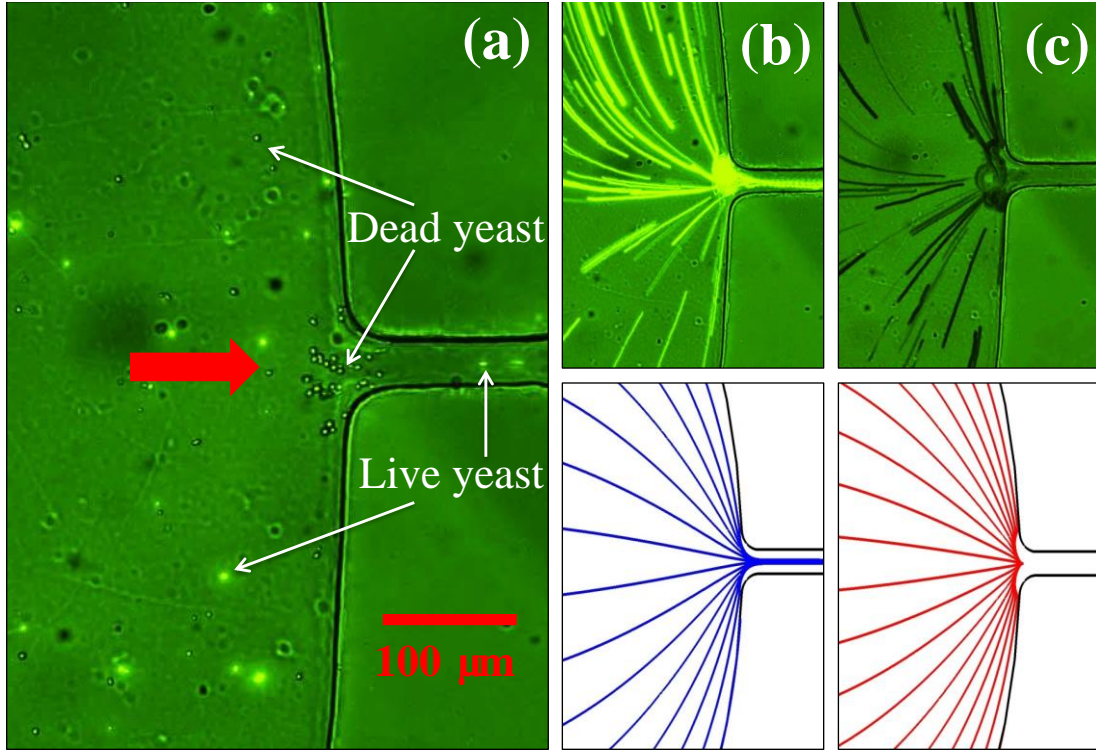


Figure 31: Demonstration of selective concentration and continuous separation of live and dead yeast cells at the reservoir-microchannel junction by rDEP. (a) is a snapshot image, and (b) and (c) compare the experimentally obtained superimposed images (top row) of live (b) and dead (c) yeast cells with the numerically predicted cell trajectories (bottom row). The cell separation was driven by a 4 V DC-biased 47.5 V AC (i.e., $\alpha = 11.875$) at 1 kHz frequency. The block arrow in (a) indicates the cell moving direction.

We admit this is just a preliminary demonstration of the continuous separation of live and dead yeast cells via rDEP. There are several issues that require further studies and may eventually be addressed. One issue is the relatively low cell throughput as the applied voltage is limited by the high-frequency voltage amplifier. This issue may be resolved by using a high-voltage amplifier (then the frequency is limited to a few kHz) or by using a very short microchannel (such as an orifice) to connect the reservoirs. Another issue is the observed dynamic movement of the trapped dead cells at the entrance of the microchannel, which also impacts the motion of the non-trapped live cells. This can be

viewed from the streak images in figure 31(b) and figure 31(c), where a circular region is formed at the reservoir-microchannel junction for each type of cells. We speculate it may be attributed to the cell-cell interactions and perhaps the cell-fluid interactions as well. Such a behavior is not captured in our numerical model as these interactions are either neglected (cell-cell interactions) or not fully considered (cell-fluid interactions).

5.6 Summary

We have developed a new method for continuous microfluidic separation of cells by viability using rDEP. The transporting, focusing, and trapping of live and dead yeast cells at the reservoir-microchannel junction have been demonstrated by simply varying the AC component (either the amplitude or the frequency) of DC-biased AC electric fields. These phenomena can all be reasonably predicted by a simple 2D numerical model. We have also carried out a fundamental study to obtain the AC to DC field ratios for trapping live and dead yeast cells separately in a range of AC field frequencies, both of which agree with the corresponding numerical prediction with a good accuracy. Within the tested frequency range, the AC to DC field ratio for live yeast trapping is higher than that for dead cells as the former experiences a weaker rDEP while having a larger electrokinetic mobility. The difference in this ratio has been utilized to implement a selective concentration and continuous separation of live yeast cells from dead ones at the reservoir-microchannel junction. Since the demonstrated cell separation takes place inside the reservoir, the clogging issue due to the trapped cells can be largely, if not entirely, removed. Moreover, the entire microchannel can be spared for post-analysis,

which makes the developed rDEP manipulation perfectly positioned for lab-on-a-chip devices towards numerous other applications.

CHAPTER 6: Enhanced Throughput for Electrical Manipulation of Particles and Cells in a Stacked Microfluidic Device Using Reservoir-based Dielectrophoresis (rDEP)

6.1 Introduction

High throughput in microfluidic devices required by commercial applications is often a challenge. To attain high throughput in microfluidic devices for cell (Wei Hou, H. 2012; Di Carlo, D. 2007; Mach, A. J. 2010) or particle (Hur, S. C. 2011; Hansson, J. 2012) manipulation and also in rapid droplet (Kim, S. H. 2013; Romanowsky, M. B. 2012) formation parallelization of microchannels is used. The method of using multilayered microchannels (i.e. stacking of PDMS layers consisting of a single microchannel on each layer) to enhance the throughput have also been utilized (Didar, T. F. 2013; Choi, S. 2011). However, the fabrication methods used in parallelization are complex and multilayered microchannels require stacking of several PDMS layers (each layer containing single microchannel) aligned on top of each other making it complicated for integration on miniaturized microfluidic devices. We propose a novel stacked microfluidic device consisting of multiple stacked polydimethylsiloxane (PDMS) layers with multiple microchannels on each layer. The microchannels in different PDMS layers are also vertically aligned so that they can be visualized in the same view field by

adjusting the vertical focus. The stacked microfluidic device proposed herein can operate in parallel on each stacked PDMS layers requiring fewer layers. Thus stacked device allows parallel operations on multiple layers which increase the throughput and reduces the complexity of fabrication. The stacked microfluidic device has the advantage of simple fabrication, is inexpensive and can attain high throughput.

6.2 Experiment

6.2.1 Stacked Microfluidic Device

To achieve high throughput we propose a stacked microfluidic device consisting of multiple layers of PDMS slabs and each layer has multiple microchannels. The microchannels in each PDMS layer were fabricated with PDMS using the standard soft lithography technique. As seen in figure 32, the stacked PDMS-glass microfluidic device has two PDMA layers bonded on top of a glass slide. Each PDMS layer has four straight microchannels of 0.5 mm in length with a 5 mm-diameter reservoir at each end. The channel is 500 μm wide and consists of a constriction with 50 μm -width and 500 μm -length at central the reservoir microchannel junction. The microchannel structure was cut and five holes were punched through the PDMS slab which served as the reservoirs in experiments. The channel side of the PDMS was then plasma treated (PDC-32 G, Harrick Scientific, Ossining, NY) for 1 min along with a clean glass slide. The two treated surfaces were bonded together to form the glass/PDMS microchannel. After plasma treatment, the top PDMS surface of the glass/PDMS microchannel was bonded to the

channel side of another identical PDMS microchannel with the five reservoirs in two PDMS layers are aligned.

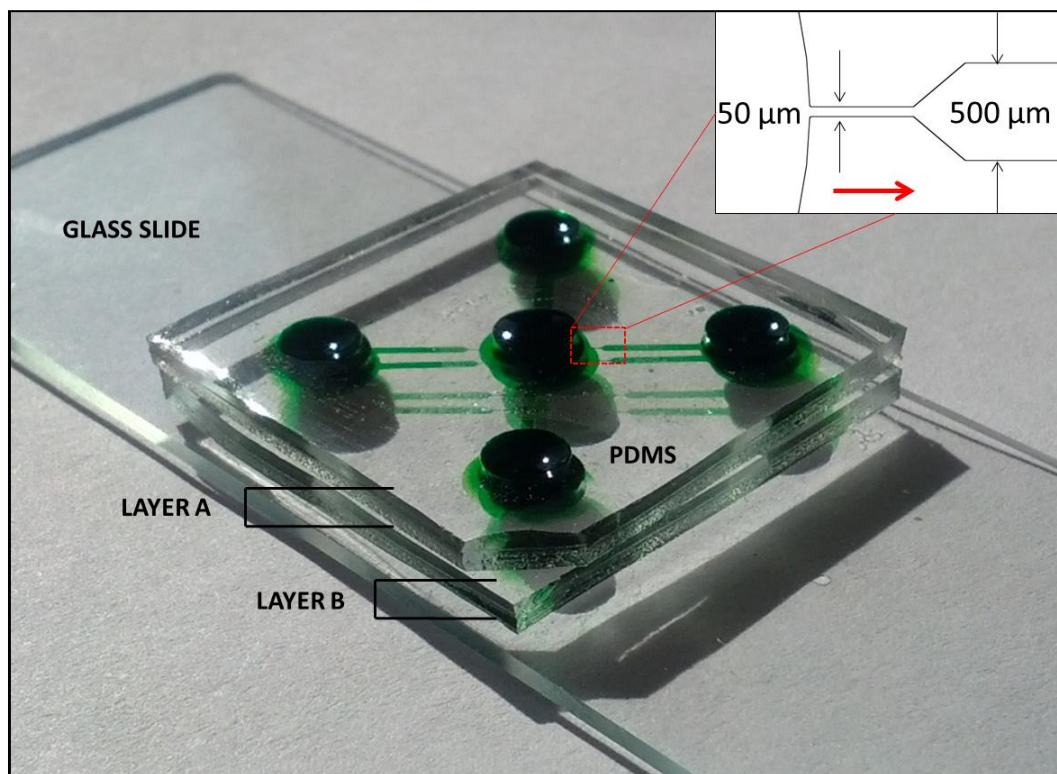


Figure 32: Illustration of a stacked PDMS-glass microfluidic device with two PDMS layers, each of which is composed of four a 0.5 mm-long straight microchannels with a 5 mm-diameter reservoir at each end. The channel is 500 μm wide and has a constriction section of 50 μm in width and 500 μm in length at the central reservoir microchannel junction (see the inset of figure. 32). The arrow in the inset indicates flow direction.

6.2.2 Particle and Cell Solution

Polystyrene particles of 5 μm and 3 μm in diameter (Sigma-Aldrich, St. Louis, MO) were used to demonstrate the size based separation. The particles were suspended in 1 mM phosphate buffer to a final concentration of 10^6 – 10^7 particles per milliliter. Tween

20 (Fisher Scientific, Waltham, MA, USA) was added to the particle solution at 0.1% v/v to suppress the aggregation of particles and their adhesion to channel walls.

Yeast cells (*Saccharomyces Cerevisiae*) were cultured using the standard procedure as detailed in section 5.2.2. *Escherichia coli* ORN178 were cultured in Tryptic Soy Broth containing Ampicillin (100 µg/ml) overnight at 37 °C. The bacterial cells were then washed and re-suspended in 1×PBS to a concentration of 2×10^5 cells/ml. Both the cells were then cleaned and re-suspended again in a 1mM phosphate buffer solution to a final concentration of 10^6 cells per ml.

6.2.3 Experimental Technique

The electrokinetic flow of the particle and cell solutions through the stacked microchannel was attained by imposing DC-biased AC electric fields across the channels. The DC-biased AC voltage was applied to the electrode in the central reservoir and the electrodes in the outer four reservoirs were grounded. The DC-biased AC electric field was supplied by a function generator (33220 A, Agilent Technologies, Santa Clara, CA) in conjunction with a high frequency power amplifier (2100HF, Trek, Inc., Medina, NY). Motion of particles and cells were monitored using an inverted microscope (Nikon Eclipse TE2000U, Nikon Instruments, Lewisville, TX), and the microchannels in the two PDMS layers were visualized by adjusting the vertical focus. The motion of particles and cells were recorded using a CCD camera (Nikon DS-Qi1Mc) connected to the microscope.

6.3 Theory

Time averaged DEP force for a spherical particle is given by (Jones, T. 1995)

$$\mathbf{F}_{DEP} = 2\pi r^3 \varepsilon_m \operatorname{Re}\{f_{CM}(\omega)\} \nabla E^2 \quad (6-1)$$

where r is the particle or cell radius, ε_m is the permittivity of the medium, $\operatorname{Re}\{f_{CM}(\omega)\}$ is the real part of the effective Clausius-Mossotti factor with ω being the angular field frequency and E is the total electric field applied. The $f_{CM}(\omega)$ is given by

$$f_{CM}(\omega) = \frac{\varepsilon_p^* - \varepsilon_m^*}{\varepsilon_p^* + 2\varepsilon_m^*} \quad (6-2)$$

where ε^* is the complex permittivity and defined as shown in Eq. (6-3). The complex permittivity is a function of permittivity ε , conductivity σ and angular frequency ω . The subscript p and m in Eq. (6-2) stands for particle and medium, respectively.

$$\varepsilon^* = \varepsilon - i \left[\frac{\sigma}{\omega} \right] \quad (6-3)$$

Based on the sign of $f_{CM}(\omega)$ particle or cell experiences positive DEP; which means translation motion towards higher electric field region, or negative DEP; which means translation motion towards lower electric field regions. The dielectrophoretic motion, \mathbf{U}_{DEP} , is induced by the inherently non-uniform electric field at the reservoir-microchannel junction.

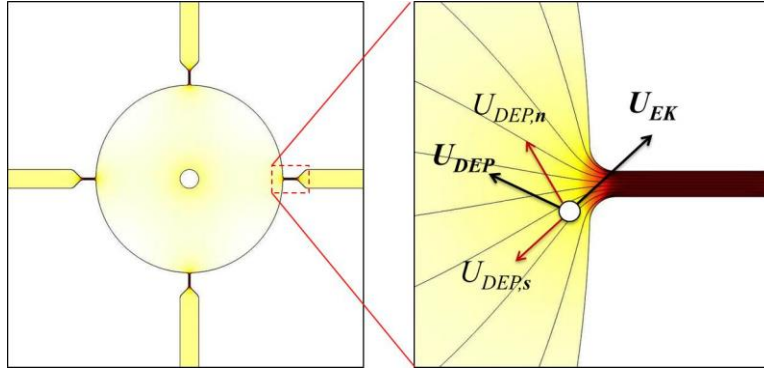


Figure 33: Velocity analysis of a particle at the reservoir-microchannel junction due to electrokinetic flow and the induced rDEP. The thin lines represent the electric field lines or equivalently fluid streamlines in the absence of the particle. The background color shows the electric field contour.

The dielectrophoretic velocity, \mathbf{U}_{DEP} can be obtained by equating \mathbf{F}_{DEP} with Stokes drag on a spherical particle. The superimposition of electrokinetic velocity and dielectrophoretic velocity results into actual particle velocity, \mathbf{U}_P at the reservoir-microchannel junction given by

$$\mathbf{U}_p = \mathbf{U}_{EK} + \mathbf{U}_{DEP} = \mu_{EK} \mathbf{E}_{DC} + \mu_{DEP} (\mathbf{E} \cdot \nabla \mathbf{E}) \quad (6-3)$$

where μ_{EK} is the electrokinetic mobility and μ_{DEP} is the dielectrophoretic mobility which is similar to ones described in earlier chapters. Particles and cells experience negative DEP at low electric field frequencies. The dielectrophoretic velocity acts counter to the electrokinetic velocity of a particle or cell as shown in figure 33. With the increase in AC electric field the DEP force increases considerably as it is function of both the DC and AC electric fields consequently increasing the DEP velocity. At sufficient AC voltages dielectrophoretic velocity counteracts the electrokinetic velocity of the particles and thus

trapping them at the reservoir-microchannel junction. The rDEP trapping can be utilized to separate particles based on size in the stacked microfluidic device as the DEP force responsible for trapping is a function of particle size. Particles attributing variation in size can be selectively separated and concentrated at the reservoir-microchannel junction in a stacked microfluidic device.

6.4 Numerical Simulation

Under thin electrical double layer approximation the DC electric field distribution, $E_{DC} = -\nabla\phi_{DC}$, is governed by 2D Laplace equation

$$\nabla^2\phi_{DC} = 0, \quad (6-4)$$

Electric insulation boundary condition is specified on the channel wall, and imposed voltages on the surfaces of the electrodes. The potential, ϕ_{DC} , is numerically solved using commercial finite element package, COMSOL Multiphysics 4.2a (Burlington, MA). With the known DC electric field the particle velocity is calculated by:

$$\mathbf{U} = \mu_{EK}\mathbf{E}_{DC} + \lambda_c\mu_{DEP}(1+\alpha)^2(\mathbf{E}_{DC}\cdot\nabla\mathbf{E}_{DC}) \quad (6-5)$$

Where, the value of λ_c accounts for the errors in the computation of particle and cell velocity caused by the perturbation of the local flow and electric fields by the presence of finite sized particle and cell. Its value varies from 0 to 1 and decreases with the increase in particle or cell size. The zeta potentials of the channel wall and particle are respectively taken to be -50 mV and -35 mV. The dielectrophoretic particle mobility, μ_{DEP} , in Eq. (6-3) was calculated using the typical dynamic viscosity, $\eta_f = 1.0 \times 10^{-3}$

kg/m•s and permittivity $\epsilon_f = 6.9 \times 10^{-10}$ C/v•m for pure water at 20 °C. The correction factors for the 5 μm and 3 μm particles are, respectively, 0.6 and 0.8, which is consistent with our previous work (Zhu, J. 2012; Patel, S. 2012). In the numerical modeling the average yeast cell diameter used is 5 μm . The CM factor for the yeast cells was calculated using multi-shell model (Patel, S. 2012).

6.5 Results and Discussion

6.5.1 5 μm Particles Concentration and Separation from 3 μm Particles

Figure 34(a)-34(c) demonstrates the electrokinetic trapping of 5 μm particles at different reservoir-microchannel junctions of the stacked device at 50 V DC and 500 V AC. A DC-biased AC voltage was applied to attain particle trapping. The DC field was fixed at 50 V DC and the AC field was varied from low to high until trapping was realized. The frequency of the AC voltage was fixed at 1 kHz, which is well below the charge relaxation frequency of the electrolyte (~ 5 MHz).

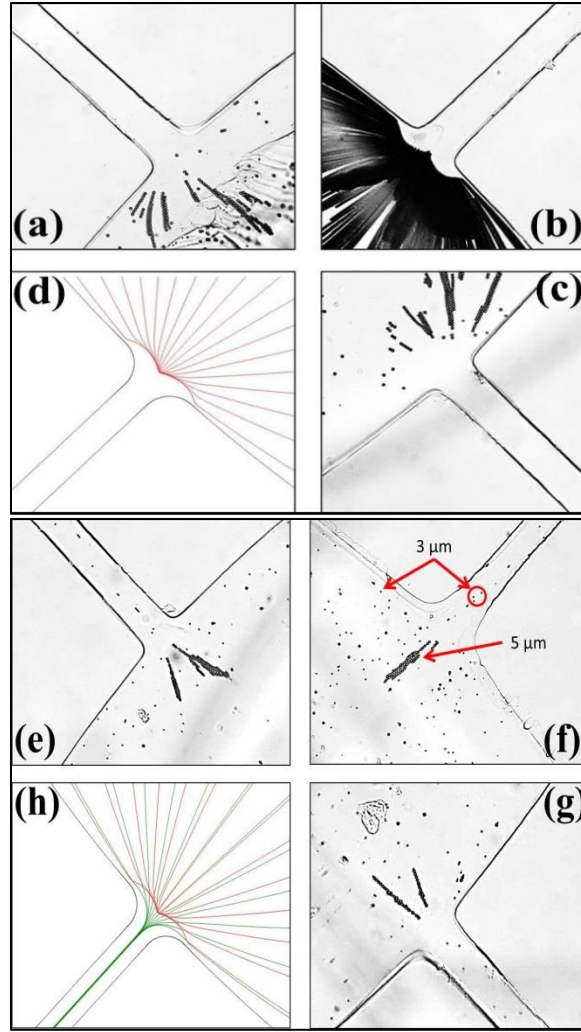


Figure 34: Comparison of experimentally obtained snapshot and superimposed images and, numerically predicted trajectories for 5 μm particles at the reservoir-microchannel junction. Where, 34(a) and 34(c) are reservoir-microchannel junctions from layer A (see figure 32) representing trapping (50V DC and 500V AC) of particles in the images. Image 34(b) represents the superimposed image of particle trapping from layer B. 34(e), 34(f) and 34(g) are experimentally obtained snapshot images demonstrating the separation of 5 μm and 3 μm particles by the rDEP. 34(d) and 34(h) represents the numerically predicted trajectories for trapping and separation respectively.

When the DEP force at the reservoir-microchannel junction is equal to or larger than the hydrodynamic forces acting on the particles they are trapped. DEP force increases as the ratio of the AC to DC field, α , increases. For AC Voltage of 500 V ($\alpha = 10$), the

DEP force becomes strong enough to overcome the hydrodynamic force acting on the particles, and the particles are thereby trapped inside the central reservoir near the central reservoir-microchannel junctions, as shown in figure 34(b) (superimposed image). The experimentally obtained results in image 34(a)-34(c) qualitatively agree with the numerically predicted particle trajectories shown in 34(d).

In figure 33 we also demonstrate the use of rDEP to separate micro-particles of different sizes at the central reservoir-microchannel junctions. Figure 34(e)-34(g) shows the experimentally observed electrokinetic separation of a mixture of 5 and 3 μm particles. The 3 μm particles are driven through the microchannel by electroosmotic flow, while the 5 μm particles are trapped and form pearl chains within the central reservoir near the entrance of the microchannels on application of 50 V DC biased 500 V AC voltages. The DEP force is also proportional to particle or cell volume. DEP force acting on the 3 μm particles is lower than that on the 5 μm particles, and is not enough to overcome the hydrodynamic force. Therefore, 3 μm particles cannot be trapped by the DEP force at the reservoir-microchannel junctions at the applied voltage, and flows through the microchannels towards the downstream reservoirs. In contrast, 5 μm particles are trapped inside the reservoir near the entrance as the DEP force generated at the applied voltage is sufficiently high to overcome hydrodynamic forces. Figure 34(e)-34(g) clearly shows that we can continuously separate 5 μm particles from 3 μm particles by rDEP. The theoretical predictions of trajectories of 3 and 5 μm particles in figure 34(h) shows that the 3 μm particles are focused and pass along the centerline of the

microchannel, while the large 5 μm particles are trapped inside the reservoir. The theoretical predictions qualitatively agree with the experimental observations.

Selective concentration and continuous separation of 5 μm from 3 μm polystyrene particles at the reservoir microchannel junction using reservoir-based dielectrophoresis (rDEP) is demonstrated in the stacked microfluidic device. The observed experimental results qualitatively agree with the predictions of a mathematical model for electrokinetic transport of the fluid and particles. Selective concentration and continuous separation of *Saccharomyces Cerevisiae* (yeast) from *Escherichia coli* (*E. coli*) at the reservoir-microchannel junction using reservoir-based dielectrophoresis (rDEP) has also been studied experimentally and is presented in the next section.

6.5.2 Yeast Cells Concentration and Separation from *E. coli*

Figure 35(a)-35(c) depicts the experimentally observed trapping of yeast cells by rDEP at the central reservoir-microchannel junctions, under the action of a DC-biased AC voltage. In the experiment, we use a lower DC voltage of 25 V to achieve the trapping at a lower AC Voltage for minimizing the Joule heating effect, which affects cells' viability. Under 25 V DC and 200 V AC voltage the yeast cells experience DEP force capable to overcome the hydrodynamic forces and are trapped at the junction. The experimental observations are in qualitative agreement with the theoretical predictions of the particle trajectories, as shown in figure 35(d). As the ratio of the AC to DC field increases, the resulting DEP force increases, leading to more yeast cells trapped at the central reservoir-microchannel junctions.

The concentration of the yeast cells trapped at the junction in the bottom microchannels is higher than that in the upper ones due to the gravitational effect. Suspended yeast cells tend to settle at the bottom of the central reservoir resulting in higher cell concentration in the bottom of the reservoir, leading to more cells trapped at the bottom junctions.

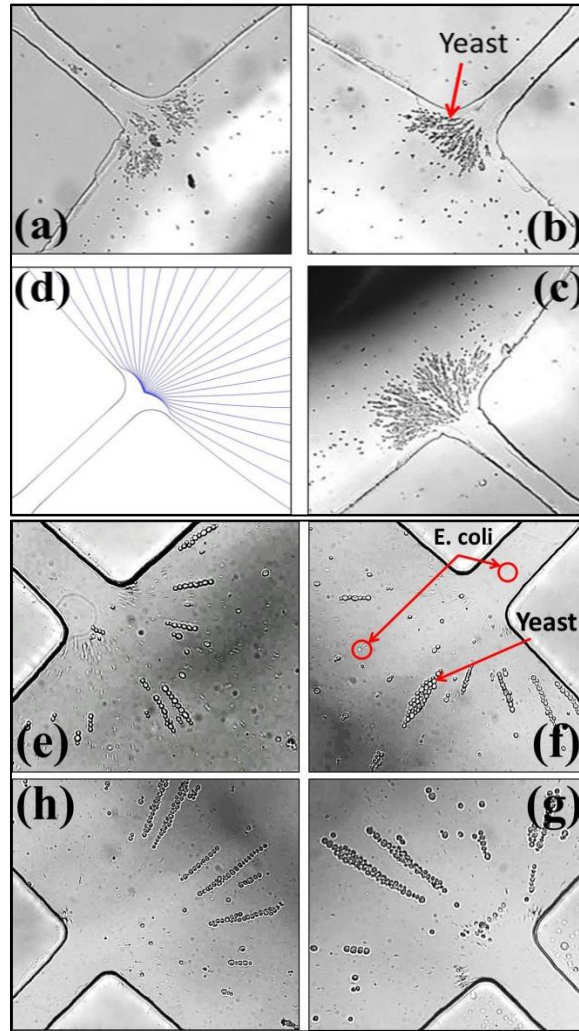


Figure 35: Experimentally obtained snapshot images of yeast cell trapping and, yeast cell and *E. coli* separation at the reservoir-microchannel junction. Images 35(a), 35(b) and 35(c) demonstrate the trapping of yeast cells (25V dc and 200V ac) at the reservoir

microchannel junction. Image 35(d) represents the numerically predicted cell trajectories. Images 35(e)-35(h) are experimentally obtained snapshot images of yeast and *E. coli* cell separation at the junction.

Figure 35(e)-35(h) shows the separation of yeast cells and *E. coli* at four different reservoir-microchannel junctions. Pressure driven flow was used utilized to achieve the cell separation shown in figure 35. The flow rate of the cell solution through the microchannels can be increased easily if pressure driven flow is utilized thus increasing the throughput considerably. Pressure driven flow is also independent of the cell surface properties (i.e. surface charge) enabling the cells to have uniform velocities. The AC DEP force generated on the application of AC electric field across each microchannel depends on the cell size which can be exploited to selectively separate and concentrate cells using rDEP. In the cell separation experiment the mixture of yeast and *E. coli* cell solution is continuously pumped from the central reservoir towards the downstream reservoirs by a pressure driven flow induced by higher liquid height in the central reservoir compared to the outer reservoir. In addition, an external AC field was applied across each microchannel to create AC DEP force at the central reservoir-microchannel junctions and the outer four reservoirs were grounded. The AC field generated DEP force is against the hydrodynamic force stemming from the pressure driven flow. Since yeast cells are much larger ($\sim 5 \mu\text{m}$ in diameter) than *E. coli* cells ($\sim 1 \mu\text{m}$ in diameter), the DEP force experienced by the yeast cells is significantly higher than that on *E. coli* cells. Therefore, yeast cells can be concentrated in the central reservoir, while *E. coli* cells are driven by the pressure-driven flow from the central reservoir through the microchannels towards the downstream reservoirs. Figure 35(e)-35(h) shows that yeast cells are trapped at the

central reservoir-microchannel junction while the *E. coli* cells can still pass through the microchannel. The *E. coli* cells being translucent and very small in size are difficult to be visualized in the images.

6.6 Summary

This work successfully demonstrates continuous separation of particles and cells by size based on rDEP occurring at the reservoir-microchannel junction. Stacked multiple microchannels are proposed and fabricated to increase the throughput. The proposed stacked microfluidic device can operate in parallel and is simple to fabricate. The device is tested by separating particles of different size and separation of yeast cells and *E. coli* bacteria. The throughput is proportional to the number of stacked PDMS layers and microchannels in each PDMS layer. One potential problem in the stacked device is the increase in the volumetric Joule heating effects which is proportional to the number of microchannels stacked in the device. Joule heating can be avoided by using 3D rDEP which can considerably reduce the electric field required for trapping and separating particles at the reservoir-microchannel junction. 3D rDEP utilizes the electric field gradients in the vertical plane along with the ones in horizontal plane. The working principle for particle manipulation using 3D rDEP is proposed in the next chapter.

CHAPTER 7: Three Dimensional Characterization of Electrokinetic Particle Entry Through Reservoir- microchannel Junction

7.1 Introduction

In Chapters 2, 3, 4, 5 and 6 micron-sized particles and cells were trapped and separated at the reservoir-microchannel junction using reservoir-based dielectrophoretic method (rDEP). For sub-micron sized particle and cell trapping at the reservoir-microchannel junction relatively larger electric fields is necessary. Application of large electric fields results into Joule heating which gives rise to electrothermal flow circulations reducing or distorting the particle trapping at the junction (Patel, S. 2013; Kale, A. 2013). In order to overcome this negative effect, we propose a three dimensional electric field gradient utilization to attain trapping of sub-micron particles at the junction. In the rDEP focusing and trapping demonstrated for the micron-sized particles the inherent electric field gradients formed in the horizontal plane of the device were used. However, if the reservoir is formed by punching a hole right at the starting of the microchannel a height difference between the reservoir and the microchannel can be created. As a result, the height difference gives rise to electric field gradients in the vertical direction as well. The increased electric field gradients at the reservoir-

microchannel junction can enhance the DEP force and reduce the overall external electric field required to trap the particles.

7.2 Experiment

The straight microchannel with constrictions at both ends was fabricated with PDMS using the standard soft lithography method, and the fabrication process is detailed in Chapter 2. The microchannel used for the experiments consists of 1 cm long straight section with 0.1 cm constrictions at both the ends. The channel is 500 μm wide in the main body and has a constriction section of 50 μm in width at both the ends. The channel has a uniform depth of 40 μm throughout. The microchannels utilized to obtain (a) two-dimensional and (b) three-dimensional characterization of particles are shown in figure 36. In the microchannel utilized for two-dimensional characterization the reservoirs are punched at an offset from the reservoir-microchannel junction. The inset in figure 36(a) is used to display the reservoir location. The reservoir when punched at an offset, created a section of reservoir that has the same depth as that of the microchannel. The microchannel in figure 36(b) is the one used to obtain three-dimensional characterization. As seen from the inset, the reservoir in this microchannel is punched right at the reservoir-microchannel interface. The resulting geometry allows for a sharp transition in the depth of the microchannel device at the reservoir-microchannel junction.

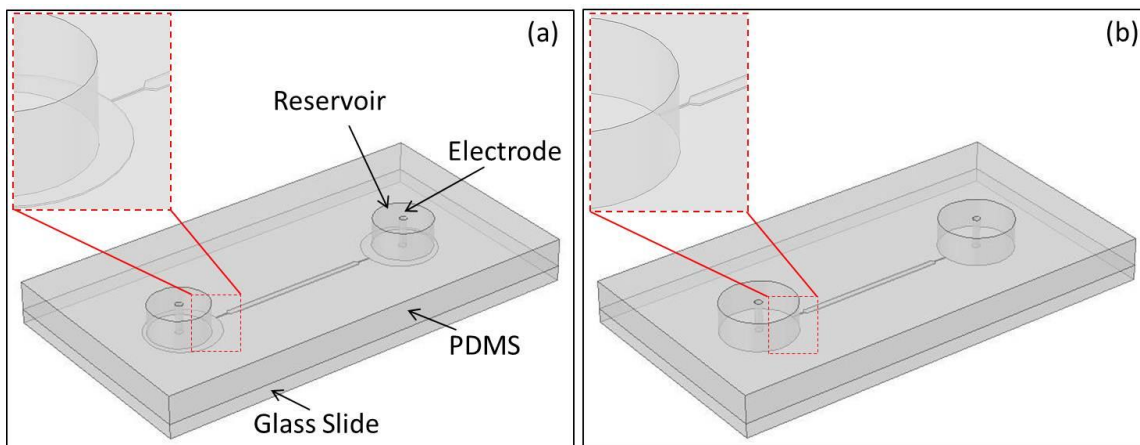


Figure 36: Schematic view of microfluidic devices used to obtain (a) two-dimensional, and (b) three-dimensional particle focusing and trapping. The inset illustrates the difference in location of the reservoirs in the devices used for two-dimensional and three-dimensional characterization of particles.

In the experiment, polystyrene particles of 5 μm diameter (Sigma-Aldrich, USA) were re-suspended in a solution made by mixing 1mM phosphate buffer and glycerol at a volume ratio of 78:22 (Chang, N. 2008). The concentration of particles in the solution is maintained to be about $10^6 - 10^7$ particles per mL. The addition of glycerol to the buffer solution at the above mentioned ratio allows for the mass density of the particles and the resulting solution to be equal. The particle transport was obtained by electric fields supplied using a function generator (33220A, Agilent Technologies, Santa Clara, CA) in conjunction with a high-voltage amplifier (609E-6, Trek, Medina, NY). The particles are visualized with a CCD camera (Nikon DS-Qi 1 Mc) through an inverted microscope (Nikon TE2000U, Nikon Instruments, Lewisville, TX).

7.3 Theory

The electric field \mathbf{E} , becomes inherently non-uniform at the reservoir-microchannel junction due the significant mismatch between size of the reservoir and microchannel. Figure 37(a) shows the contour of electric field magnitude, \mathbf{E} , in the microchannel from the top view and the side view at the junction. Particles experience a dielectrophoretic force, \mathbf{F}_{DEP} , when they move electrokinetically through the reservoir-microchannel junction. Figure 37(a) shows the dielectrophoretic force, \mathbf{F}_{DEP} , generated due to the electric field gradients at the reservoir-microchannel junction. The time averaged dipole moment approximation of \mathbf{F}_{DEP} on an isolated spherical particle is given by (Jones, T. 1995)

$$\mathbf{F}_{DEP} = \frac{1}{2} \pi \epsilon_f d^3 f_{CM} (\mathbf{E} \cdot \nabla \mathbf{E}) \quad (7-1)$$

where ϵ_f is the fluid permittivity, d the particle diameter, f_{CM} the Clausius-Mossotti factor which is a function of particle and fluid conductivities.

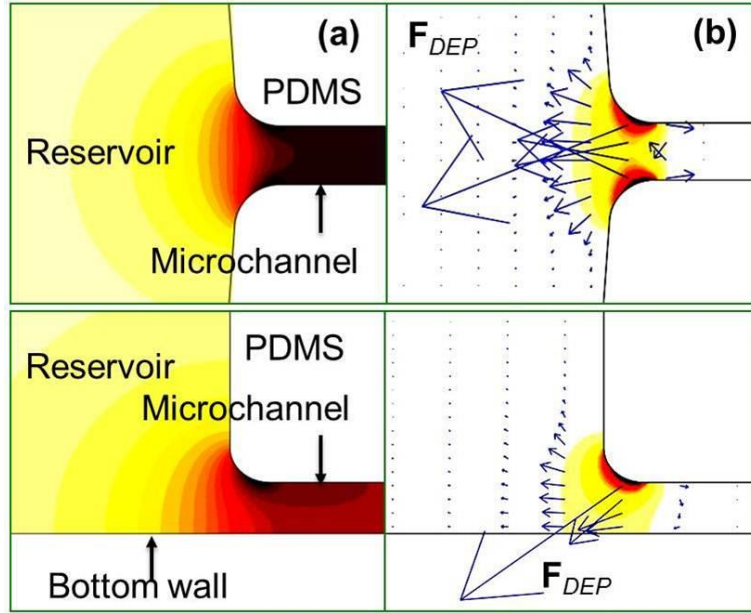


Figure 37: Illustration of (a) electric field \mathbf{E} and (b) dielectrophoretic force, \mathbf{F}_{DEP} distribution at the reservoir-microchannel junction. The top and bottom image on the left represents the top view and the side view of electric field distribution at the reservoir-microchannel junction. The images on the right represent the dielectrophoretic force (\mathbf{F}_{DEP}) distribution at the junction.

The polystyrene particles typically are poor conductors in DC and low-frequency AC electric fields, leading to negative dielectrophoresis. Thus, \mathbf{F}_{DEP} on these particles is directed towards the lower electric field regions as indicated by the arrows in figure 37(b). The underlying physics for two-dimensional focusing and trapping is extensively explained in the previous chapters. As seen in figure 37(c), \mathbf{F}_{DEP} is directed towards the centerline and the also towards the bottom wall of the microchannel in the horizontal and vertical planes respectively. As discussed earlier, if the height difference between the microchannel and the reservoir is large, particles should experience three-dimensional focusing at the reservoir-microchannel junction. In contrast to two-dimensional, three-dimensional focusing utilizes electric field gradients in both the horizontal and vertical

directions. Therefore, we may be able to focus and trap particles at a lower voltage ratios in three-dimensional compared to two-dimensional. Also, we may be able to trap particles of sub-micron range by simply reducing the microchannel depth.

7.4 Numerical Simulation

The computational domain considers full scale three-dimensional microfluidic device used in the experiments (refer to figure 36). It considers the fluid in the microchannel and the inlet/outlet reservoirs. The simulation of the electrokinetic particle motion from reservoir to the microchannel was conducted in COMSOL 4.3b (Burlington, MA) using particle tracing function. The model utilized accounts for the effect of electric and flow fields on the particles. However, the perturbation of electric and flow field due to the presence of the particle is neglected. To account for the effects of the particle size on the dielectrophoretic velocity, a correction factor, c , is introduced. The particle velocity is written as

$$\mathbf{U}_p = \mu_{EK} \mathbf{E} + c \mu_{DEP} (\mathbf{E} \cdot \nabla \mathbf{E}) \quad (7-2)$$

where μ_{EK} denotes the electrokinetic mobility, a combination of electroosmotic and electrophoretic mobility. μ_{DEP} is the dielectrophoretic mobility of the particle obtained from substituting values of material properties used during the experiments. All the particles are assumed to be massless and uniformly distributed when entering the microchannel. The DC electric field, $\mathbf{E} = -\nabla \phi$, is obtained by solving the Laplace

equation $\nabla^2\phi = 0$ in COMSOL. The electric voltage was imposed on the electrode in the inlet reservoir and the electrode in the outlet reservoir was grounded. All the microchannel walls were imposed with an electrical insulation condition. The electrokinetic mobility, μ_{EK} was obtained by tracing individual particles in a straight channel where DEP is negligible. The measured electrokinetic mobility for the 5 μm particles were $3.2 \times 10^{-8} \text{ (m}^2/\text{V}\cdot\text{s)}$. The value of -0.5 was used for the Clausius-Mossotti factor. The numerical value for the correction factor, c , that accounts for the perturbation of fields due to finite particle size was taken as 0.5. The value was determined by fitting the predicted particle trajectories to the observed particle streak lines at the reservoir-microchannel junction.

7.5 Results and Discussion

7.5.1 Comparison Between Two-dimensional and Three-dimensional Particle Focusing

Figure 38 demonstrates 5 μm particle focusing in the two-dimensional (refer figure 36(a)) microchannel under various DC-biased AC voltages. Under pure DC field of 25 V as seen in figure 38(a), the 5 μm particles occupy the full channel width. The DEP force experiences by the particles in the absence of AC field at the reservoir-microchannel junction is low and hence the particles are not deflected towards the center of the microchannel. From the snapshot images on the left, the particles can be seen in different plane. Some particles are optically well focused compared to others suggesting

that the particles occupy the channel in depth-wise direction as well. The figure 38(a) on the right is of experimentally obtained superimposed and numerically predicted trajectories of the 5 μm particles. There is a close agreement between the experimentally obtained and numerically predicted trajectories. On application of AC field of 150 V along with the DC field of 25 V, the particles experience a DEP force and are pushed towards the center of the microchannel. As seen in figure 38(b), the particle stream is narrow and does not occupy the full channel width. The narrow particle stream width suggests that they are undergoing two-dimensional focusing. In the experimentally obtained snapshot images in figure 38(b), it can be seen that all the particles are not very well optically focused. This suggests that particles occupy the channel depth in different plane and are not focused well in the depth-wise direction. Finally, on application of 300 V AC along with 25 V DC, the particles pass through the center of the channel in a single file suggesting a very good two-dimensional focusing. However, on observing the snapshot image of the same in figure 38(c), we can still see particles optically not focused. The snapshot images suggest that even on application of high DC-biased AC voltages the particles are only focused in the horizontal plane (two-dimensional) and the focusing in the vertical plane is absent. The experimentally obtained snapshot and superimposed images agree closely with the numerically predicted trajectories of the particles.

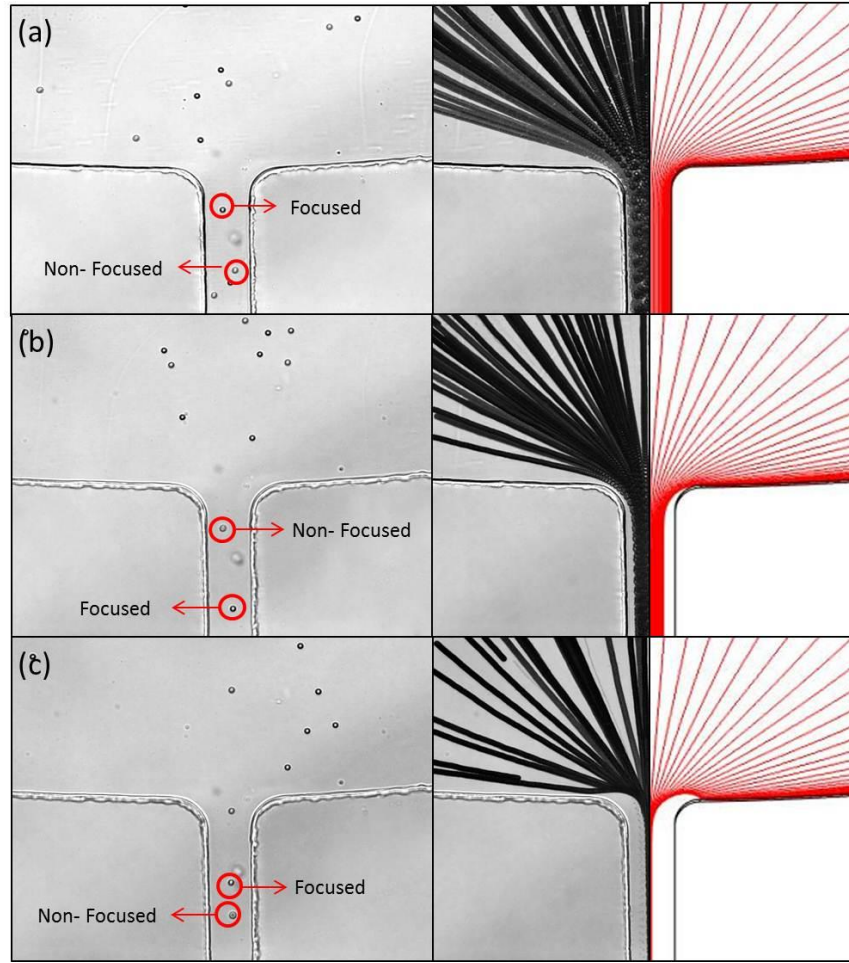


Figure 38: Comparison between experimentally obtained (snapshot and superimposed) and numerically predicted trajectories of 5 μm particles subjected to two-dimensional focusing at the reservoir-microchannel junction under the influence of rDEP at various DC-biased AC voltages. The DC voltage applied, is fixed at 25 V and the AC (RMS) voltage at 1 kHz frequency is varied from (a) 0 V ($\alpha=0$) to (b) 150 V ($\alpha=6$), and (c) 300 V ($\alpha=12$).

Figure 39 demonstrates 5 μm particle focusing in the 2-dimesional (refer figure 36(b)) microchannel under various DC-biased AC voltages. Under pure DC field of 25 V as seen in figure 38(a), the 5 μm particles occupy the full channel width. The DEP force experiences by the particles in the absence of AC field at the reservoir-microchannel junction is low and hence the particles are not deflected towards the center of the

microchannel. From the snapshot images on the left, the particles can be seen in different plane. Some particles are optically well focused compared to others suggesting that the particles occupy the channel in depth-wise direction as well. On application of AC field of 150 V along with the DC field of 25 V, the particles experience a DEP force and are pushed towards the center of the microchannel. As seen in figure 39(b), the particle stream is narrow and does not occupy the full channel width. The narrow particle stream width suggests that they are undergoing focusing in the horizontal plane. In the experimentally obtained snapshot images in figure 39(b), it can be seen that all the particles are not very well optically focused. This suggests that particles occupy the channel depth in different plane and are not focused well in the depth-wise direction. However, the particles have a better resolution compared to the 25 V pure DC case. This suggests that the particles are gradually undergoing focusing in vertical plane as well. Finally, on application of 300 V AC along with 25 V DC, the particles pass through the center of the channel in a single file suggesting a very good horizontal plane focusing. On observing the snapshot image of the same in figure 39(c), we can observe that all the particles are optically focused. The snapshot images suggest that on application of high DC-biased AC voltages the particles are not only focused in the horizontal plane but also in the vertical plane. The particles occupy the center of the channel and are also optically focused, suggesting a good 3-dimesional focusing. The experimentally obtained snapshot and superimposed images agree closely with the numerically predicted trajectories of the particles.

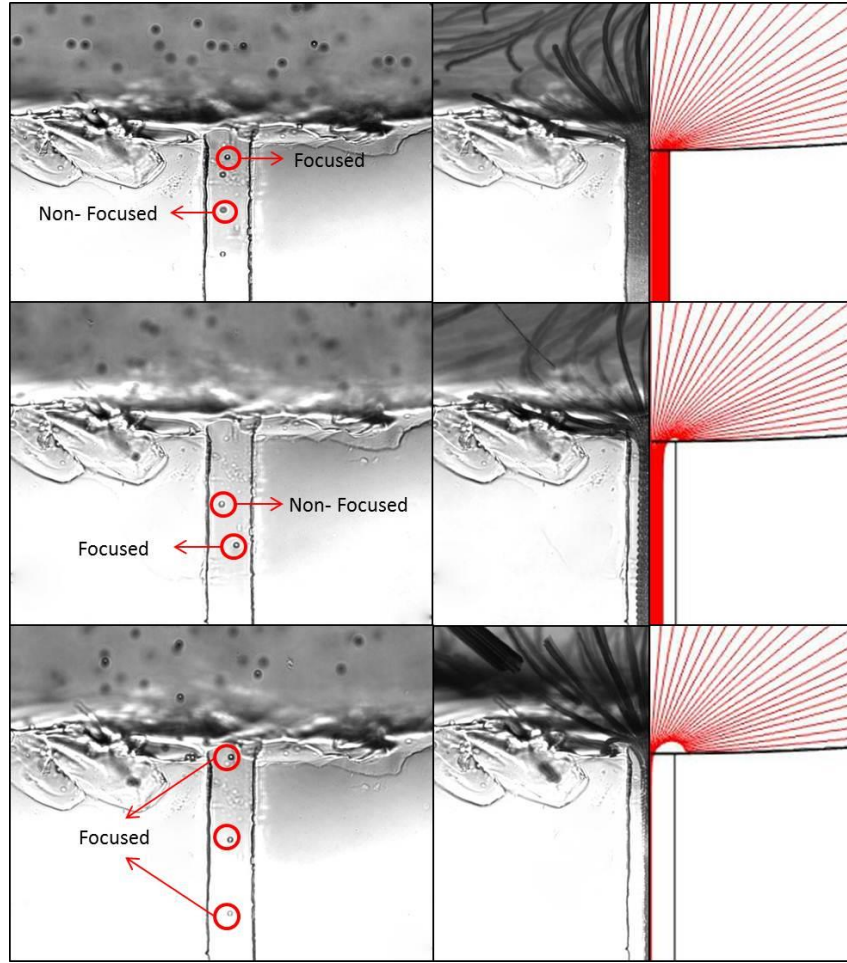


Figure 39: Comparison between experimentally obtained (snapshot and superimposed) and numerically predicted trajectories of 5 μm particles subjected to three-dimensional focusing at the reservoir-microchannel junction under the influence of rDEP at various DC-biased AC voltages. The DC voltage applied, is fixed at 25 V and the AC (RMS) voltage at 1 kHz frequency is varied from (a) 0 V ($\alpha=0$) to (b) 150 V ($\alpha=6$), and (c) 300 V ($\alpha=12$).

7.5.2 Comparison Between Two-dimensional and Three-dimensional Particle Trapping

Experimentally obtained snapshots and superimposed images of 5 μm particle trapping using two-dimensional and three-dimensional method is shown in figure 40.

When the stream-wise dielectrophoretic velocity counteracts the electrokinetic velocity particles are trapped at the reservoir-microchannel junction. The $5\text{ }\mu\text{m}$ particles as shown in figure 40(a), are trapped at the junction in the two-dimensional channel on application of 25 V DC and 425 V AC whereas in the three-dimensional channel the particles are trapped on application of 25 V DC and 375 V AC. We can observe that the voltage required for trapping of $5\text{ }\mu\text{m}$ particles in three-dimensional channel is lower compared to two-dimensional channel. The sharp transition between the depth of the reservoir and the microchannel produces an electric field gradient in the depth direction which is absent in the two-dimensional channel. The additional gradients in three-dimensional channel produce a larger opposing DEP force compared to two-dimensional channel, trapping the particles at a lower DC-biased AC voltage. The experimentally obtained snapshot and superimposed images are also compared with that of the numerically predicted trajectories for both the channel geometries and they agree closely well with each other.

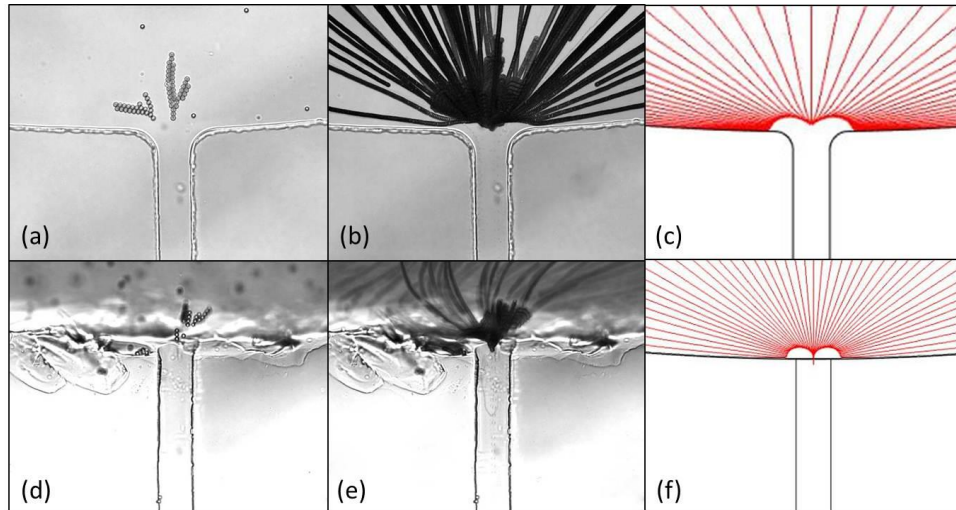


Figure 40: Comparison of experimentally obtained snapshots and superimposed images with numerically predicted trajectories of 5 μm particles subjected to (a) two-dimensional and (d) three-dimensional trapping at the reservoir-microchannel junction under the influence of rDEP. The DC voltage applied is 25 V and the AC (RMS) voltage at 1 kHz frequency is 375 V ($\alpha=15$) for two-dimensional, and 425 ($\alpha=17$) for three-dimensional trapping.

Particles trapping in both, two-dimensional and three-dimensional channel was performed using rDEP at different DC-biased AC voltages. Figure 41 shows the experimentally obtained and numerically predicted trapping voltages at different DC-biased AC voltages in both the two-dimensional and three-dimensional channels. With the increase in DC field the electrokinetic velocity of the particles increases and a larger opposing DEP force is required to trap the particles. From the plot in figure 41, we can see that with larger DC field, the AC field required to produce an opposing DEP force is also larger.

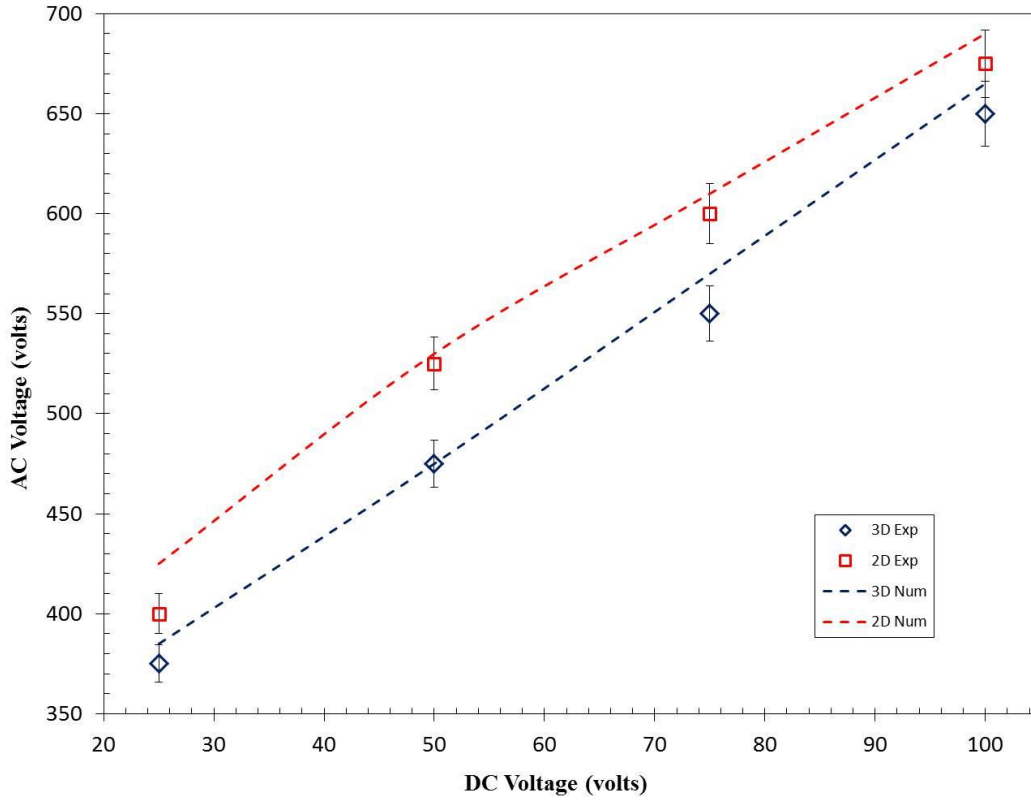


Figure 41: Comparison between two-dimensional and three-dimensional particle trapping under various DC-biased AC voltages under the influence of rDEP at the reservoir-microchannel junction.

On comparison between the voltages required to trap $5\ \mu\text{m}$ particles in two-dimensional and three-dimensional channel, we can observe that the AC voltages required for trapping particles at the same DC voltages are different. The DC-biased AC voltage required to trap particles in three-dimensional channel is lower in all the four cases compared to two-dimensional channel studied above. The lower voltage requirements can be attributed to the additional electric field gradient present in the depth direction in the three-dimensional channel. The additional electric field gradient produces a larger DEP force at the same applied voltage in a three-dimensional channel compared

to two-dimensional channel. This unique feature in the three-dimensional channel can be utilized to trap particles at lower voltages, reducing the side effects of Joule heating. While trapping of sub-micron particles in a two-dimensional channel can be difficult, three-dimensional channels can be potentially used to trap sub-micron particles by altering the depth of the channel compared to the reservoir.

7.6 Summary

This work demonstrates continuous particle focusing and trapping based on rDEP occurring at the reservoir-microchannel junction in two-dimensional and three-dimensional channel geometries. Three-dimensional focusing and trapping is proposed to reduce the applied voltages required to trap particles and also to focus particles in horizontal and vertical planes. Joule heating can be avoided by using 3D rDEP which can considerably reduce the electric field required for trapping and separating particles at the reservoir-microchannel junction. 3D rDEP utilizes the electric field gradients in the vertical plane along with the ones in horizontal plane. 3D rDEP can be potentially utilized to manipulate and concentrate sub-micron size particles without producing Joule heating owing to low voltage requirements compared to traditional two-dimensional trapping.

CHAPTER 8: Conclusion and Future Work

8.1 Conclusions

In this thesis, electrokinetic and dielectrophoretic motions of particles and, cells at the reservoir-microchannel junction is extensively studied using both experimental and numerical approach. Initially, particle electrokinetic motion at the reservoir-microchannel junction undergoing reservoir-based dielectrophoresis is studied. The factors that affect the electrokinetic and dielectrophoretic motion of the particles are studied in detail. Size based particle separation was attained utilizing the size dependence of the dielectrophoretic force acting at the reservoir-microchannel junction. Surface charge differences for monodisperse particles were utilized to attain charge based separation. Particles with varied surface charge possess different electrokinetic velocity which was exploited to attain charge based separation. Membrane of a cell that loses its viability gets distorted resulting into higher inflow and outflow of ions; increasing its conductivity compared to viable cells. The conductivity difference results into different Clausius-Mossotti factor for viable and non-viable cells which was utilized to continuously separate live yeast cells from the dead ones. Furthermore, we used a stacked microfluidic device that has multiple levels with multiple microchannels at each level to continuously concentrate and, selectively separate particles and cells. A stacked microfluidic device was utilized to considerably increase the microfluidic throughput. At last, we utilize the rDEP method to attain three dimensional reservoir-based dielectrophoretic focusing and

trapping of particles. The detailed conclusion of major contributions of this thesis work is listed below.

1. In Chapter 2, the electrokinetic particle motion at the reservoir-microchannel junction under the effect of rDEP was studied. The effect of AC electric fields, DC electric fields and particle size on focusing at reservoir-microchannel junction was extensively studied. Trapping of different sized particles at various DC-biased AC fields was investigated. Validation of the experimentally obtained result was done using a 2D numerical model developed in COMSOL 3.5a (Birmingham, MA). The numerically obtained results agreed qualitatively with the experimentally obtained results. Particle focusing was found to increase with the magnitude of the in AC electric field and with the particle size but decrease with the DC electric field. From the investigation, it was also found that larger particles can be trapped at lower electric fields compared to smaller counterparts. Therefore, reservoir-based dielectrophoresis can be utilized to trap and separate particles/cells.

2. In Chapter 3, we demonstrated size based particle separation at the reservoir-microchannel junction using reservoir-based dielectrophoresis. Continuous separation of particles with different size was obtained at the reservoir-microchannel junction. The separation process utilized inherent electric field gradients formed at the reservoir-microchannel junction due to the size difference between the two micro-device components. The particles were trapped inside the reservoir during the separation process aiding in the utilization of the microchannel for post processing. Inter-particle

interactions however tend to reduce the separation efficiency at the junction. The effect of enhanced electrokinetic flow on the separation process was investigated experimentally. The separation efficiency was observed to be increasing with enhanced electrokinetic flow.

3. In Chapter 4, reservoir-based dielectrophoretic approach was applied to separate particle based upon surface charge. Same sized particles with difference in surface charge were separated inside the microfluidic reservoir. It was found that the streaming particles interacted with the trapped particles and reduced the separation efficiency. However, the influences from the undesired particle trapping have been found through experiments to decrease with the enhanced electrokinetic flow and the lowered AC electric field frequency. It was concluded that the channel width and depth along with solution ionic concentration can also impact the charge based particle separation.

4. In Chapter 5, continuous microfluidic separation of cells by viability using reservoir-based dielectrophoresis was attained. Live and dead yeast cells were trapped separately at different AC field frequencies under various DC-biased AC fields. The experimental results agreed closely with the corresponding numerical results. Within the tested field frequencies, the AC to DC ratio for live yeast trapping was higher than that for the dead cells as the former experiences a weaker rDEP while having a larger electrokinetic mobility. The difference in the AC to DC ratio required for trapping was utilized to selective concentrate and continuously separate dead yeast cells from live ones

at the reservoir-microchannel junction. The rDEP sorter can be perfectly positioned inside a lab-on-a-chip device as it spares the entire microchannel for post analysis.

5. In Chapter 6, we implemented a stacked microfluidic device for continuous concentration and separation of particles/cells at the reservoir-microchannel junction. A stacked microfluidic device consists of multiple levels with multiple microchannels at each level. Stacked device was utilized to manipulate polystyrene particles and cells at the reservoir-microchannel junction. Using a stacked device considerably increased the throughput compared to a single channel device. Low throughput is a major concern in microfluidics, implementing such a device can significantly increase the experimental throughput.

6. In Chapter 7, a comparison between two-dimensional and three-dimensional particle focusing and trapping is presented. A microchannel which utilizes electric field gradients in all the three directions was fabricated by punching the reservoir right at the reservoir-microchannel junction thus utilizing the depth-wise gradient to focus and trap particles. Three-dimensional particle focusing was observed in above mentioned microchannel configuration contrary to two-dimensional configuration used in previous chapters. A comparison of trapping voltages between three-dimensional and two-dimensional configuration was studied. The experimental and numerical results showed that the three-dimensional configuration required lower AC voltages to trap particles at all the different base DC voltages compared to two-dimensional configuration. As three-dimensional configuration utilizes the electric field gradients in both vertical and

horizontal plane, thus the voltage required to trap particles is lowered considerably, reducing the effects of Joule heating.

8.2 Future Work

The microfluidic method of reservoir-based dielectrophoresis can be effectively utilized to manipulate micron sized particles. However, manipulation of sub-micron sized particles using this method would require application of a larger electric field which can in turn result into Joule heating. Joule heating at the reservoir-microchannel junction can greatly disturb the particle focusing and trapping. Future work would include detailed investigation of Joule heating effects on particle manipulation at the reservoir-microchannel junction. In all our current work we utilize negative dielectrophoresis for separation of particles and cells. Particle or cell separation can also be attained by positive dielectrophoresis. Specifically, if separation is attained by forcing particular kind of particles to undergo positive dielectrophoresis and other kind to undergo negative dielectrophoresis, the inter-particle interactions at the junction can be greatly reduced. This would enable us to obtain very high separation efficiency and can be investigated as a part of future work. Moreover, the effects of channel length, constriction width, and buffer solution conductivity on particle and cell separation process can also be investigated.

REFERENCES

- Adams, J. D., U. Kim, and H. T. Soh. "Multitarget Magnetic Activated Cell Sorter." *Proceedings of the National Academy of Sciences of the United States of America* 105, no. 47 (Nov 25 2008): 18165-18170. PMID: 19015523.
- Ai, Y., A. Beskok, D. T. Gauthier, S. W. Joo, and S. Qian. "Dc Electrokinetic Transport of Cylindrical Cells in Straight Microchannels." *Biomicrofluidics* 3, no. 4 (Nov 24 2009): 44110. PMID: 20216972.
- Ai, Y., S. W. Joo, Y. Jiang, X. Xuan, and S. Qian. "Transient Electrophoretic Motion of a Charged Particle through a Converging-Diverging Microchannel: Effect of Direct Current-Dielectrophoretic Force." *Electrophoresis* 30, no. 14 (Jul 2009): 2499-2506. PMID: 19639572.
- Ai, Y., S. Park, J. Zhu, X. Xuan, A. Beskok, and S. Qian. "DC Electrokinetic Particle Transport in an L-Shaped Microchannel." *Langmuir : The ACS Journal of Surfaces and Colloids* 26, no. 4 (Feb 16 2010): 2937-2944. PMID: 19852473.
- Alghane, M., Y. Q. Fu, B. X. Chen, Y. Li, M. P. Y. Desmulliez, and A. J. Walton. "Frequency Effect on Streaming Phenomenon Induced by Rayleigh Surface Acoustic Wave in Microdroplets." *Journal of Applied Physics* 112, no. 8 (2012).
- Anderson, J. *Colloid Transport by Interfacial Forces*. Annual Review of Fluid Mechanics, 1989.
- Balagadde, F. K., L. You, C. L. Hansen, F. H. Arnold, and S. R. Quake. "Long-Term Monitoring of Bacteria Undergoing Programmed Population Control in a Microchemostat." *Science (New York, N.Y.)* 309, no. 5731 (Jul 1 2005): 137-140. PMID: 15994559.
- Berthier, J., and P. Silberzan. *Microfluidics for Biotechnology*. norwood, MA: Artech House, 2006.
- Bhagat, A. A., H. Bow, H. W. Hou, S. J. Tan, J. Han, and C. T. Lim. "Microfluidics for Cell Separation." *Medical & Biological Engineering & Computing* 48, no. 10 (Oct 2010): 999-1014. PMID: 20414811.
- Cetin, B., and D. Li. "Dielectrophoresis in Microfluidics Technology." *Electrophoresis* 32, no. 18 (Sep 2011): 2410-2427. PMID: 21922491.

Chen, Z., S. Zhang, Z. Tang, P. Xiao, X. Guo, and Z. Lu. *Surface and Interface Analysis* 38 (2006): 996.

Chen, L., J. Choo, and B. Yan. "The Microfabricated Electrokinetic Pump: A Potential Promising Drug Delivery Technique." *Expert Opinion on Drug Delivery* 4, no. 2 (Mar 2007): 119-129. PMID: 17335410.

Cheng, I. F., H. C. Chang, D. Hou, and H. C. Chang. "An Integrated Dielectrophoretic Chip for Continuous Bioparticle Filtering, Focusing, Sorting, Trapping, and Detecting." *Biomicrofluidics* 1, no. 2 (May 10 2007): 21503. PMID: 19693376.

Choi, S., T. Ku, S. Song, C. Choi, and J. K. Park. "Hydrophoretic High-Throughput Selection of Platelets in Physiological Shear-Stress Range." *Lab on a Chip* 11, no. 3 (Feb 7 2011): 413-418. PMID: 21072435.

Choi, S., S. Song, C. Choi, and J. K. Park. "Continuous Blood Cell Separation by Hydrophoretic Filtration." *Lab on a Chip* 7, no. 11 (Nov 2007): 1532-1538. PMID: 17960282.

Church, C., J. Zhu, G. Wang, T. R. Tzeng, and X. Xuan. "Electrokinetic Focusing and Filtration of Cells in a Serpentine Microchannel." *Biomicrofluidics* 3, no. 4 (Nov 24 2009): 44109. PMID: 20216971.

Cummings, E. B., S. K. Griffiths, R. H. Nilson, and P. H. Paul. "Conditions for Similitude between the Fluid Velocity and Electric Field in Electroosmotic Flow." *Analytical Chemistry* 72, no. 11 (Jun 1 2000): 2526-2532. PMID: 10857630.

Davis, J. A., D. W. Inglis, K. J. Morton, D. A. Lawrence, L. R. Huang, S. Y. Chou, J. C. Sturm, and R. H. Austin. "Deterministic Hydrodynamics: Taking Blood Apart." *Proceedings of the National Academy of Sciences of the United States of America* 103, no. 40 (Oct 3 2006): 14779-14784. PMID: 17001005.

Davison, S. M., and K. V. Sharp. "Boundary Effects on the Electrophoretic Motion of Cylindrical Particles: Concentrically and Eccentrically-Positioned Particles in a Capillary." *Journal of Colloid and Interface Science* 303, no. 1 (Nov 1 2006): 288-297. PMID: 16920138.

Del Bene, F., M. Germani, G. De Nicolao, P. Magni, C. E. Re, D. Ballinari, and M. Rocchetti. "A Model-Based Approach to the in Vitro Evaluation of Anticancer Activity." *Cancer Chemotherapy and Pharmacology* 63, no. 5 (Apr 2009): 827-836. PMID: 18663447.

DeWitt, S. H. "Microreactors for Chemical Synthesis." *Current Opinion in Chemical Biology* 3, no. 3 (Jun 1999): 350-356. PMID: 10359719.

Di Carlo, D. "Inertial Microfluidics." *Lab on a Chip* 9, no. 21 (Nov 7 2009): 3038-3046. PMID: 19823716.

Di Carlo, D., D. Irimia, R. G. Tompkins, and M. Toner. "Continuous Inertial Focusing, Ordering, and Separation of Particles in Microchannels." *Proceedings of the National Academy of Sciences of the United States of America* 104, no. 48 (Nov 27 2007): 18892-18897. PMID: 18025477.

Didar, T. F., K. Li, M. Tabrizian, and T. Veres. "High Throughput Multilayer Microfluidic Particle Separation Platform using Embedded Thermoplastic-Based Micropumping." *Lab on a Chip* 13, no. 13 (Jul 7 2013): 2615-2622. PMID: 23640083.

Docoslis, A., L. A. Espinoza, B. Zhang, L. L. Cheng, B. A. Israel, P. Alexandridis, and N. L. Abbott. "Using Nonuniform Electric Fields to Accelerate the Transport of Viruses to Surfaces from Media of Physiological Ionic Strength." *Langmuir : The ACS Journal of Surfaces and Colloids* 23, no. 7 (Mar 27 2007): 3840-3848. PMID: 17323980.

Docoslis, A., N. Kalogerakis, L. A. Behie, and K. V. Kaler. "A Novel Dielectrophoresis-Based Device for the Selective Retention of Viable Cells in Cell Culture Media." *Biotechnology and Bioengineering* 54, no. 3 (May 5 1997): 239-250. PMID: 18634090.

Doh, I., and H. Y. Chou. *Sensors and Actuators A* (2005).

Ermolina, I., and H. Morgan. "The Electrokinetic Properties of Latex Particles: Comparision of Electrophoresis and Didelectrophoresis." *J. Colloid Interface Science* 285 (2005): 419.

Friend, J., and L. Yeo. "Microscale Acoustofluidics: Microfluidics Driven Via Acoustics and Ultrasonics." *Reviews of Modern Physics* 83, no. (2011): 647.

Fu, A. Y., H. P. Chou, C. Spence, F. H. Arnold, and S. R. Quake. "An Integrated Microfabricated Cell Sorter." *Analytical Chemistry* 74, no. 11 (Jun 1 2002): 2451-2457. PMID: 12069222.

Fu, A. Y., C. Spence, A. Scherer, F. H. Arnold, and S. R. Quake. "A Microfabricated Fluorescence-Activated Cell Sorter." *Nature Biotechnology* 17, no. 11 (Nov 1999): 1109-1111. PMID: 10545919.

Gagnon, Z. R. "Cellular Dielectrophoresis: Applications to the Characterization, Manipulation, Separation and Patterning of Cells." *Electrophoresis* 32, no. 18 (Sep 2011): 2466-2487. PMID: 21922493.

Gale, B. K., K. D. Caldwell, and A. B. Frazier. "A Micromachined Electrical Field-Flow Fractionation (Mu-EFFF) System." *IEEE Transactions on Bio-Medical Engineering* 45, no. 12 (Dec 1998): 1459-1469. PMID: 9835194.

Gascoyne, P. R., and J. Vykoukal. "Particle Separation by Dielectrophoresis." *Electrophoresis* 23, no. 13 (Jul 2002): 1973-1983. PMID: 12210248.

Giddings, J. C. "Field-Flow Fractionation: Analysis of Macromolecular, Colloidal, and Particulate Materials." *Science (New York, N.Y.)* 260, no. 5113 (Jun 4 1993): 1456-1465. PMID: 8502990.

Gijs, M. A., F. Lacharme, and U. Lehmann. "Microfluidic Applications of Magnetic Particles for Biological Analysis and Catalysis." *Chemical Reviews* 110, no. 3 (Mar 10 2010): 1518-1563. PMID: 19961177.

Gordon, J. E., Z. Gagnon, and H. C. Chang. "Dielectrophoretic Discrimination of Bovine Red Blood Cell Starvation Age by Buffer Selection and Membrane Cross-Linking." *Biomicrofluidics* 1, no. 4 (Nov 27 2007): 44102. PMID: 19693401.

Gossett, D. R., W. M. Weaver, A. J. Mach, S. C. Hur, H. T. Tse, W. Lee, H. Amini, and D. Di Carlo. "Label-Free Cell Separation and Sorting in Microfluidic Systems." *Analytical and Bioanalytical Chemistry* 397, no. 8 (Aug 2010): 3249-3267. PMID: 20419490.

Grom, F., J. Kentsch, T. Muller, T. Schnelle, and M. Stelzle. "Accumulation and Trapping of Hepatitis A Virus Particles by Electrohydrodynamic Flow and Dielectrophoresis." *Electrophoresis* 27, no. 7 (Apr 2006): 1386-1393. PMID: 16568408.

Hakoda, M., Y. Wakizaka, and Y. Hirota. "Separation of Viable and Nonviable Animal Cell using Dielectrophoretic Filter." *Biotechnology Progress* 26, no. 4 (Jul-Aug 2010): 1061-1067. PMID: 20205163.

Hansson, J., J. M. Karlsson, T. Haraldsson, H. Brismar, W. van der Wijngaart, and A. Russom. "Inertial Microfluidics in Parallel Channels for High-Throughput Applications." *Lab on a Chip* 12, no. 22 (Nov 21 2012): 4644-4650. PMID: 22930164.

Hawkins, B. G., A. E. Smith, Y. A. Syed, and B. J. Kirby. "Continuous-Flow Particle Separation by 3D Insulative Dielectrophoresis using Coherently Shaped, Dc-Biased, Ac Electric Fields." *Analytical Chemistry* 79, no. 19 (Oct 1 2007): 7291-7300. PMID: 17764153.

Hirvonen, J., and R. H. Guy. "Iontophoretic Delivery Across the Skin: Electroosmosis and its Modulation by Drug Substances." *Pharmaceutical Research* 14, no. 9 (Sep 1997): 1258-1263. PMID: 9327458.

Holmes, D., M. E. Sandison, N. G. Green, and H. Morgan. "On-Chip High-Speed Sorting of Micron-Sized Particles for High-Throughput Analysis." *Nanobiotechnology, IEE Proceedings* - 152, no. 4 (2005): 129-135.

Hong, J. W., V. Studer, G. Hang, W. F. Anderson, and S. R. Quake. "A Nanoliter-Scale Nucleic Acid Processor with Parallel Architecture." *Nature Biotechnology* 22, no. 4 (Apr 2004): 435-439. PMID: 15024389.

Hsu, J. P., and Z. S. Chen. "Electrophoresis of a Sphere Along the Axis of a Cylindrical Pore: Effects of Double-Layer Polarization and Electroosmotic Flow." *Langmuir : The ACS Journal of Surfaces and Colloids* 23, no. 11 (May 22 2007): 6198-6204. PMID: 17469861.

Hsu, J. P., M. H. Ku, and C. Y. Kao. "Electrophoresis of a Spherical Particle Along the Axis of a Cylindrical Pore: Effect of Electroosmotic Flow." *Journal of Colloid and Interface Science* 276, no. 1 (Aug 1 2004): 248-254. PMID: 15219456.

Huang, L. R., E. C. Cox, R. H. Austin, and J. C. Sturm. "Continuous Particle Separation through Deterministic Lateral Displacement." *Science (New York, N.Y.)* 304, no. 5673 (May 14 2004): 987-990. PMID: 15143275.

Huang, Y., R. Holzel, R. Pethig, and X. B. Wang. "Differences in the AC Electrodynamics of Viable and Non-Viable Yeast Cells Determined through Combined Dielectrophoresis and Electrorotation Studies." *Physics in Medicine and Biology* 37, no. 7 (Jul 1992): 1499-1517. PMID: 1631195.

Hughes, M. P. "Strategies for Dielectrophoretic Separation in Laboratory-on-a-Chip Systems." *Electrophoresis* 23, no. 16 (Aug 2002): 2569-2582. PMID: 12210160.

Huh, D., J. H. Bahng, Y. Ling, H. H. Wei, O. D. Kripfgans, J. B. Fowlkes, J. B. Grotberg, and S. Takayama. "Gravity-Driven Microfluidic Particle Sorting Device with Hydrodynamic Separation Amplification." *Analytical Chemistry* 79, no. 4 (Feb 15 2007): 1369-1376. PMID: 17297936.

Hunter, J. *Foundation of Colloid Sciences*. 2nd ed. Oxford, UK: Oxford University Press, (2001).

Hur, Soojung Claire, Albert J. Mach, and Dino Di Carlo. "High-Throughput Size-Based Rare Cell Enrichment using Microscale Vortices." *Biomechanics* 5, no. 2 (2011).

Hyoung Kang, Kwan, Xiangchun Xuan, Yuejun Kang, and Dongqing Li. "Effects of Dc-Dielectrophoretic Force on Particle Trajectories in Microchannels." *Journal of Applied Physics* 99, no. 6 (2006).

Jellema, L. C., T. Mey, S. Koster, and E. Verpoorte. "Charge-Based Particle Separation in Microfluidic Devices using Combined Hydrodynamic and Electrokinetic Effects." *Lab on a Chip* 9, no. 13 (Jul 7 2009): 1914-1925. PMID: 19532967.

Jen, C. P., and W. F. Chen. "An Insulator-Based Dielectrophoretic Microdevice for the Simultaneous Filtration and Focusing of Biological Cells." *Biomicrofluidics* 5, no. 4 (Dec 2011): 44105-4410511. PMID: 22662057.

Jesus-Perez, N. M., and B. H. Lapidco-Encinas. "Dielectrophoretic Monitoring of Microorganisms in Environmental Applications." *Electrophoresis* 32, no. 17 (Sep 2011): 2331-2357. PMID: 21823133.

Jones, T. *Electromechanics of Particles*. New York City, NY: Cambridge University Press, 1995.

Jones, P. V., S. J. Staton, and M. A. Hayes. "Blood Cell Capture in a Sawtooth Dielectrophoretic Microchannel." *Analytical and Bioanalytical Chemistry* 401, no. 7 (Oct 2011): 2103-2111. PMID: 21830138.

Kadaksham, J., P. Singh, and N. Aubry. "Dielectrophoresis Induced Clustering Regimes of Viable Yeast Cells." *Electrophoresis* 26, no. 19 (Oct 2005): 3738-3744. PMID: 16152665.

Kale, A., S. Patel, G. Hu, and X. Xuan. "Numerical Modeling of Joule Heating Effects in Insulator-Based Dielectrophoresis Microdevices." *Electrophoresis* 34, no. 5 (Mar 2013): 674-683. PMID: 23192532.

Kang, Y., D. Li, S. A. Kalams, and J. E. Eid. "DC-Dielectrophoretic Separation of Biological Cells by Size." *Biomedical Microdevices* 10, no. 2 (Apr 2008): 243-249. PMID: 17899384.

Kartalov, E. P., and S. R. Quake. "Microfluidic Device Reads Up to Four Consecutive Base Pairs in DNA Sequencing-by-Synthesis." *Nucleic Acids Research* 32, no. 9 (May 20 2004): 2873-2879. PMID: 15155856.

Keh, H. J., and J. L. Anderson. "Boundary Effects on Electrophoretic Motion of Colloidal Spheres." *Journal of Fluid Mechanics* 153 (1985): 417-439.

Keh, Huan J., and Jinn Y. Chiou. "Electrophoresis of a Colloidal Sphere in a Circular Cylindrical Pore." *AIChE Journal* 42, no. 5 (1996): 1397-1406.

Keh, Huan J., and Liang C. Lien. "Electrophoresis of a Colloidal Sphere Along the Axis of a Circular Orifice Or a Circular Disk." *Journal of Fluid Mechanics* 224 (1991): 305-333.

Kersaudy-Kerhoas, M., R. Dhariwal, and M. P. Desmulliez. "Recent Advances in Microparticle Continuous Separation." *IET Nanobiotechnology / IET* 2, no. 1 (Mar 2008): 1-13. PMID: 18298195.

Kim, S. B., S. Y. Yoon, H. J. Sung, and S. S. Kim. "Cross-Type Optical Particle Separation in a Microchannel." *Analytical Chemistry* 80, no. 7 (Apr 1 2008): 2628-2630. PMID: 18275223.

Kim, S. H., J. Nam, J. W. Kim, D. H. Kim, S. H. Han, and D. A. Weitz. "Formation of Polymersomes with Double Bilayers Templated by Quadruple Emulsions." *Lab on a Chip* 13, no. 7 (Apr 7 2013): 1351-1356. PMID: 23380918.

Kohlheyer, D., J. C. Eijkel, A. van den Berg, and R. B. Schasfoort. "Miniaturizing Free-Flow Electrophoresis - a Critical Review." *Electrophoresis* 29, no. 5 (Mar 2008): 977-993. PMID: 18232029.

Krivankova, L., and P. Bocek. "Continuous Free-Flow Electrophoresis." *Electrophoresis* 19, no. 7 (Jun 1998): 1064-1074. PMID: 9662166.

Kua, C. H., Y. C. Lam, I. Rodriguez, C. Yang, and K. Youcef-Toumi. "Dynamic Cell Fractionation and Transportation using Moving Dielectrophoresis." *Analytical Chemistry* 79, no. 18 (Sep 15 2007): 6975-6987. PMID: 17702529.

Kuntaegowdanahalli, S. S., A. A. Bhagat, G. Kumar, and I. Papautsky. "Inertial Microfluidics for Continuous Particle Separation in Spiral Microchannels." *Lab on a Chip* 9, no. 20 (Oct 21 2009): 2973-2980. PMID: 19789752.

L. Yu, C. Iliescu, G. Xu and F.E.H. Tay. "Sequential Field-Flow Cell Separation Method in a Dielectrophoretic Chip with 3D Electrodes, JMEMS." 5, no. 16 (2007): 1120.

Lapizco-Encinas, B. H., B. A. Simmons, E. B. Cummings, and Y. Fintschenko. "Dielectrophoretic Concentration and Separation of Live and Dead Bacteria in an Array of Insulators." *Analytical Chemistry* 76, no. 6 (Mar 15 2004): 1571-1579. PMID: 15018553.

"Insulator-Based Dielectrophoresis for the Selective Concentration and Separation of Live Bacteria in Water." *Electrophoresis* 25, no. 10-11 (Jun 2004): 1695-1704. PMID: 15188259.

Laurell, T., F. Petersson, and A. Nilsson. "Chip Integrated Strategies for Acoustic Separation and Manipulation of Cells and Particles." *Chemical Society Reviews* 36, no. 3 (Mar 2007): 492-506. PMID: 17325788.

Lei, U., P. H. Sun, and R. Pethig. "Refinement of the Theory for Extracting Cell Dielectric Properties from Dielectrophoresis and Electrorotation Experiments." *Biomicrofluidics* 5, no. 4 (Dec 2011): 44109-4410916. PMID: 22662061.

Lenshof, A., and T. Laurell. "Continuous Separation of Cells and Particles in Microfluidic Systems." *Chemical Society Reviews* 39, no. 3 (Mar 2010): 1203-1217. PMID: 20179832.

Lettieri, G. L., A. Dodge, G. Boer, N. F. de Rooij, and E. Verpoorte. "A Novel Microfluidic Concept for Bioanalysis using Freely Moving Beads Trapped in Recirculating Flows." *Lab on a Chip* 3, no. 1 (Feb 2003): 34-39. PMID: 15100803.

Lewpiriyawong, N., K. Kandaswamy, C. Yang, V. Ivanov, and R. Stocker. "Microfluidic Characterization and Continuous Separation of Cells and Particles using Conducting Poly(Dimethyl Siloxane) Electrode Induced Alternating Current-Dielectrophoresis." *Analytical Chemistry* 83, no. 24 (Dec 15 2011): 9579-9585. PMID: 22035423.

Lewpiriyawong, N., C. Yang, and Y. C. Lam. "Dielectrophoretic Manipulation of Particles in a Modified Microfluidic H Filter with Multi-Insulating Blocks." *Biomicrofluidics* 2, no. 3 (Aug 11 2008): 34105. PMID: 19693372.

Li, D. *Electrokinetics in Microfluidics*. New York: Elsevier Academic Press, (2004).

Li, H., and R. Bashir. *Sensors and Actuators B*. (2002).

Li, J. Q., Q. Zhang, J. Yang, and J. and Tian. "Fabrication of Carbon Nanotubes Field Effect Transistors by AC Dielectrophoresis Method. Carbon ." , no. 42 (2011): 2263.

Li, R., and R. Bashir. *Dielectrophoretic Separation and Manipulation of Live and Heat-Treated Cells of Listeria on Microfabricated Devices with Interdigitated Electrodes*. (2002).

Li, D., and Y. Daghighi. "Eccentric Electrophoretic Motion of a Rectangular Particle in a Rectangular Microchannel." *Journal of Colloid and Interface Science* 342, no. 2 (Feb 15 2010): 638-642. PMID: 19944427.

Liang, L., Y. Ai, J. Zhu, S. Qian, and X. Xuan. "Wall-Induced Lateral Migration in Particle Electrophoresis through a Rectangular Microchannel." *Journal of Colloid and Interface Science* 347, no. 1 (Jul 1 2010): 142-146. PMID: 20400083.

Liang, L., S. Qian, and X. Xuan. "Three-Dimensional Electrokinetic Particle Focusing in a Rectangular Microchannel." *Journal of Colloid and Interface Science* 350, no. 1 (Oct 1 2010): 377-379. PMID: 20650465.

Linan Jiang, J. Mikkelsen, Jae-Mo Koo, D. Huber, Shuhuai Yao, L. Zhang, P. Zhou, J. G. Maveety, R. Prasher, J. G. Santiago, T. W. Kenny, and Kenneth E. Goodson. "Closed-Loop Electroosmotic Microchannel Cooling System for VLSI Circuits." *Components and Packaging Technologies, IEEE Transactions on* 25, no. 3 (2002): 347-355.

Liu, H., S. Qian, and H. H. Bau. "The Effect of Translocating Cylindrical Particles on the Ionic Current through a Nanopore." *Biophysical Journal* 92, no. 4 (Feb 15 2007): 1164-1177. PMID: 17142291.

Liu, J., C. Hansen, and S. R. Quake. "Solving the "World-to-Chip" Interface Problem with a Microfluidic Matrix." *Analytical Chemistry* 75, no. 18 (Sep 15 2003): 4718-4723. PMID: 14674446.

Mach, A. J., and D. Di Carlo. "Continuous Scalable Blood Filtration Device using Inertial Microfluidics." *Biotechnology and Bioengineering* 107, no. 2 (Oct 1 2010): 302-311. PMID: 20589838.

Markx, G. H., M. S. Talary, and R. Pethig. "Separation of Viable and Non-Viable Yeast using Dielectrophoresis." *Journal of Biotechnology* 32, no. 1 (Jan 15 1994): 29-37. PMID: 7764449.

Masliyah, J., and S. Bhattacharjee. *Electrokinetic and Colloid Transport Phenomena*. John Wiley & Sons, Inc, 2005.

Miltenyi, S., W. Muller, W. Weichel, and A. Radbruch. "High Gradient Magnetic Cell Separation with MACS." *Cytometry* 11, no. 2 (1990): 231-238. PMID: 1690625.

Morgan, H., and N. Green. *AC Electrokinetics: Colloids and Nanoparticles*. Hertfordshire, UK: Research Studies, (2002).

Nam, K. H., W. J. Chang, H. Hong, S. M. Lim, D. I. Kim, and Y. M. Koo. "Continuous-Flow Fractionation of Animal Cells in Microfluidic Device using Aqueous Two-Phase Extraction." *Biomedical Microdevices* 7, no. 3 (Sep 2005): 189-195. PMID: 16133806.

Pamme, N. "Continuous Flow Separations in Microfluidic Devices." *Lab on a Chip* 7, no. 12 (Dec 2007): 1644-1659. PMID: 18030382.

Pamme, N. "Magnetism and Microfluidics." *Lab on a Chip* 6, no. 1 (Jan 2006): 24-38. PMID: 16372066.

Parikesit, G. O., A. P. Markesteijn, O. M. Piciu, A. Bossche, J. Westerweel, I. T. Young, and Y. Garini. "Size-Dependent Trajectories of DNA Macromolecules due to Insulative Dielectrophoresis in Submicrometer-Deep Fluidic Channels." *Biomicrofluidics* 2, no. 2 (May 6 2008): 24103. PMID: 19693406.

Park, J., B. Kim, S. K. Choi, S. Hong, S. H. Lee, and K. I. Lee. "An Efficient Cell Separation System using 3D-Asymmetric Microelectrodes." *Lab on a Chip* 5, no. 11 (Nov 2005): 1264-1270. PMID: 16234950.

Patel, S., S. Qian, and X. Xuan. "Reservoir-Based Dielectrophoresis for Microfluidic Particle Separation by Charge." *Electrophoresis* 34, no. 7 (Apr 2013): 961-968. PMID: 23161644.

Patel, S., D. Showers, P. Vedantam, T. R. Tzeng, S. Qian, and X. Xuan. "Microfluidic Separation of Live and Dead Yeast Cells using Reservoir-Based Dielectrophoresis." *Biomicrofluidics* 6, no. 3 (Jul 13 2012): 34102. PMID: 23853679.

Pethig, R., and G. H. Markx. "Applications of Dielectrophoresis in Biotechnology." *Trends in Biotechnology* 15, no. 10 (Oct 1997): 426-432. PMID: 9351287.

Pethig, Ronald. "Preface to Special Topic: Dielectrophoresis." *Biomicrofluidics* 4, no. 2 (2010).

Pikal, M. J. "The Role of Electroosmotic Flow in Transdermal Iontophoresis." *Advanced Drug Delivery Reviews* 46, no. 1-3 (Mar 1 2001): 281-305. PMID: 11259844.

Pohl, H. A. *Dielectrophoresis*. Cambridge, UK: Cambridge University Press, (1978).

Pysher, M. D., and M. A. Hayes. "Electrophoretic and Dielectrophoretic Field Gradient Technique for Separating Bioparticles." *Analytical Chemistry* 79, no. 12 (Jun 15 2007): 4552-4557. PMID: 17487977.

Qian, S., S. W. Joo, W. S. Hou, and X. Zhao. "Electrophoretic Motion of a Spherical Particle with a Symmetric Nonuniform Surface Charge Distribution in a Nanotube." *Langmuir : The ACS Journal of Surfaces and Colloids* 24, no. 10 (May 20 2008): 5332-5340. PMID: 18399647.

Qian, S., A. Wang, and J. K. Afonien. "Electrophoretic Motion of a Spherical Particle in a Converging-Diverging Nanotube." *Journal of Colloid and Interface Science* 303, no. 2 (Nov 15 2006): 579-592. PMID: 16979648

Regtmeier, J., R. Eichhorn, M. Viefhues, L. Bogunovic, and D. Anselmetti. "Electrodeless Dielectrophoresis for Bioanalysis: Theory, Devices and Applications." *Electrophoresis* 32, no. 17 (Sep 2011): 2253-2273. PMID: 23361920.

Rodriguez, M. A., and D. W. Armstrong. "Separation and Analysis of colloidal/nano-Particles Including Microorganisms by Capillary Electrophoresis: A Fundamental Review." *Journal of Chromatography.B, Analytical Technologies in the Biomedical and Life Sciences* 800, no. 1-2 (Feb 5 2004): 7-25. PMID: 14698231.

Romanowsky, M. B., A. R. Abate, A. Rotem, C. Holtze, and D. A. Weitz. "High Throughput Production of Single Core Double Emulsions in a Parallelized Microfluidic Device." *Lab on a Chip* 12, no. 4 (Feb 21 2012): 802-807. PMID: 22222423.

Rosenthal, A., and J. Voldman. "Dielectrophoretic Traps for Single-Particle Patterning." *Biophysical Journal* 88, no. 3 (Mar 2005): 2193-2205. PMID: 15613624.

Sethu, P., A. Sin, and M. Toner. "Microfluidic Diffusive Filter for Apheresis (Leukapheresis)." *Lab on a Chip* 6, no. 1 (Jan 2006): 83-89. PMID: 16372073.

Shafiee, H., J. L. Caldwell, M. B. Sano, and R. V. Davalos. "Contactless Dielectrophoresis: A New Technique for Cell Manipulation." *Biomedical Microdevices* 11, no. 5 (Oct 2009): 997-1006. PMID: 19415498.

Shafiee, H., M. B. Sano, E. A. Henslee, J. L. Caldwell, and R. V. Davalos. "Selective Isolation of live/dead Cells using Contactless Dielectrophoresis (cDEP)." *Lab on a Chip* 10, no. 4 (Feb 21 2010): 438-445. PMID: 20126683.

Shugai, A. A., and S. L. Carnie. "Electrophoretic Motion of a Spherical Particle with a Thick Double Layer in Bounded Flows." *Journal of Colloid and Interface Science* 213, no. 2 (May 15 1999): 298-315. PMID: 10222069.

Sridharan, Sriram, Junjie Zhu, Guoqing Hu, and Xiangchun Xuan. "Joule Heating Effects on Electroosmotic Flow in Insulator-Based Dielectrophoresis." *Electrophoresis* 32, no. 17 (2011): 2274-2281.

Srivastava, S. K., A. Gencoglu, and A. R. Minerick. "DC Insulator Dielectrophoretic Applications in Microdevice Technology: A Review." *Analytical and Bioanalytical Chemistry* 399, no. 1 (Jan 2011): 301-321. PMID: 20967429.

Subirats, X., D. Blaas, and E. Kenndler. "Recent Developments in Capillary and Chip Electrophoresis of Bioparticles: Viruses, Organelles, and Cells." *Electrophoresis* 32, no. 13 (Jun 2011): 1579-1590. PMID: 21647924.

Suehiro, J., G. Zhou, M. Imamura, and M. Hara. "Dielectrophoretic Filter for Separation and Recovery of Biological Cells in Water." *Industry Applications, IEEE Transactions on* 39, no. 5 (2003): 1514-1521.

Talary, M. S., J. Burt, J. Tame, and P. Pething. "Electromanipulation and Separation of Cells using Traveling Electric Fields." 29 (1996): 2203.

Tatosian, D. A., and M. L. Shuler. "A Novel System for Evaluation of Drug Mixtures for Potential Efficacy in Treating Multidrug Resistant Cancers." *Biotechnology and Bioengineering* 103, no. 1 (May 1 2009): 187-198. PMID: 19137589.

Tsutsui, H., and C. M. Ho. "Cell Separation by Non-Inertial Force Fields in Microfluidic Systems." *Mechanics Research Communications* 36, no. 1 (Jan 1 2009): 92-103. PMID: 20046897.

Unni, H. N., H. J. Keh, and C. Yang. "Analysis of Electrokinetic Transport of a Spherical Particle in a Microchannel." *Electrophoresis* 28, no. 4 (Feb 2007): 658-664. PMID: 17304499.

Urdaneta, M., and E. Smela. "Multiple Frequency Dielectrophoresis." *Electrophoresis* 28, no. 18 (Sep 2007): 3145-3155. PMID: 17703466.

Voldman, J. "Electrical Forces for Microscale Cell Manipulation." *Annual Review of Biomedical Engineering* 8 (2006): 425-454. PMID: 16834563.

Wang, M. M., E. Tu, D. E. Raymond, J. M. Yang, H. Zhang, N. Hagen, B. Dees, E. M. Mercer, A. H. Forster, I. Kariv, P. J. Marchand, and W. F. Butler. "Microfluidic Sorting of Mammalian Cells by Optical Force Switching." *Nature Biotechnology* 23, no. 1 (Jan 2005): 83-87. PMID: 15608628.

Watts, P., and S. J. Haswell. "Microfluidic Combinatorial Chemistry." *Current Opinion in Chemical Biology* 7, no. 3 (Jun 2003): 380-387. PMID: 12826126.

Wei Hou, Han, Hiong Yap Gan, Ali Asgar S. Bhagat, Leon D. Li, Chwee Teck Lim, and Jongyoon Han. "A Microfluidics Approach Towards High-Throughput Pathogen Removal from Blood using Margination." *Biomicrofluidics* 6, no. 2 (2012).

Weigl, Bernhard. *Microfluidics-Based Lab-on-a-Chip Systems*. IVD Technology, 2000.

Wheeler, A. R., W. R. Throdsset, R. J. Whelan, A. M. Leach, R. N. Zare, Y. H. Liao, K. Farrell, I. D. Manger, and A. Daridon. "Microfluidic Device for Single-Cell Analysis." *Analytical Chemistry* 75, no. 14 (Jul 15 2003): 3581-3586. PMID: 14570213.

Wolff, A., I. R. Perch-Nielsen, U. D. Larsen, P. Friis, G. Goranovic, C. R. Poulsen, J. P. Kutter, and P. Telleman. "Integrating Advanced Functionality in a Microfabricated High-Throughput Fluorescent-Activated Cell Sorter." *Lab on a Chip* 3, no. 1 (Feb 2003): 22-27. PMID: 15100801.

Xuan, X. "Joule Heating in Electrokinetic Flow." *Electrophoresis* 29, no. 1 (Jan 2008): 33-43. PMID: 18058768.

Xuan, X., S. Raghizadeh, and D. Li. "Wall Effects on Electrophoretic Motion of Spherical Polystyrene Particles in a Rectangular Poly(Dimethylsiloxane) Microchannel." *Journal of Colloid and Interface Science* 296, no. 2 (Apr 15 2006): 743-748. PMID: 16226268.

Xuan, X., B. Xu, and D. Li. "Accelerated Particle Electrophoretic Motion and Separation in Converging-Diverging Microchannels." *Analytical Chemistry* 77, no. 14 (Jul 15 2005): 4323-4328. PMID: 16013842.

Xuan, X., C. Ye, and D. Li. "Near-Wall Electrophoretic Motion of Spherical Particles in Cylindrical Capillaries." *Journal of Colloid and Interface Science* 289, no. 1 (Sep 1 2005): 286-290. PMID: 16009235.

Yamada, M., V. Kasim, M. Nakashima, J. Edahiro, and M. Seki. "Continuous Cell Partitioning using an Aqueous Two-Phase Flow System in Microfluidic Devices." *Biotechnology and Bioengineering* 88, no. 4 (Nov 20 2004): 489-494. PMID: 15459911.

Yamada, M., M. Nakashima, and M. Seki. "Pinched Flow Fractionation: Continuous Size Separation of Particles Utilizing a Laminar Flow Profile in a Pinched Microchannel." *Analytical Chemistry* 76, no. 18 (Sep 15 2004): 5465-5471. PMID: 15362908.

Yamada, M., and M. Seki. "Microfluidic Particle Sorter Employing Flow Splitting and Recombining." *Analytical Chemistry* 78, no. 4 (Feb 15 2006): 1357-1362. PMID: 16478134.

Yamada, M., and M. Seki. "Hydrodynamic Filtration for on-Chip Particle Concentration and Classification Utilizing Microfluidics." *Lab on a Chip* 5, no. 11 (Nov 2005): 1233-1239. PMID: 16234946.

Yang, L., P. P. Banada, A. K. Bhunia, and R. Bashir. "Effects of Dielectrophoresis on Growth, Viability and Immuno-Reactivity of *Listeria Monocytogenes*." *Journal of Biological Engineering* 2 (Apr 16 2008): 6-1611-2-6. PMID: 18416836.

Yang, S., A. Undar, and J. D. Zahn. "A Microfluidic Device for Continuous, Real Time Blood Plasma Separation." *Lab on a Chip* 6, no. 7 (Jul 2006): 871-880. PMID: 16804591.

Yariv, E., and H. Brenner. "The Electrophoretic Mobility of an Eccentrically Positioned Spherical Particle in a Cylindrical Pore." *Physics of Fluids (1994-Present)* 14, no. 9 (2002): 3354-3357.

Zhang, X., J. M. Cooper, P. B. Monaghan, and S. J. Haswell. "Continuous Flow Separation of Particles within an Asymmetric Microfluidic Device." *Lab on a Chip* 6, no. 4 (Apr 2006): 561-566. PMID: 16572220.

Zhu, J., G. Hu, and X. Xuan. "Electrokinetic Particle Entry into Microchannels." *Electrophoresis* 33, no. 6 (Mar 2012): 916-922. PMID: 22528411.

Zhu, J., T. R. Tzeng, and X. Xuan. "Continuous Dielectrophoretic Separation of Particles in a Spiral Microchannel." *Electrophoresis* 31, no. 8 (Apr 2010): 1382-1388. PMID: 20301126.

Zhu, J., and X. Xuan. "Curvature-Induced Dielectrophoresis for Continuous Separation of Particles by Charge in Spiral Microchannels." *Biomicrofluidics* 5, no. 2 (Jun 2011): 24111. PMID: 21792385.

Zhu, J., and X. Xuan. "Dielectrophoretic Focusing of Particles in a Microchannel Constriction using DC-Biased AC Electric Fields." *Electrophoresis* 30, no. 15 (Aug 2009): 2668-2675. PMID: 19621378.

Zhu, J., and X. Xuan. "Particle Electrophoresis and Dielectrophoresis in Curved Microchannels." *Journal of Colloid and Interface Science* 340, no. 2 (Dec 15 2009): 285-290. PMID: 19782995.

Zhu, L., Q. Zhang, H. Feng, S. Ang, F. S. Chau, and W. T. Liu. "Filter-Based Microfluidic Device as a Platform for Immunofluorescent Assay of Microbial Cells." *Lab on a Chip* 4, no. 4 (Aug 2004): 337-341. PMID: 15269801.